Structural and Functional Characterization of Neurotoxic Oligomers of Pro-aggregant Tau Repeat Domain : A model for Tauopathy disease

Dissertation

zur

Erlangung des Doktorgrades (Dr. rer. nat.)

der

Mathematisch-Naturwissenschaftlichen Fakultät

der

Rheinischen Friedrich-Wilhelms-Universität Bonn

vorgelegt von

Senthilvelrajan Kaniyappan

Sivakasi, INDIA

2015

Angefertigt mit Genehmigung der Mathematisch-Naturwissenschaftlichen Fakultät der Rheinischen Friedrich-Wilhelms-Universität Bonn

1. Gutachter : Prof. Dr. Eckhard Mandelkow

2. Gutachter : Prof. Dr. Micheal Hoch

Tag der Promotion: 24-11-2015

Erscheinungsjahr: 2016

Contents

Abbreviations

°C – degree Celsius

µg – micro gram

µl – micro liter

µm – micro meter

µM – micro molar

aa- amino acid

AFM – Atomic Force Microscopy

ANS – 8 anilino napthaleno sulfate

APC - Allophycocyanin

BCA – Bicinchoninic acid

BSA – Bovine serum albumin

Butyl FF – Butyl Fast Flow column

CCD – Charged Coupled Device

CD – Circular Dichroism

CNS – Central Nervous System

CV – Column Volume

DLS – Dynamic Light Scattering

DMEM – Dulbecco Minimal Essential Medium

DMSO – Dimethyl Sulfoxide.

DSS – Disuccinimidyl suberate

DTT – Dithiothreitol

E18 – Embryonic day 18

EGCG – Epigallocatechin Gallate

EM – Electron Microscope

FCS – Fetal Calf Serum

FTDP – Fronto Temporal Dementia linked with Parkinsonism

GA – Glutaraldehyde

GTO – Granular Tau Oligomers

HBSS – Hank's Balanced Salt Saline solution

HCl – Hydrochloric Acid

HIC – Hydrophobic Interaction Chromatography

HPLC – High Performance Liquid Chromatography

kHz – kilo Hertz

M – Molar

mA – milli Ampere

MAP – Microtubule Associated Proteins

MBS - m-maleimidobenzoyl-N-hydroxysuccinimide ester

mg – milli gram

ml – milli liter

mm – milli meter

mM – milli molar

MTBR – MicroTubule Binding Region

MWCO – Molecular Weight Cut Off

NaN_3 – Sodium Azide

NFT – Neuro Fibrillary Tangles

ng – nano gram

nm – nano meter

nM – nano molar

NMR – Nuclear Magnetic Resonance

OD – Optical Density

OHSC – Organotypic Hippocampal Slice Culture

PAGE – Poly Acrylamide Gel Electrophoresis

PBS – Phosphate Buffer Saline

PDM - Phenylenedimaleimide

PHF – Paired Helical Filaments

PNS – Peripheral Nervous System

PVDF – Poly Vinylidene DiFluoride

Rpm – Rotations per minute

RT – Room Temperature

SDS – Sodium Dodecyl Sulfate

SEC – Size Exclusion Chromatography

$Tau^{RD\Delta}$ – Tau Repeat Domain protein with deletion of lysine at 280 position

Tau^{FL} – Full length Tau protein

TEA – Tri Ethanol Amine

ThS – Thioflavin S

V – Volt

WT – Wild Type

Summary

Tau protein is a microtubule associated protein present abundantly in the neurons of the central nervous system where it stabilizes the axonal microtubules thereby providing structural architecture for the axons of neurons. Aggregation of Tau occurs in many neurodegenerative diseases collectively termed tauopathies including Alzheimer disease (AD) and frontotemporal dementia (FTD). The mutation ΔK280 of Tau was originally discovered in cases of FTD (Rizzu et al., 1999). In vitro it leads to a pronounced propensity of the protein to aggregate (Barghorn et al., 2000). The repeat domain of Tau protein with this pro-aggregant mutation ($Tau^{RD\Delta}$) induces toxicity in transgenic mice and organotypic hippocampal slice culture models (Sydow et al., 2011, Messing et al., 2013). One current concept of Tau-mediated toxicity in Alzheimer disease and related tau dependent pathologies is that it is based on low-n oligomeric species, rather than higher aggregated forms (fibers and neurofibrillary tangles). To test this we characterized oligomers from $Tau^{RD\Delta}$ protein assembled and purified in vitro. Since Tau oligomers are in dynamic equilibrium during aggregation, we tried to capture and stabilize only the oligomeric forms of Tau using EGCG (Epigallocatechin gallate). EGCG reduces the formation of fibrils and increases the SDS stable oligomers. However, the oligomers are not separable by gel filtration chromatography. Therefore we stabilized the tau oligomers using a low concentration of glutaraldehyde as a cross-linking reagent. This yielded SDS stable low-n oligomers predominantly in the form of dimers, trimers, tetramers with very low amounts of higher order species. The cross-linked $Tau^{RD\Delta}$ oligomers can be purified by hydrophobic interaction chromatography with ~95% purity. They exhibit enhanced fluorescence with the dye ANS, arguing for an altered conformation (compared with monomers) and possibly exposed hydrophobic surface patches. However, they do not contain substantial ß-sheet structure, as analyzed by thioflavin S fluorescence and circular dichroism. Atomic force microscopy (AFM) of $Tau^{RD\Delta}$ oligomers reveals that the particles are roughly globular in shape, with diameters in the range 1.6-5.4 nm (AFM height values). The hydrodynamic radius of $Tau^{RD\Delta}$ oligomers (~5.2 nm) is dominated by that of tetramers, as measured by dynamic light scattering. The size of $Tau^{RD\Delta}$ oligomers reveals that they contain up to 4-5 molecules of Tau, consistent with the SDS gel analysis. The $Tau^{RD\Delta}$ oligomers do not exhibit global toxicity towards rat primary neurons when applied to the extracellular medium, as judged by MTT and LDH assays. However, functional impairment can be deduced from a

pronounced (up to 50%) decrease of dendritic spines and a shift from mushroom-shaped to stubby spines. Consistent with this, the expression of cytoskeletal proteins which are necessary to maintain the mushroom spines is reduced. The neurons also show an increase in reactive oxygen species and influx of calcium. In summary, low-n oligomers of $Tau^{RD\Delta}$ do not cause gross changes in viability, but induce subtle functional defects, leading to an increase in Ca++ and ROS, and consequently to loss of spines and associated shape changes.

Since Tau is an intracellular protein and the formation of oligomers occurs inside the cells, we introduced low-n Tau oligomers by protein transfection into SH-SY5Y cells and primary rat hippocampal neurons and analyzed them by flow cytometry and western blot analysis. This showed that only the cells transfected with $Tau^{RD\Delta}$ oligomers (but not monomers) induce the intracellular aggregation of Tau and recruitment of endogenous Tau into the aggregates. This is accompanied by the hyperphosphorylation of aggregated Tau. Although $Tau^{RD\Delta}$ oligomer transfected cells do not undergo cell death within 15 h of transfection, we found the presence of annexin V positive cells. When compared to monomers and fibrils, the oligomer transfected cells show a 5 fold increase in annexin V positive cells suggesting enhanced apoptosis. We conclude that $Tau^{RD\Delta}$ oligomers applied extracellularly cause degeneration of spines without affecting cell viability, whereas introducing oligomers intracellularly leads to Tau aggregation and apoptosis.

List of tables

List of figures

1 Introduction

1.1 Neurodegenerative diseases

Selective and progressive loss of structure and functions of neurons, including neuronal death is generally called neurodegeneration (Dickson et al., 2010). Neurodegeneration can be caused by genetic mutations in some neurodegenerative diseases, but more generally by a combination of causes related to advanced age (metabolic stress, failure of proteostasis, etc). Many neurodegenerative diseases are characterized by the abnormal aggregation of misfolded proteins collectively called proteopathies. For example α-synuclein protein is aggregated in Parkinson disease, amyloid ß and Tau are aggregated in Alzheimer disease.

1.2 Tauopathies

Tau protein is a natively unfolded soluble protein primarily located on the microtubules of axons (Weingarten et al., 1974). It stabilizes the microtubules thereby maintaining the structural architecture of the axons. Among the tauopathies characterized by aggregated tau, the best known disease is Alzheimer disease where the Tau protein is aggregated into neurofibrillary tangles within neurons. There are several other tauopathies like frontotemporal dementia (FTD), progressive supranuclear palsy (PSP) and traumatic brain encephalopathy (TBE) where Tau protein aggregates into filaments. In case of Pick disease and corticobasal neurodegeneration (CBD), the Tau protein accumulates into inclusion bodies rather than into neurofibrillary tangles (Arai et al., 2001). As of 2013, there were an estimated 44.4 million people with dementia worldwide. 50-75% of these are afflicted with AD (the most common neurodegenerative disease), 2/3 are women. This number will increase to an estimated ~75.6 million in 2030, and to 135.5 million in 2050 (http://www.alz.co.uk/research/statistics).

Alzheimer disease is characterized by selective loss of neurons and synapses (Morrison and Hof, 1997). The major hallmark of the disease is the presence of extracellular amyloid plaques containing fibrillar amyloid ß peptide (Glenner and Wong, 1984, Glenner et al., 1984, Masters et al., 1985), and neurofibrillary tangles consisting of hyperphosphorylated Tau protein (Grundke-Iqbal et al., 1986, Bancher et al., 1989). These histological findings were described in 1906 by the German psychiatrist Alois Alzheimer (Alzheimer, 1907).

1.3 Tau and Alzheimer disease

Tau protein is encoded by a single gene (MAPT) of >100kb long on human chromosome 17q21 (Neve et al., 1986). The Tau gene contains 16 exons. The promoter region of this gene lies in the exon1 of the gene. Exons 2, 3, and 10 undergo alternative splicing to form the six main isoforms of Tau in the human CNS. Their ratio changes with brain development and in the various CNS compartments (Andreadis, 2006).

1.3.1 Tau protein structure

There are a variety of microtubule-associated proteins which vary between cell types and organisms. Some can be grouped together on the basis of their similar domain structure, such as the brain MAPs Tau and MAP2, and the ubiquitous MAP4, and there are several alternatively spliced isoforms whose expression is developmentally regulated (Cassimeris and Spittle, 2001).

The longest isoform of Tau in the human central nervous system contains 441 amino acid residues. It can be subdivided into several domains (Gustke et al., 1994), roughly an N-terminal domain, a microtubule binding domain and C-terminal tail (Figure 1.2). The N-terminal half does not bind to microtubules, projects away from the microtubule surface, and hence is called "projection domain" Most of the C-terminal half contributes to the interaction with microtubules, facilitates their assembly and hence it is called assembly domain.

The C-terminal half contains three or four semi-conserved repeated sequences of 31 or 32 amino acids, termed R1, R2, R3 and R4. Repeat R2 corresponds to exon 10 which can undergo alternative splicing. The N-terminal domain contains two inserts of 29 amino acids each termed N1 and N2 which correspond to the alternatively spliced exon2 and 3. Thus the alternative splicing of exons 2, 3 and 10 leads to six splice forms of Tau of various lengths between 352 and 441 residues, termed 0N3R (smallest isoform) to 2N4R (largest isoform) (Figure 1.1) (Goedert and Jakes, 1990). In the peripheral nervous system there is an additional Tau isoform called “Big Tau” which contains additional 242 residues from exon 4a (Table 1.1)(Couchie et al., 1992, Goedert et al., 1992).

Other mammalian organisms like mouse, rat, and cow have similar amino acid sequences of Tau with few variations, located mostly in the N-terminal domain. For example mouse Tau differs from human Tau only by 11 amino acids, ranging from 341 to 430 amino acid residues (Lee et al., 1988).

Clones	**Inserts/Repeats**	**Number of amino acids**	**Molecular weight (kDa)**
hTau40	2N4R	441	45.9
hTau34	1N4R	412	43
hTau24	0N4R	383	40
hTau39	2N3R	410	42.6
hTau37	1N3R	381	39.7
hTau23	0N3R	352	36.7
Big Tau	2N4R+ exon 4a	695	72.7

Table 1.1 Isoforms of Tau

hTau – Human Tau. The number designates the clone number. (Mandelkow and Mandelkow, 2012, Goedert and Jakes, 1990)

Overall Tau has an unusually hydrophilic composition, consistent with its high solubility and natively unfolded structure. The N-terminal 120 residues are highly acidic (pI 3.8) followed by the basic proline-rich region (residues 150-240 residues, pI 11.4), similar to the repeat domain (residues 240-368, pI 10.8) (Sergeant et al., 2008). The proline-rich region contains numerous prolines, mainly in the form of SP (Ser-Pro) or TP (Thr-Pro) motifs. These motifs can be phosphorylated by proline-directed kinases (such as MAP kinase, GSK3β, cdk5), and there are seven PXXP motifs which can form binding sites for proteins containing SH3 domains (Mandelkow and Mandelkow, 2012, Hanger et al., 2009). Figure 1.2 shows an overview of Tau domains, structural elements, and interaction partners (Mandelkow and Mandelkow, 2012, Mukrasch et al., 2009).

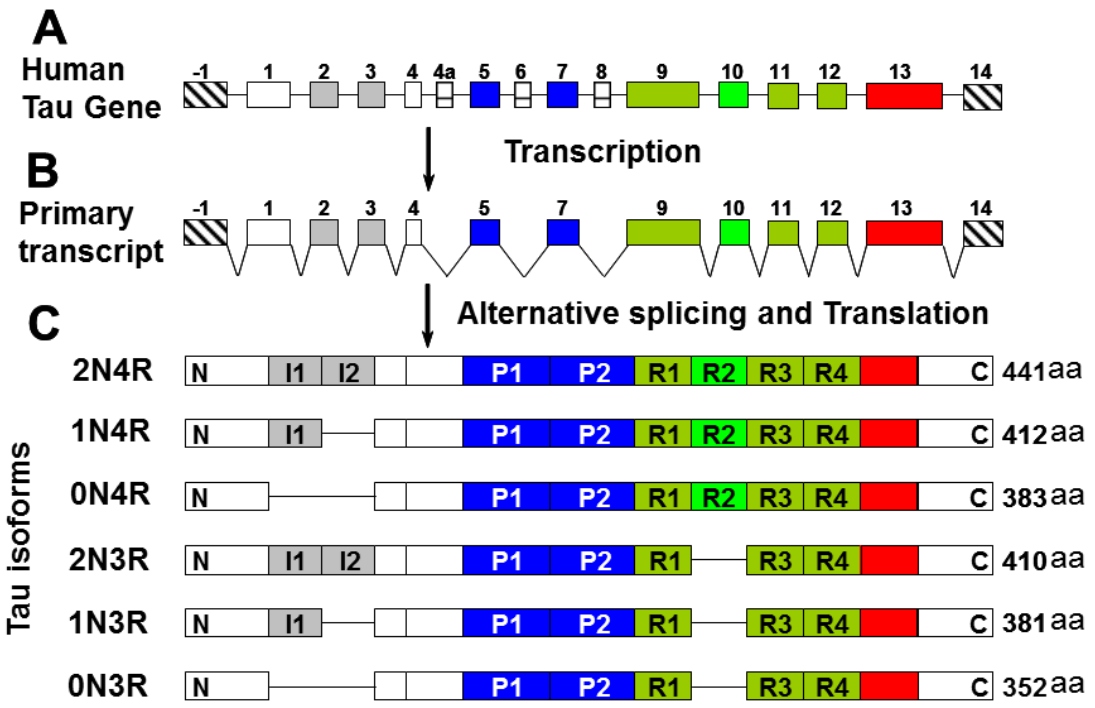

Figure 1.1 Tau structure and its isoforms
A) Diagramatic representation of human Tau gene located at chromosome 17q21. The boxes are exons and the number denotes the exon numbers. The lines between the boxes are introns. **B)** The primary mRNA transcribed from the Tau gene. **C)** There are 6 different isoforms of Tau with different chain lengths. Alternative splicing of exon 2 (Insert I1), 3(Insert I2) and 10 (R2) determines the length of the various isoforms. P1 and P2 = Proline rich region. aa = amino acids. Figure from S. Barghorn, PhD thesis, 2002.

Tau protein is resistant to mild heat and acid treatment, which does not destroy its ability to interact with microtubules (Cleveland et al., 1977a). Biophysical studies showed that Tau protein is natively unfolded because of its hydrophilic nature (Gamblin, 2005, von Bergen et al., 2005, Jeganathan et al., 2008, Schweers et al., 1994). Nuclear magnetic resonance spectroscopy and small angle X-ray scattering methods confirmed the natively unfolded conformation and dynamics of this protein with high resolution (Mukrasch et al., 2005, Shkumatov et al., 2011). Tau protein contains only a low content of secondary structure (α-helix and ß-strand) (Figure 1.2). This also opens the opportunity for other proteins to interact with Tau readily in the crowded environment of the cell. Due to its unfolded nature, the domains of Tau could also interact with themselves. An example is the paperclip conformation where the N-terminal and C-terminal domains of Tau interact with the repeat domain (Jeganathan et al., 2006).

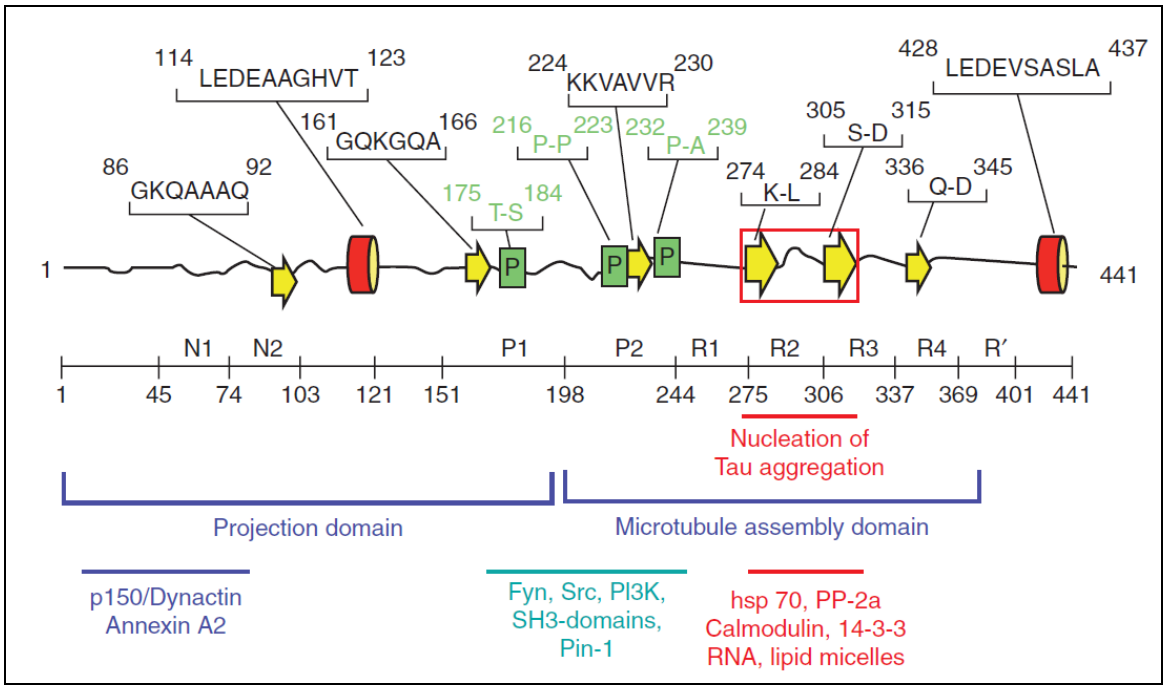

Figure 1.2 Domains of Tau protein
Representation of Tau structure deduced from NMR analysis. Most of the chain is unfolded (black lines), with a few short and transient elements of secondary structure (α-helix red, ß-strands yellow, poly proline helix green). The red box indicates the region of the two hexapeptide motifs responsible for Tau aggregation (von Bergen et al., 2000). The carboxy terminal half promotes microtubule assembly, and the amino-terminal half projects out from the microtubule surface. NI, N2 and R2 may be absent owing to alternative splicing. R1-R4 represents the repeat domain; together with the flanking domains, this represents the microtubule interaction domain. Bottom: Approximate location of interaction sites with other proteins. Figure adapted from (Mukrasch et al., 2009).

1.3.2 Functions of Tau protein

Tau protein was originally isolated as an interacting partner of microtubules (Cleveland et al., 1977b, Weingarten et al., 1974). Microtubules are assembled as polymers of α-ß-tubulin heterodimers. Microtubules have diverse tasks for example maintenance of the cytoskeleton architecture of a cell, separation of chromosomes during mitosis, or as tracks for intracellular transport by motor proteins. Tau promotes the assembly of microtubules and stabilizes them in neuronal axons; this interaction is based on the Tau repeat domain plus flanking regions (Mukrasch et al., 2005, Gustke et al., 1994).

The microtubule assembly mediated by Tau can be modulated by its posttranslational modifications especially phosphorylation (Brandt et al., 2005). Two different types of kinases can phosphorylate Tau protein. The proline directed kinases target the SP and TP amino acid motifs. Examples are GSK3ß, CDK5, and MAPK. Other kinases

target KXGS motifs in Tau repeat domain which control the interaction with microtubules. For instance, phosphorylation at S262 strongly reduces the interaction of Tau with microtubules (Biernat et al., 1993). Figure 1.3 shows the kinases and the phosphorylation sites of Tau.

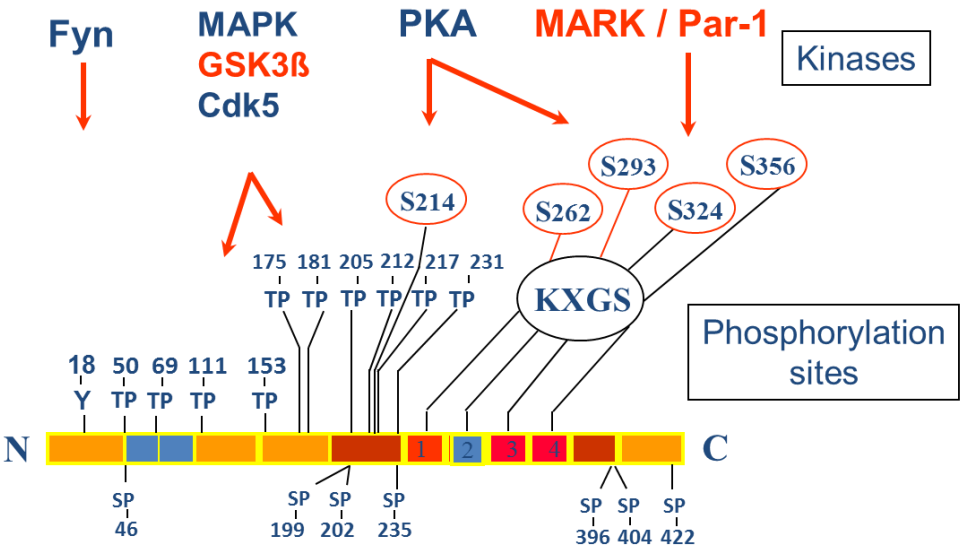

Figure 1.3 Kinases and Phosphorylation sites of Tau
This diagram shows the number of sites available for phosphorylation in Tau protein. The proline directed kinases are targeting the SP and TP amino acid sequences, whereas KXGS motifs are targeted by kinases like MARK. Figure adapted from (Schneider and Mandelkow, 2008).

Detachment of Tau from microtubules by phosphorylation facilitates the attachment of motor proteins to walk on the microtubule track for intracellular transport (Trinczek et al., 1999). In addition to microtubules, Tau has numerous binding partners including signaling molecules and cytoskeletal proteins. Tau protein interacts with spectrin and actin filaments (Yu and Rasenick, 2006, He et al., 2009) which allows the Tau stabilized microtubule to interconnect with neurofilaments. This restricts the flexibility of microtubules (Farias et al., 2002). Tau as a scaffold protein modulates the activity of Src tyrosine kinases, c-Src and Fyn, and thereby facilitates c-Src-mediated actin rearrangements (Figure 1.4) (Sharma et al., 2007). During the development of a neuron, Tau protein interacts with actin in a microtubule independent manner and promotes neurite outgrowth (Yu and Rasenick, 2006). In the nucleolar organizing region of the cell, Tau is thought to be involved in DNA repair and heat shock responses (Sultan et al., 2011). For reviews of Tau biology, see recent review by (Mandelkow and Mandelkow, 2012).

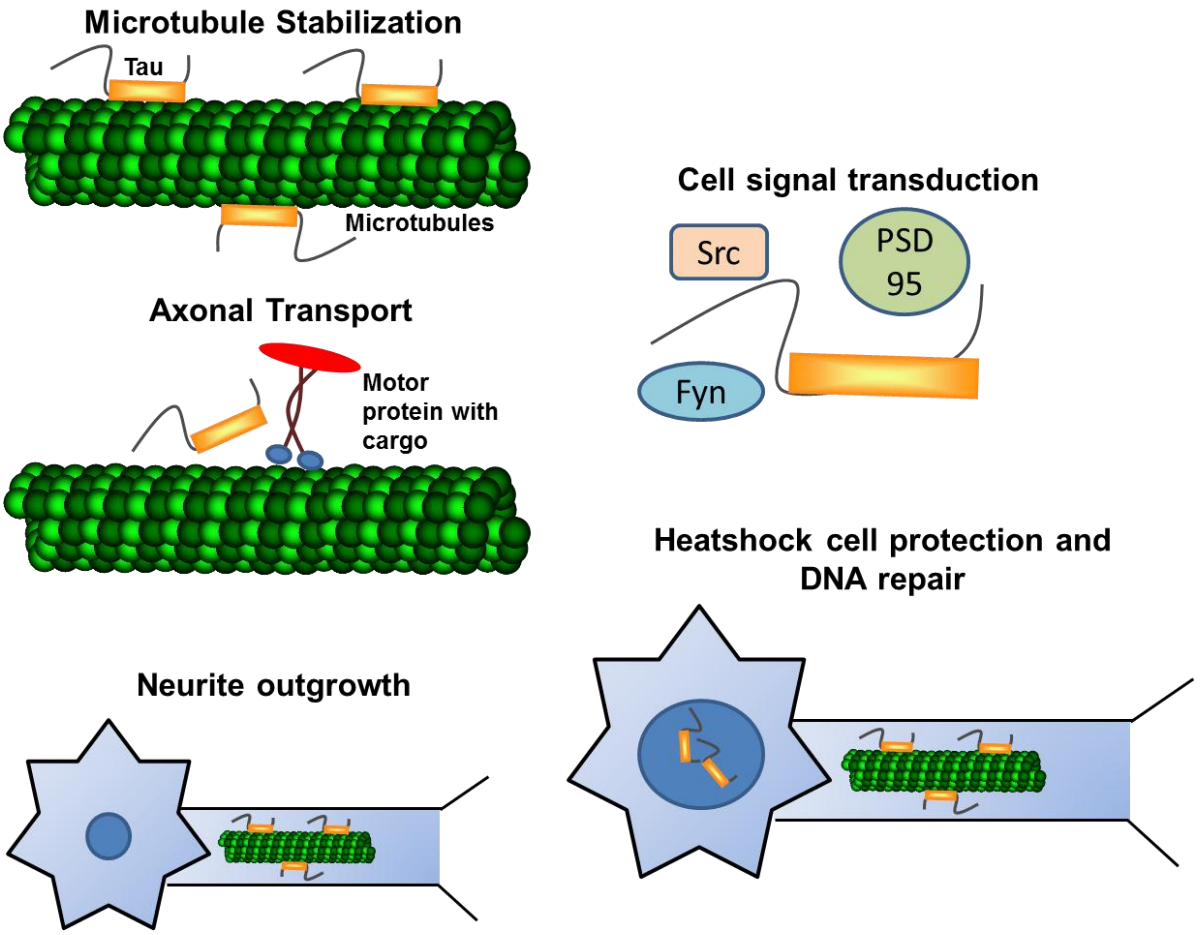

Figure 1.4 Tau as a multi-functional protein.
As a microtubule-associated protein, Tau contributes to microtubule dynamics and participates in neurite outgrowth and axonal transport. Moreover, Tau participates in cell signal transduction through the modulation of the activity of Src and Fyn kinases and PSD95 protein. In the nucleolar organizing region of the cell, Tau can also be involved in DNA repair and heat shock responses. Figure modified from (Mietelska-Porowska et al., 2014)

1.3.3 Changes of Tau in Alzheimer disease

In Alzheimer disease, Tau protein is thought to become detached from microtubules and loses its normal function of stabilizing microtubules. The free Tau molecules can become misfolded and interact with each other to form the filamentous structures ("paired helical filaments") in the degenerating neurons (Hyman et al., 2005, Ghoshal et al., 2002, Garcia-Sierra et al., 2003). There has been a debate whether Tau is obligatory for disease or just a byproduct of some disease process. In case of Alzheimer disease the debate is still ongoing, as Tau is thought to be the mediator of Aß induced toxicity (Haass and Selkoe, 2007). However, it is now clear that Tau protein alone is sufficient to cause neurodegeneration and dementia, because mutations only in the TAU gene can cause the neurodegeneration and dementia in Fronto Temporal Dementia with Parkinsonism linked to choromosome-17 (FTDP-17)

(Goedert and Spillantini, 2001). Tau mutations have been found in progressive supra nuclear palsy (PSP), Pick disease (PiD) and other tauopathies. Increased expression of Tau protein alone can be a risk factor, as demonstrated by individuals carrying the H1c haplotype (Myers et al., 2007). These findings illustrate the causative role of Tau protein in neurodegenerative diseases.

In Alzheimer disease and other Tauopathies, Tau protein undergoes several modifications including phosphorylation, acetylation, nitrosylation (Horiguchi et al., 2003), oxidation (Schweers et al., 1995), ubiquitination (Cripps et al., 2006), glycosylation, glycation (Kuhla et al., 2007, Yan et al., 1994, Nacharaju et al., 1997), and proteolytic processing (Wang et al., 2007). These posttranslational modifications can disrupt the normal functions of Tau and may contribute to the formation of aggregates (Mandelkow and Mandelkow, 2012). However, it is not clear which of these post translational modifications are specific and necessary to cause the disease phenotype because many post translation modifications are present even under physiological condition. Aggregation of Tau is the most common modification in many Tauopathies including Alzheimer disease.

1.3.4 Tau aggregation

Although Tau is a highly hydrophilic and unfolded protein, it aggregates into well-structured fibers in Alzheimer disease and other tauopathies. The mechanism of Tau aggregation is reasonably well understood from *in vitro* studies. Tau protein in solution is not able to aggregate because of its hydrophilic composition. *In vitro* aggregation is achieved by polyanionic cofactors like heparin or heparan sulfate which compensates the basic charge of the Tau (Goedert et al., 1996). Other polyanionic nucleation factors include nucleic acids (Kampers et al., 1996) , acidic lipid micelles, e.g. from arachidonic acid (Wilson and Binder, 1995) (Chirita et al., 2003), acidic peptides resembling the C-terminus of tubulin (Friedhoff et al., 1998a) and carboxylated microbeads (Chirita et al., 2005) .

Another important factor necessary for Tau aggregation is the ß propensity of hexapeptide motifs present in the beginning of repeat region R2 (VQIINK) and R3 (VQIVYK) (von Bergen et al., 2000). Mutations (ΔK280 and P301L) in Tau protein increase the ß-propensity and accelerate the aggregation (von Bergen et al., 2001) (Figure 1.5). Tau aggregates have been analyzed in detail by various biophysical and

microscopic techniques which confirm the presence of ß-sheet structure (Barghorn et al., 2004, von Bergen et al., 2005, Mukrasch et al., 2005, Mukrasch et al., 2009) and twisted helical structure respectively (Figure 1.6). The core region of PHF is the repeat domain of Tau. The N-terminal and C-terminal regions spread away from the core structure and represent the fuzzy coat of PHF (Crowther and Wischik, 1985). This coat is still highly mobile even in the aggregated state (Sillen et al., 2005). This fuzzy coat has the characteristics of a “soft polymer brush” extending from the PHF core and is able to interact with other cellular components (Wegmann et al., 2013, Wegmann et al., 2010).

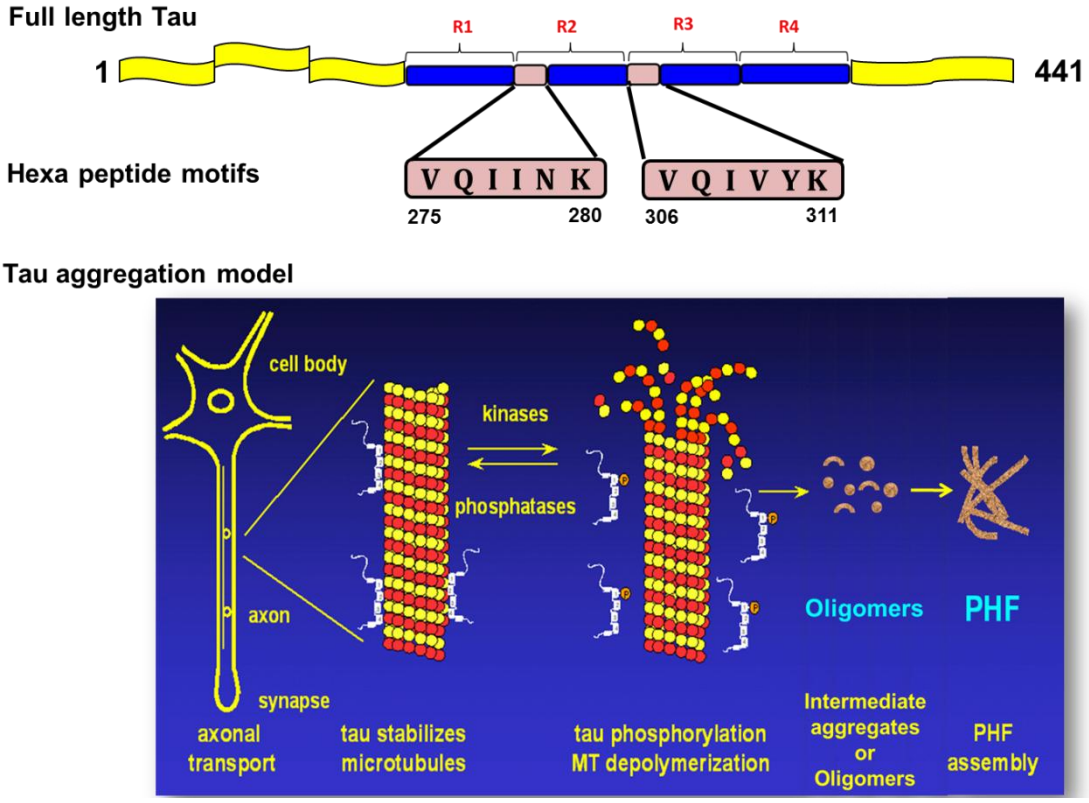

Figure 1.5 Hexapeptide motifs and Tau aggregation pathway
The longest isoform of Tau has 441 amino acids. Two hexapeptide motifs (275 VQIINK 280 and 306 VQIVYK 311) are present at the beginning of repeat region R2 and R3 which are necessary for the ß-sheet formation which is a core of the paired helical filaments. The bottom picture represents the formation of paired helical filaments. The post translation modifications detach the Tau molecules from microtubules and the free Tau molecule aggregates into oligomers and paired helical filaments. Figure adapted from (Schneider and Mandelkow, 2008).

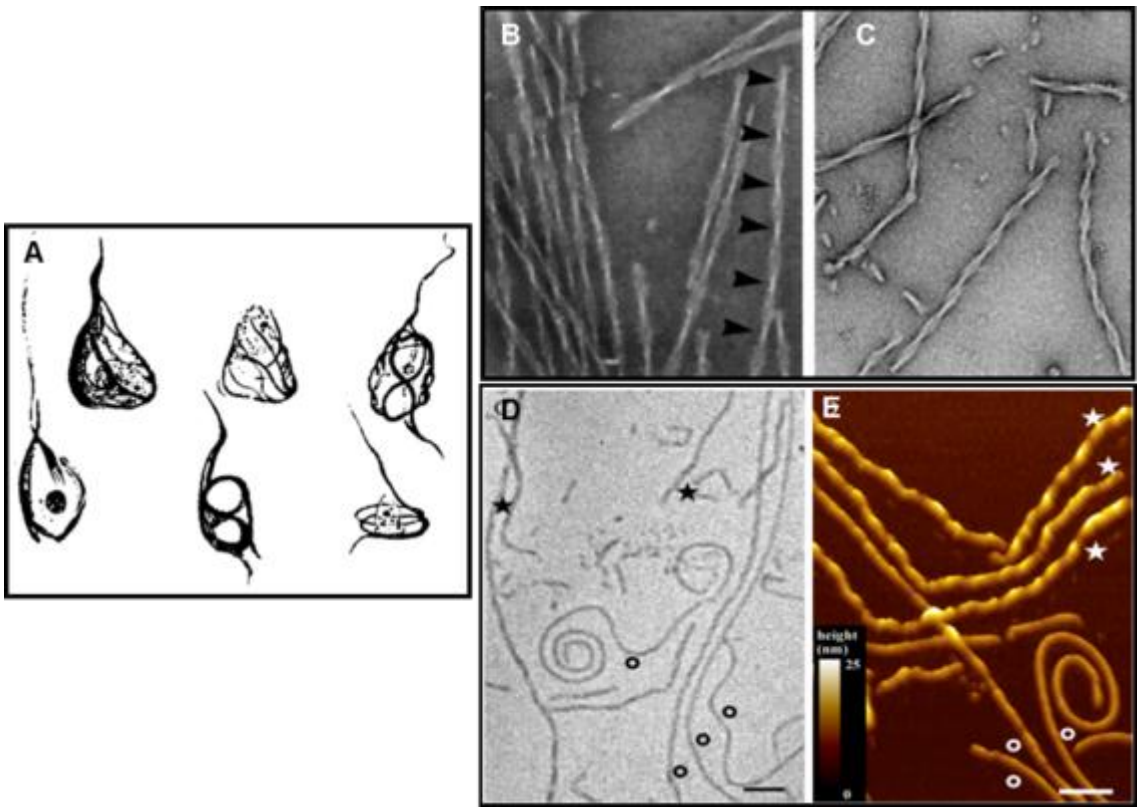

Figure 1.6 Paired helical filaments and NFTs
A) Neurofibrillary tangles formed in neurons of Auguste D, drawn by Alzheimer. Figure from (Maurer et al., 1997) **B)** Electron micrograph of twisted fibers appearing as "paired helical filaments" isolated from Alzheimer brain tissue, with ~80 nm periodicity (arrowheads). **C)** Fibers assembled in vitro from the proaggregant Tau repeat domain ($Tau^{RD\Delta}$). Note the similarity of the twisted structures, even though the repeat domain contains only ~27% of the full-length protein. Figures B and C from (Mandelkow and Mandelkow, 2012). **D)** EM images of in vitro hTau40 fibril preparations show a heterogeneous mixture of fibril shapes. **E)** AFM topographs of the same fibril preparation confirm the heterogeneity of fibril structures but reveal details with superior contrast. Figures D and E from (Wegmann et al., 2010).

1.3.4.1 Stages of Tau aggregation

An important question in the field of proteinopathies is the mechanism of aggregation of a protein. Tau aggregates like PHFs (fibers) and NFTs (assemblies of fibers) are formed by successive aggregation of monomers and/or smaller soluble oligomers (Cowan and Mudher, 2013). Partially folded Tau monomer favors the spontaneous formation of dimers (Chirita et al., 2005). Dimers are the important intermediate species which control the rate of aggregation (Schweers et al., 1995, Wille et al., 1992). Consistent with this, the *in vitro* generated Tau dimers form larger oligomers and aggregates (Sahara et al., 2007, Patterson et al., 2011). Apart from dimers, low-n oligomers such as trimers and tetramers are also involved in the formation of polymers or Tau filaments(Lasagna-Reeves et al., 2010).

Many sporadic Tauopathies have mutations in the MAPT gene. Several mouse models with mutations in the Tau gene have been created to understand the aggregation process in vivo. Expression of human Tau isoforms with or without mutations cause a neurodegenerative disease phenotype proving the role of Tau in memory impairment and neuronal loss (Ramalho et al., 2008, Yoshiyama et al., 2007, Santacruz et al., 2005, Mocanu et al., 2008, Sydow et al., 2011, Eckermann et al., 2007). Most of these mutations are in or near the repeat domain of Tau. These mutations tend to weaken the binding of Tau to microtubules and enhance the aggregation of Tau (Brunden et al., 2009, Combs and Gamblin, 2012). Mutations in the Tau genes are represented in Figure 1.7.The list of the mutations of Tau can be found in www.alzforum.org.

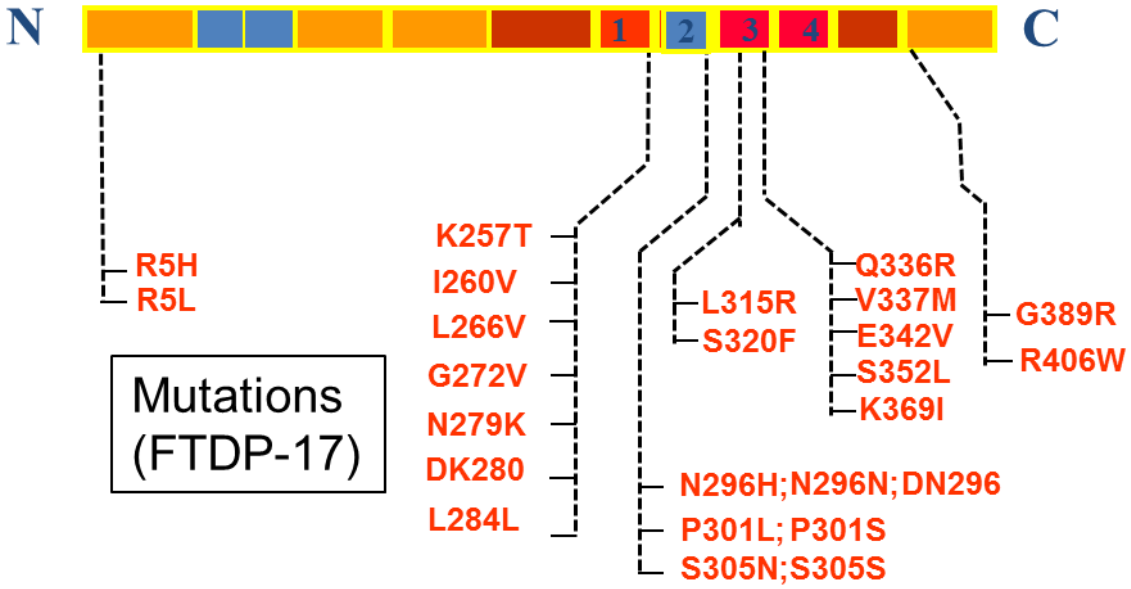

Figure 1.7 Mutations of tau gene
This diagram represents the sites of Tau which are mutated in frontotemporal dementia with parkinsonism. Exons 9,10,11,12 and 13 of repeat domain of Tau have many mutations. However, the N-terminal and proline rich regions also have some mutations. Figure adapted from (Schneider and Mandelkow, 2008).

1.3.5 Toxicity of Tau aggregates

A major concern in the field of tauopathies is the mechanism of toxicity of Tau. The supporting and opposing arguments for the toxicity of different forms of Tau summarized below.

1.3.5.1 Toxicity of NFTs

In Alzheimer disease and other Tauopathies, cognitive decline and neuronal loss are well correlated with the presence of NFTs (Tomlinson et al., 1970, Braak and Braak, 1991b, Arriagada et al., 1992, Dickson et al., 1995, Nagy et al., 1995). The formation of NFTs and the loss of neurons are observed in parallel in the same regions of the brains of AD mouse models. For example, expression of P301L mutant Tau in the mouse under the Thy 1.2 promoter causes neuronal apoptosis and formation of NFTs in the same location (Gotz et al., 2001). More direct evidence emerged from mouse and *C elegans* models expressing both pro-aggregant (promotes ß-structure formation) and anti-aggregant (does not form ß-structure) mutant forms of Tau. Expression of the pro-aggregant $Tau^{RD\Delta}$ mutant in the mouse brain evokes neuronal loss and NFT formation in the CA3 region of the hippocampus (Mocanu et al., 2008). When the expression of the pro-aggregant Tau ($Tau^{RD\Delta}$) is switched off in the mouse model, the toxic effects were reversible including memory decline (Sydow et al., 2011). By contrast expression of anti-aggregant Tau ($Tau^{RD\Delta\text{-}PP}$) does not cause memory decline in transgenic mice. Similarly, pro-aggregant $Tau^{RD\Delta}$ expression in worms also leads to aggregation and synapse loss, but treating the pro-aggregant worms with certain aggregation inhibitors rescues the toxic effects (Fatouros et al., 2012). In several *Drosophila* models of AD and Tauopathies, expression of human Tau leads to neurodegeneration without the formation of NFTs (Williams et al., 2000, Wittmann et al., 2001, Mudher et al., 2004). Similarly, mouse models expressing non mutant human Tau do form NFTs, but the cognitive deficits occur much earlier than NFT formation (Andorfer et al., 2005). In case of two inducible mouse models, expressing either full length Tau-ΔK280 mutation (Eckermann et al., 2007) or P301L (Spires et al., 2006), switching off the expression of mutant Tau after the NFT formation and cognitive decline rescues the memory, stabilizes the cell loss yet NFTs remain. These evidences suggest that NFTs or PHFs do not cause toxicity and imply that there are smaller species of Tau which might be necessary for Tau related toxicity..

1.3.5.2 Toxicity of insoluble Tau oligomers

As NFTs or PHFs may not be the toxic species, the focus shifted to the species preceding the filaments. Earlier it was shown that soluble Tau is not toxic in an inducible cell model. However, cells expressing pro-aggregant mutant Tau died even

before the NFT formation (Khlistunova et al., 2006) which suggest that there is an intermediate species of aggregation which could be toxic, such as higher-n oligomers (pre aggregated oligomers). Insoluble oligomers occur also in the synaptosome fractions of AD brain which impair the ubiquitin proteasome system (Tai et al., 2012). These findings suggest that insoluble oligomers are toxic.

1.3.6 Small soluble Tau oligomers

The terminology and definition for Tau oligomers is not yet well defined. Thus, molecules as small as dimers and up to prefibrillar forms of Tau are collectively called Tau oligomers. The *in vitro* prepared Tau oligomers are formed from non-phosphorylated Tau monomers. But in the case of AD, Tau oligomers mostly consist of hyperphosphorylated Tau. Methods like electron microscopy, atomic force microscopy and pelleting assays allow one to determine the different stages of Tau aggregation as follows.

- Low-n oligomers (<10 mers) are visible on SDS gels after pelleting, and can be seen in the AFM, but not by EM.These species are soluble.
- There are larger oligomers usually visible as blobs by EM. These are really polymers (hundreds of subunits), which one could consider as granular Tau oligomers.
- Insoluble Tau oligomers obtained by pelleting assay consist >70 subunits. By contrast, even fairly high-n oligomers (>10 but <70) are still “soluble” by pelleting criterion but can be distinguished from low-n oligomers by AFM.

1.3.6.1 Formation of Tau oligomers *in vitro*

Several groups studied Tau oligomerization *in vitro*. The 3R construct (K12) readily forms dimers in non-reducing conditions. Cross-linking of 3R tau protein with PDM and MBS yielded dimers and oligomers. The authors also showed that the dimers formed are in anti-parallel orientations (Wille et al., 1992). Oxidation of Cys 322 in 3R tau constructs (K12) lead to the formation of dimers, trimers and higher order oligomers. The C322A mutant of the Tau-K12 construct did not form filaments suggesting the importance of Cys 322 in aggregation (Schweers et al., 1995). Other authors showed that two distinct Tau dimers could be generated *in vitro* in the presence of heparin 6,000. These dimers are either Cysteine dependent or independent. Cysteine dependent dimers were observed before the increase in the

ThT fluorescence signal. Hence they suggest that intermolecular disulfide cross-linking mediated by the PHF6 hexapeptide facilitates the Tau oligomerization (Sahara et al., 2007).

The aggregation of Tau could be monitored in real time using the ThS or ThT dye which detects the ß-sheet structure in the aggregates (Friedhoff et al., 1998a). The ß-sheet content increases with aggregate size. The higher rate of ß-sheet structure occurs after the formation of oligomers comprised of 8-14 monomers as they act as nucleation seeds for PHFs (Friedhoff et al., 1998b). Full length Tau constructs with the deletion of the hexapeptide motif PHF6 (306-VQIVYK-311) sequence formed only dimers and trimers after prolonged incubation with heparin which shows that this sequence is important for the formation of oligomers and aggregates. This construct could also form some aggregates (without pronounced ß-sheet structure), but do not form filamentous structures when analyzed by AFM (Sahara et al., 2007). These results indicate that intermolecular disulfide crosslinking along with PHF6 hexapeptide facilitates tau oligomerization and aggregation.

Mutations in the Tau gene found in frontotemporal dementias are known to accelerate the neurodegeneration. An example is the deletion mutation of lysine 280 of Tau which promotes ß-sheet formation, rapid aggregation (von Bergen et al., 2000) and toxicity, presumably through oligomers (Khlistunova et al., 2006, Kumar et al., 2014, Mocanu et al., 2008, Sydow et al., 2011).

1.3.6.2 Toxicity of soluble Tau oligomers

Formerly it was thought that neuronal loss and cognitive impairment was caused by NFTs whose distribution was well correlated with disease progression (Arriagada et al., 1992, Braak and Braak, 1991b, Gomez-Isla et al., 1997), but more recent evidences shifted the emphasis to Tau oligomers. Neurodegeneration can occur even before the NFT formation, and in certain mouse lines expressing human Tau the NFTs do not correlate well with neuronal loss (Andorfer et al., 2003). Another mouse model expressing P301L Tau, showed synapse loss and microgliosis even before the NFT formation (Yoshiyama et al., 2007). An inducible mouse model expressing full length human Tau with the ΔK280 mutation (pro-aggregant), even at low expression level causes Tau hyperphosphorylation, missorting, microgliosis, astrocytosis, synapse loss, pathological conformation by MC1 antibody, but no tangle

formation or neuronal loss. Still this mouse shows strong cognitive decline. Switching off the expression of the human Tau recovered the synapse loss, LTP and memory (Van der Jeugd et al., 2012).

In order to validate the oligomer hypothesis, several groups have purified the full length tau oligomers *in vitro* and also from AD brains. The toxic effects of these Tau oligomers prepared by cross-seeding with Aß were analyzed in both cell and animal systems. *In vitro* prepared SDS stable dimers and trimers reduced the cell viability in SH-SY5Y cells up to 80%, neuronal loss in mouse hippocampus (Tau oligomers injected), whereas monomers and fibrils did not compromise the cell viability and neuronal loss (Lasagna-Reeves et al., 2010, Lasagna-Reeves et al., 2011).

Some laboratories generated antibodies against Tau oligomers to characterize oligomers and to use them for staging or treating AD. Using these antibodies (T22 and TOMA), Kayed and coworkers found that Tau oligomers are present in AD and other neurodegenerative diseases. These authors observed that there is a rapid accumulation of Tau oligomers in the rat model of traumatic brain injury (Hawkins et al., 2013) . Increased Tau oligomers were also observed in progressive supranuclear palsy patients(Gerson et al., 2014), consistent with patients carrying the Tau-A152T mutation, as risk factor for PSP (Coppola et al., 2012) . Other Tau oligomers specific antibody includes TOC1 antibody which recognize the pre-fibrillar Tau aggregates and used as a tool in assessing the disease progression (Patterson et al., 2011, Ward et al., 2013).

1.4 Inhibition of Tau aggregation

Given that the ability of Tau to aggregate is considered to be detrimental to neurons one may expect that Tau aggregation inhibitors could be protective. Therefore several groups searched for aggregation inhibitors (Bulic et al., 2009, Brunden et al., 2009, Schafer et al., 2013, Wischik et al., 2014, Wobst et al., 2015). Indeed beneficial effect could be shown in several cell and animal models. Members of different substance classes, such as antraquinones, N-phenyl amines, phenylthiazolhydrazides and rhodanines can inhibit Tau aggregation and also disassemble existing filaments (Pickhardt et al., 2005). For example bb14, a rhodanine based Tau aggregation inhibitor inhibits the aggregation of Tau in organotypic hippocampal slice culture expressing pro-aggregant $Tau^{RD\Delta}$. bb14

treated slices showed improvement in LTP and prevent the calcium dysregulation and synapse loss (Messing et al., 2013). Similarly, B4D3, D1C11 and B4A1 was shown to inhibit the aggregation of Tau and also to disassemble preformed aggregates (Khlistunova et al., 2006). Phenothiazines such as methylene blue inhibit Tau aggregation as well as oligomerization of Aß. Methylene blue is neuroprotective by inhibiting the aggregation of Tau (Hochgrafe et al., 2015, Schirmer et al., 2011, Lira-De Leon et al., 2013) and by inhibiting the reactive oxygen species production (Begum et al., 2008). Another compound (cmp-16) is shown to inhibit aggregation of Tau in C elegans models of Tauopathy (Fatouros et al., 2012). Although these compounds inhibit aggregation, it is not clear whether they also clear the Tau oligomers. Recently, it has been shown that curcumin is able to suppress soluble Tau dimers, there by rescuing the synaptic and behavioral deficits (Ma et al., 2013). Another compound, polyphenol epigallocatechin gallate (EGCG) efficiently inhibits the fibrillogenesis of both α-synuclein and amyloid ß. The mechanism is that EGCG directly binds to the natively unfolded polypeptides and prevents their conversion into toxic, on-pathway aggregation intermediates and reduces cellular toxicity (Bieschke et al., 2010) (Ehrnhoefer et al., 2008). EGCG coated nanoparticles are efficient in reducing the amyloid beta aggregation and the cell toxicity. (Zhang et al., 2014). Similarly, the Tau aggregation inhibitors might also induce the formation of off-pathway oligomers. These observations show that it is important to target Tau oligomers by different approaches in order to find a cure against the toxic species of Tau.

2 Aims of the study:

The aims of the project were to develop procedures for the purification of oligomers of $Tau^{RD\Delta}$ protein, characterize their biochemical and biophysical properties, and test their ability to induce toxicity in neurons.

The following problems were investigated in detail:

1. In vitro characterization of $Tau^{RD\Delta}$ protein aggregation to understand the stages of aggregation
2. Stabilization oligomers of $Tau^{RD\Delta}$ by different methods and characterization of the oligomers formed
3. Development of methods to prepare and purify oligomers of $Tau^{RD\Delta}$in vitro
4. Biophysical and biochemical characterization of in vitro purified oligomers of $Tau^{RD\Delta}$
5. Structural characterization of $Tau^{RD\Delta}$ oligomers using microscopy and dynamic light scattering methods
6. Functional characterization of $Tau^{RD\Delta}$ oligomers in cell culture models using different types of assays
7. Functional characterization of $Tau^{RD\Delta}$ oligomers in tissue culture models.

3 Materials and Methods

3.1 Materials (Instruments and equipment)

3.1.1 Centrifuges

Name	Company
Eppendorf centrifuge 5415C	Eppendorf, Hamburg
Eppendorf centrifuge 5810R	Eppendorf, Hamburg
Eppendorf centrifuge 5810	Eppendorf, Hamburg
Optima^{TM} LE-80K Ultracentrifuge	Beckman Coulter, München
Avanti^{R}Centrifuge J-26 XP	Beckman Coulter, München
Optima^{TM} Max Ultracentrifuge	Beckman Coulter, München

3.1.2 HPLC

Name	Company
Äkta micro system	GE Healthcare Life Sciences, Freiburg
Äkta explorer100	GE Healthcare Life Sciences, Freiburg

3.1.3 Columns

Name	Company
Superose PC12 (3.2mm x 300mm)	Amersham Biosciences, Freiburg
Superdex G200 HR 16/60	Amersham Biosciences, Freiburg
Superdex G75 HR 16/60	Amersham Biosciences, Freiburg
Superdex peptide	Amersham Biosciences, Freiburg
SP Sepharose 16/10	Amersham Biosciences, Freiburg
HiTrap HIC Selection Kit	GE Healthcare Life Sciences, Freiburg
HiPrep Butyl FF 16/10	GE Healthcare Life Sciences, Freiburg
PD 10 column	GE Healthcare Life Sciences, Freiburg
NAP5 column	Pharmacia Biotech
HiTrap NHS-activated HP 1ml	GE Healthcare Life Sciences, Freiburg

3.1.4 Spectrophotometers

Name	Company
Ultrospec 3100 *pro*	Amersham Biosciences, Freiburg
Tecan Spectrophotometer	Lab System, Frankfurt
Spex Fluoromax spectrophotometer	Polytec, Waldbronn

Dynamic Light Scattering Nano S	MALVERN, Germany
Jasco J-810 CD spectrometer	Jasco, Gross-Umstadt

3.1.5 Microscopes

Name	Company
Electron Microscope	JEOL
Atomic Force Microscope (Dimension model 3100)	Veeco
Olympus CK2 microscope	Olympus, Japan
LSM 700 Confocal Microscope	Zeiss
Cell observer	Zeiss
Lambda 10-2 (Shutter for calcium imaging)	Visitron Systems
Dissection microscope	Olympus SZX9

3.1.6 Cell culture equipment

Name	Company
HERA Safe Laminar air flow	Heraeus Instruments, Germany
HER Cell 240 CO_2Incubator	Heraeus Instruments, Germany
Preparation laminar air flow	Thermo Scientific
Tissue Chopper	Mickle Laboratory Engineering co.ltd
Light source KL 1500 LED	Schott
Neubauer chamber	MARIENFELD, Germany
HERA Safe Laminar air flow	Heraeus Instruments, Germany
HER Cell 240 CO_2Incubator	Heraeus Instruments, Germany

3.1.7 Others

Name	Company
French Press	G-Heinemann Ultraschall und labrotechnik
Ice flaking machine (SPR 80)	Nord Cap
Water filtration apparatus	Millipore
Deep freezer (-80°C)	SANYO
Image Quant LAS 4000 mini	GE Healthcare Life Sciences, Freiburg

Blotting Apparatus	BIO-RAD trans-blot SD transfer cell
Gel apparatus for SDS-PAGE	SE 250, Hoefer
Electrophoresis power supply	Pharmacia Biotech
Micropipettes (2, 10, 20, 100, 200 and 1000µl)	GILSON
Weighing balance BP 310S	Sartorius
Incubators	Memmert
Incubator with shaker	INFORS HT Multitron
Heating-agitator	Eppendorf
Incubator with rotator	Shake and Stack, HYBAID
Laminar flow for bacterial inoculation	LaminAir HB 2448, Heraeus Instruments
pH-Meter	Schott Instruments
Water bath	GFL AND JULABO UC
Vortexer	JANKE & KUNKEL. IKA-WERK
Pasteur pipette	Assistant
well plates (6,12,24,48, and 96)	Corning
SNL 10 cantilever	Bruker, München
Glass wares	VWR international
PVDF membrane (0.45µm pore siz**e)**,	Millipore transfer membrane
Quartz microcuvettes	Hellma, Muhlheim, Germany
Magnetic steel disks (diameter 12mm)	Ted Pella, Inc., Redding, CA, USA
Teflon sheets (0.2 mm thickness)	Maag Technic AG, Birsfelden, Switzerland
Mica sheets	Muscovite, Kolkatta, India
Cantilever (Si_3N_4)	Di-Veeco, Santa Barbara, California, USA

3.1.8 Chemicals

Chemicals of highest quality were purchased from the following suppliers:
Sigma, Merck, Gerbu, Amersham Pharmacia Biotech, AppliChem, Molecular Probes, Fluka, Serva

3.2 Methods

Note: The buffer compositions are listed in the appendix section.

3.2.1 Protein preparation and purification

100 ml of LB broth was prepared and autoclaved. The antibiotic carbenecillin (50µg/ml) was added to the broth. The glycerol stock of $Tau^{RD\Delta}$ BL21 (DE3) was inoculated by taking a pinch at the end of pipette tip. This pre-culture was grown at 37°C at 180rpm in a shaker incubator overnight. 2 liters of “terrific broth” was prepared and autoclaved. The antibiotic ampicillin (100mg/l) was added to the terrific broth. 100ml of pre-culture was inoculated to the fresh 2 liters of terrific broth. Before inoculating, 2ml of terrific broth was used for optical density (OD) measurement as 0 time point control. The inoculated culture was grown at 37°C with 180rpm rotation until the OD reached a minimum of 0.8 (approximately 4 h) as determined photometrically at 600 nm (Ultrospec 3100 pro, Amersham Biosciences, Freiburg) at 600nm. The sample was induced by IPTG to a final concentration of 0.4mM for 3 h. The culture was pelleted by centrifuging at 7000 rpm for 12 min (JLA-8.1000 rotor, AvantiRCentrifuge J-26 XP, Beckman Coulter, München). The pellet was collected in 90 ml of resuspension buffer and mixed at 4°C by magnetic stirring. (The cells can be frozen at this stage for later usage. The cells should be defrosted slowly in water).

The resuspended pellet was homogenized using a French press. This homogenization was repeated once more to completely break down the cell wall, DNA and other cell components. The homogenized cells were collected in 50ml Falcon tubes. NaCl and DTT were added at a final concentration of 500mM and 5mM respectively. This sample was mixed well and boiled at 97°C for 20 min. The temperature was maintained carefully throughout the boiling step. (Note: The lid of the Falcon tube should be opened slowly during boiling and then closed again). The solution was mixed well, then ultracentrifuged (Ti 45 rotor) at 40,000 rpm, for 1 h at 4°C (OptimaTM LE-80K Ultracentrifuge, Beckman Coulter, München). The supernatant was collected and dialyzed with a 45kDa MWCO membrane. The supernatant was dialyzed twice in Mono S A buffer with a single exchange of buffer at 4°C. One round of dialysis was done overnight. (Note: The volume of dialysis buffer should be at least 10 times higher than the sample volume). The dialyzed supernatant was centrifuged (Ti 45 rotor) at 40,000 rpm, for 1 h at 4°C. The supernatant was removed and added to the 150ml super loop for purification. (Note:

Air bubbles must be avoided when filling in the super loop). The protein was purified by anion exchange chromatography using the Äkta Explorer100 (GE Healthcare Life Sciences, Freiburg) system fitted with a SP Sepharose 16/10 column (Amersham Biosciences, Freiburg). The column was equilibrated with 5 column volumes (CV) of Mono S A buffer. Once the sample was injected, the purified protein was eluted with Mono S A and Mono S B buffer in a gradient segment (Mono S B 60% gradient for 5CV and 100% gradient for 1CV). The column was cleaned with Mono S B buffer for 4CV. The purified protein was eluted in 2ml fraction volume. The fractions were run on a 17% SDS gel and stained with Coomassie Blue. The protein containing fractions were pooled and concentrated using 3000 MWCO centrifugal filters (Amicon Ultra, Millipore, Ireland). Then the protein was further purified by gel filtration chromatography using a Superdex G75 column in the Äkta Explorer 100. PBS pH 7.4 with 1mM DTT was used as a mobile phase. The eluted protein was concentrated using 3kDa MWCO amicon filters and then the protein concentration was measured using the BCA method.

3.2.2 Determination of protein concentration (BCA assay)

The BCA method (BCA protein assay reagent, Sigma) was used to determine the concentrations of proteins. A standard curve was prepared using BSA at different concentrations (40 -200µg/ml). The protein sample and standard sample were diluted in 50µl of H2O and mixed with 1 ml of reagent mixture consisting of 1 ml copper (II) sulfate (Sigma) 4% (w/v) and 50 ml biocinchoninic acid solution (Sigma). The mixture was incubated at 60°C for 30 min, and the absorption was measured at 562 nm in a spectrophotometer (Ultrospec 3100 Pro Pharmachia Biotech). For the blank reference, H2O was used instead of the protein solution..

3.2.3 Aggregation of $Tau^{RD\Delta}$

3.2.3.1 Polymerization (into filaments) of $Tau^{RD\Delta}$

For preparation of fibrils, $Tau^{RD\Delta}$ monomer was diluted to 50 µM in PBS pH 7.4 or in TBS pH 9.0 supplemented with 1mM DTT and heated at 95°C for 15 min in order to disrupt disulfide cross-links. Then the sample was brought to room temperature. This monomer solution was incubated at 37°C for different time intervals (0, 0.5, 1, 2, 4, 8, 24, 48 and 72 h) for the aggregation kinetics assay. For EGCG experiments, EGCG was added prior to the incubation. The formation of aggregates was monitored by

ThS fluorescence and the morphology of filaments was analyzed by electron microscopy.

3.2.3.2 Oligomerization of Tau$^{RD\Delta}$

50µM Tau$^{RD\Delta}$ monomer was incubated in either PBS pH 7.4 or in TBS pH 9.0 for 30 min at 37°C without DTT. (Since DTT breaks disulfide cross-links, we omitted it in order to avoid disassembly of formed oligomers). The aggregated samples (oligomers) were cross-linked using 0.01% glutaraldehyde (EM grade) for 10 min at 37°C. The reaction was stopped by final addition of 10mM Tris-Cl, pH 8.8.

3.2.3.3 Sedimentation assay

The aggregated samples of Tau$^{RD\Delta}$ (72 h of incubation; concentration 50µM in phosphate buffer pH 7.4 in the presence or absence of EGCG) were centrifuged at 61000 rpm (TLA 100.3) for 1 h at 4°C to generate a pellet fraction of aggregated Tau protein. After centrifugation, the supernatant and pellet was separated. The pellet was resuspended in the same volume as the supernatant. The SDS sample buffer was added to pellets and supernatants, followed by heating at 95°C for 10 min. The samples were run on a 17% SDS-PAGE gel and the amount of Tau protein in the supernatants and pellets were quantified by densitometry of the Coomassie Brilliant Blue R-250 stained gels using Image J analysis software (Schneider et al., 2012).

3.2.3.4 SDS gel analysis

The samples (fractions from HPLC, pelleting assay, cell lysates, brain homogenates) were mixed with 1X sample buffer and heated at 95°C for 15 min. Then samples were run on 17% SDS gel at constant 120V for 2 h at room temperature. For the primary neuronal cell lysates, the samples were run on 10% SDS gel at 120V for 1.5 h at room temperature. The gels were stained with Coomassie and silver in case of in vitro samples. The brain homogenate samples were run and transferred to a PVDF membrane for western blot analysis.

3.2.3.5 Coomassie staining

An SDS gel was transferred to the Coomassie stain solution for 30 min to 1 h. The gel was then transferred to the destaining solution (intensive) for another one h. If normal destaining solution was used then the gel was left overnight. All these steps

were done at room temperature on a shaker. Afterwards the gel was scanned and used for analysis.

3.2.3.6 Silver staining

The SDS gel was transferred to fixative solution and incubated for 15 min then transferred to cross-linking solution and incubated for 30 min up to overnight. The gels were washed with doubly distilled water three times for 10 min each. Then the gels were incubated with silver nitrate staining solution for 20 min. Then the gels were briefly washed with doubly distilled water for 30 seconds. The developing solution was added to the gels after discarding the water. After the detection the stopping reagent was added immediately to avoid further development. All these steps were done on the shaker at room temperature.

3.2.3.7 Western blotting

The SDS gels were incubated in 50ml of 1X transfer buffer for 15-20 min at RT. Then 3 pieces of wet Whatman filter papers were placed in the transfer apparatus plus a single PVDF membrane. The PVDF membrane was activated by soaking it in methanol for 1 minute and then washing in transfer buffer thoroughly. The gel was placed on the PVDF membrane. Another 3 pieces of Whatman filter paper were placed on the gel. The transfer was started at 100mA (for a gel area of 67.5 cm^2 i.e. 1.5 mA per cm^2) for 2 h (depending on the molecular weight of the protein to be analyzed). The transfer was checked by prestained markers on the blot. The blot was incubated with 5% fat dry milk powder in TBST for 1 h at RT on a shaker and incubated with primary antibody overnight at 4°C. Unbound antibodies were washed with 1X TBST, 3 times, 10 min each. The secondary antibody was added to the blot and incubated at 37°C for 1 h and then the unbound antibodies were washed away using 1X TBST (3 times, 10 min each). Finally, the membrane was developed using the ECL reagent kit and the images were acquired using LAS ImageQuant application software developed by GE Healthcare.

3.2.4 Separation of oligomers of $Tau^{RD\Delta}$

3.2.4.1 Size exclusion chromatography (Superose PC12 column)

Size-exclusion chromatography (SEC) is a chromatographic method in which molecules in solution are separated by their size, and molecular weight. The columns

have a matrix with a particular pore size. The molecules run on SEC column will travel through the whole matrix. The larger molecule will not travel through all the pores thereby elute earlier whereas the smaller molecule will pass through all the pores and elutes later.

A sample of $Tau^{RD\Delta}$ oligomers formed in PBS buffer, pH 7.4 was used to standardize the separation of oligomers from the monomers. An analytical Superose PC 12 column was used. The column was pre equilibrated with elution buffer (PBS pH 7.4) for 10X column volume (CV) and calibrated with the standard proteins. Approximately 50-100µl sample of oligomers containing solution of $Tau^{RD\Delta}$ was injected in to the ÄKTA micro system fitted with the Superose PC 12 column. If stable oligomers are present, they will elute earlier than the monomer in the chromatogram. The system was run at 40 -100µl/min flow rate and the elution was monitored at 214, 252 and 280nm. The fractions were collected in 96 well plates. The column was washed with distilled water for 5 CV and re equilibrated with 5 CV of elution buffer. The protein fractions were run on 17% SDS gel to analyze the quality of separation.

3.2.4.2 Large scale preparation using a Superdex G-200 column

The column was pre equilibrated with elution buffer (2x column volume (CV)) and calibrated with the standard proteins. For separation of $Tau^{RD\Delta}$ oligomers an ÄKTA explorer 100 system was used. 2 ml of a solution containing oligomers of $Tau^{RD\Delta}$ was injected into Superdex G-200 column and run at 0.5-1ml /min flow rate. The elution was monitored at 214, 252 and 280nm. The fractions were collected in 2ml volumes. The column was washed with the distilled water (2x CV) and re equilibrated with 2x CV of elution buffer. The protein fractions were run on 17% SDS gels to analyze the quality of separation.

3.2.4.3 Hydrophobic interaction chromatography (HIC)

The cross-linked $Tau^{RD\Delta}$ oligomers were separated on a HIC column. For standardizing the purification method, the HIC selection kit from GE Healthcare was used. 1M ammonium sulphate was used as adsorption buffer. The elution buffers were TBS pH 9.0 or PBS pH 7.4 and doubly distilled water. All HiTrap 1ml HIC columns were equilibrated with adsorption buffer (10x column volume) before injecting the sample (300µl – 900µl). The hydrophilic proteins do not bind to the column (unbound protein) and were collected as flow-through. The bound

hydrophobic proteins were eluted in an TBS pH 9.0 and water. The eluted fractions were run on 17% SDS gel and the separation was checked by staining the gels with silver.

A Butyl FF column 16/10 was used for further large scale purification. The column was pre equilibrated with adsorption buffer (3-5x CV) and then the samples (1.8ml) were injected into the column. Unbound proteins were collected as flow-through. The bound proteins were eluted as fractions of 2-3ml with a gradient of doubly distilled water with TBS pH 9.0. The fractions were run on the SDS gels and then the quality was confirmed by silver staining.

The fractions containing pure oligomers were pooled together and concentrated using 3kDa MWCO Amicon filters at 4000 rpm for 1.5 – 2 h at 4°C. These concentrated oligomers were transferred to PBS pH 7.4 buffer using PD 10 buffer exchange column. The PD 10 column was equilibrated with 5ml elution buffer (PBS pH 7.4). This equilibration step was repeated 4 times. Then 2.5 ml of pooled protein fractions were loaded on top of the bed. If the initial volume of the sample was smaller it was topped up with PBS to 2.5ml. The flow-through was collected for further analysis. Then the protein was eluted in 3.5ml of PBS. The column was never allowed to dry during the procedure. Protein estimation was done by BCA method.

3.2.5 Biophysical methods

3.2.5.1 Thioflavin S (ThS) assay

The formation of filamentous polymers of $Tau^{RD\Delta}$ was monitored by the ThS fluorescence assay (Friedhoff et al., 1998b). The binding and subsequent increase in ThS fluorescence is specific for the cross ß-structure that is typical of amyloid fibers.

5 µM final concentration of the PHF reaction mixture was mixed with PBS pH 7.4 or ammonium acetate buffer, pH 7.0 containing 20 µM ThS and transferred into a 384-well plate (black microtiter 384 plate round well, ThermoLabsystems, Dreieich). The measurements were carried out at 25˚C in a TECAN spectrofluorimeter (Ascent, Lab systems, Frankfurt) using an excitation wavelength of 440 nm, an emission wavelength of 521 nm and spectral bandwidths of 2.5 and 2.5 nm for emission and excitation respectively. Background fluorescence from ThS alone was subtracted when needed and the measurements were carried out in triplicates always.

3.2.5.2 ANS fluorescence measurement

The formation of polymers of $Tau^{RD\Delta}$ was also monitored by ANS fluorescence which increases when the dye binds to solvent exposed hydrophobic patches and positively charged amino acids (Slavik, 1982). 5µM final concentration of PHF reaction mixture was mixed with 45 µl of 50 mM ammonium acetate pH 7.0 containing 20µM ANS and transferred into a 384-well plate (black micro titer 384 plate round well, ThermoLabsystems, Dreieich). The measurements were carried out at 25˚C in a TECAN spectrofluorimeter (Ascent, Lab Systems, Frankfurt) using an excitation wavelength of 390 nm, an emission wavelength of 475 nm and spectral bandwidths of 2.5 and 2.5 nm for emission and excitation respectively.

3.2.5.3 Circular Dichroism

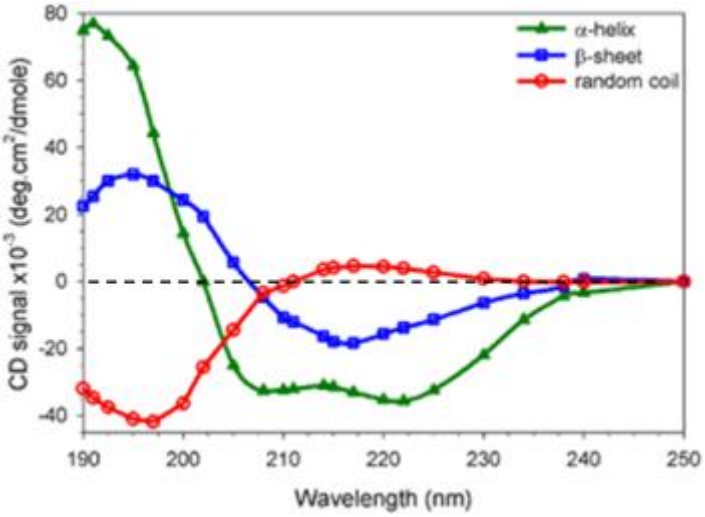

Figure 3.1 CD spectra of reference structure.
Representative CD spectra of proteins are shown. A protein with α-helix structure has a two spectral peak minima at 208 and 222nm.A protein with ß-sheet structure has a single spectral minimum at 215nm and a random coiled protein has a spectral minimum at 198nm. Picture reproduced from http://www.fbs.leeds.ac.uk/facilities/cd/images/1.png

The circular dichroism spectroscopy method measures the differences between the absorption of left handed circularly polarized and right handed polarized light. A typical CD curve contains both negative and positive values depending on the wavelength. The far UV spectral range (190- 250 nm) is used to study the secondary structure of the protein. Structures such as α-helix, ß-sheet, and random coiled give rise to characteristic shapes and amplitudes of the CD spectrum (Figure 3.1). All CD measurements were carried out with a Jasco J-810 CD spectrometer (Jasco, Gross-Umstadt, Germany) in a cuvette with a path length of 0.1 cm. The parameters were:

scanning speed – 100 nm/min; bandwidth - 0.1 nm; response time - 4 s; measurement temperature, 20°C.

3.2.5.4 Light Scattering (90°)

The basic principle of light scattering is that the size of a molecule (with certain approximations) is directly proportional to the amount of scattered light. Hence this method is used to monitor the aggregation of $Tau^{RD\Delta}$. Measurements were performed with a Spex Fluromax spectrophotometer (Polytec, Waldbronn, Germany), using 3x3 mm quartz microcuvettes (Hellma, Muhlheim, Germany) with 20µl of sample volume at concentration of 50µM. Experimental parameters were excitation and emission wavelength at 350 nm (90° scattering); scan range 320-400 nm: excitation slit width - 5 nm; emission slit width - 5 nm; integration time - 1 s; photomultiplier - 950 V. Each time two spectra were scanned and averaged. The scattering of the buffer was always subtracted.

3.2.5.5 Dynamic (quasielastic) Light Scattering

The principle of dynamic light scattering (or quasielastic light scattering) is based on fluctuations of the scattering particles caused by Brownian motion, which in turn depends on particle size and shape. The method allows one to analyze contributions from different types of particles (e.g. monomers and oligomers) provided that the size differences are sufficiently large (about 5-fold or more). Measurements of FPLC fractions were performed with a Zetasizer Nano ZS (Malvern, Herrenberg, Germany) containing a 5-milliwatt Helium-neon 633-nm laser at 173° measurement angle. The system was calibrated with latex beads of 30 and 150nm. The samples were diluted to 10µM in water. 20µl of sample in a low-volume quartz batch cuvette (ZEN2112) was used and the samples were thermally equilibrated at 25 °C for 2 min. Particle size was obtained as an average of three measurements with 20 runs each and expressed as intensity or volume distribution.

3.2.6 Imaging methods:

3.2.6.1 Transmission electron microscopy

Electron microscopy is an imaging technique in which a beam of electrons passes through a specimen and scattered electrons form a magnified high resolution image on a photographic film or on a CCD camera. To enhance the structural details of a

sample, staining with heavy metals such as osmium, lead or uranium can be used because the heavy atoms, having dense nuclei, scatter the electrons out of the optical path and hence areas where electrons are scattered appear dark on the screen or on a positive image.

The protein samples were diluted to 16.6 µM and placed on 200 mesh carbon coated copper grids which were glow discharged to generate a hydrophilic surface. The samples were incubated on grids for 3 min, washed thrice with H_2O and negatively stained with 2 % filtered uranyl acetate for 45-90 seconds (depending on the sample) followed by a final wash with H_2O. The specimens were examined with a JEOL electron microscope at 200 kV at the Electron Imaging facility of CAESAR. Images of aggregated samples were captured with a CCD camera using EMMENU 4 software.

3.2.6.2 Atomic force microscopy

Atomic force microscopy (AFM) is a technique to obtain images at a high (nanometer) resolution by scanning the sample surface with a very sharp (end radius ca. 10 nm) probe (cantilever) and recording the deflection of a cantilever. When the probe is brought close to the sample surface, forces between the probe and sample leads to the deflection which is received in the photodiode and is proportional to the height of the particle.

AFM sample preparation: Magnetic steel disks 12mm diameter were used as a base. 10-15 mm diameter disc shaped Teflon sheets were glued using Loctite 406 on magnetic steel disks. 10mm diameter disc shaped mica sheets (AFM grade - thickness 0.5mm) were glued on the Teflon sheets using the two component epoxy glue Araldite-Rapid after cleaving the bottom layer of the mica sheets and allowing it to dry overnight at room temperature. The fluid cell was washed thoroughly and attached to the AFM head before the sample preparation. 1-2µM of protein sample in adsorption buffer (oligomer, monomer, and/or fibril) was placed on the freshly cleaved mica sheets and allowed to adhere to the surface for 10-20 min at room temperature. The non-adherent proteins were removed by washing with imaging buffer carefully 4-5 times by pipetting.

AFM Imaging: AFM imaging was done in oscillation mode for all Tau samples. The cantilever was inserted in the cantilever holder attached with fluid cell. This assembled setup was attached to the AFM head. The laser was aligned on the end

of the tip and the set up was thermally equilibrated for 10-20 min at room temperature. The initial approach of the cantilever to the surface was performed in the constant force mode with the relative set point of 1V and the scan size was at 0nm. The cantilever was retracted to 50µm from the surface. The oscillation of frequency and drive amplitude for oscillation mode imaging was chosen using the in-built auto-tuning procedure (using an SNL 10 cantilever). Frequency sweep was performed to find the first resonance peak of the cantilever. In air the first resonance peak appeared around 60 kHz. The sweeping was done on the liquid and the first resonance peak in the liquid was between 5-6 kHz. A 5% offset of oscillation amplitude was applied to the operating frequency of the cantilever and the target amplitude was set at 1V. The parameters such as x, y offset were kept at 0 nm and the z offset was kept at maximum. The surface was approached in oscillation mode with an amplitude set point of 50-60% of the target amplitude. Once the surface was reached, the minimal contact between the sample and cantilever was maintained by altering the amplitude set point manually. The images were acquired at a scan rate of 1Hz with the resolution of 512 by 512 pixels. The scan size for the overview images were scanned for either 10µm or 5µm. For oligomers, 1µm scan size images were acquired. During the scanning the gains and amplitude set points were altered manually often to keep a minimal force between the cantilever and the sample. The images were acquired using the Nanoscope III microscope facility at CAESAR. The acquired images were processed by the Nanoscope III software.

3.2.7 Cell culture

3.2.7.1 SH-SY5Y cells maintenance

The SH-SY5Y cells were grown in DMEM medium supplemented with 15% FCS and 1X penicillin and streptomycin antibiotics (Complete medium). The cells were generally cultured up to 70-80% confluence at 37°C with 5% CO_2 in a CO_2 incubator. The cells were subcultured by the trypsin digestion method as follows. Cells were washed with tissue culture grade PBS. 1ml of trypsin EDTA solution was added to the SH-SY5Y cells (T25 flasks) and incubated at 37°C in the CO_2 incubator for 2-3 min. 4ml of the complete medium was added to the cells to prevent the excessive digestion by trypsin. The cells were centrifuged at 1250rpm for 1-2 min to pellet down the cells and sub cultured (1:5 – 1:10 ratio) in 5ml of complete medium.

3.2.7.2 Freezing of SH-SY5Y cells

The freezing media (50% FCS+30% DMEM+20% DMSO) was prepared and filter sterilized using syringe filters. The cells grown in T-75 flasks were trypsinized for 2-3 min. 4ml of the complete medium was added to the cells to prevent the excessive digestion. The cells were centrifuged at 1250rpm for 5 min at RT. The medium was removed and the cells were resuspended in 2-3 ml of freezing medium. The number of cells was counted in a Neubauer chamber. $1x10^6$ cells/cryo vial was prepared and stored in an isopropanol container for 24 h at -80°C and then transferred to the liquid nitrogen tank for longer storage.

3.2.7.3 Preparation of primary neuronal cells

Before the preparation, all surgical instruments were sterilized in 70% ethanol followed by heat sterilization. A pregnant rat at E18 days was anesthetized using 3-4 ml of dichloromethane and sacrificed by cervical dislocation method. The uterus with the embryo was removed by making an incision on the stomach. Embryos were collected by removing the embryonic sac. The heads were removed and placed it on ice cold HBSS. By holding the eyes of the embryo using a forceps, an insertion was made in the middle of the brain (forebrain - midbrain junction). Using a sharp forceps the skull was removed without damaging the brain. The tissues covering the hippocampus were removed by micro scissors. The meninges (a layer which covers the brain) were removed out and then the cortex and hippocampus were dissected out. The tissues were minced into small pieces and collected in 15ml conical tube to settle down. The supernatant was discarded and 5ml of trypsin was added to the cortex tissue (1-2ml of trypsin for hippocampal tissue). The tissues were incubated in a water bath at 37°C for 8 min and then twice the volume of plating medium was added. The tissues were allowed to settle down and the supernatant was removed. For a pair of hippocampi, 0.5ml of HBSS was added and the cells were dissociated by pipetting. For cortical cells, 50 ml of HBSS were directly added after dissociation in 2-3 ml of HBSS buffer. 10µl of dissociated cells were mixed with 10µl of 0.4% trypan blue for 5 min at room temperature and then the cell number was counted using a Neubauer chamber. Rat primary cortical and hippocampal neurons were plated on 96 well plate (15,000 cells/well) or 6 well plate (250,000 cells/well). After 3 h the cells were changed to Neurobasal medium. After 3 days AraC was added to the medium to arrest the growth of the glial cells. Then the cells were grown for 21-28 days.

3.2.7.4 Protein transfection

SH-SY5Y cells were plated at a density of 150,000 cells/well in 6 well plates and left overnight at 37°C. Xfect protein transfection reagent kit (Clontech) was used to transfect the protein of our interest into the neurons. 15µl of Xfect transfection reaction mixture was mixed with 85µl of deionized water in a tube. In another tube the protein of interest and the Xfect transfection buffer was made up to the final volume of 100µl. Both the reaction mixture were added together and mixed well by pipetting them up and down slowly for 10-15 times and then incubating them at RT for 30 min. 400µl of serum free medium was added to this mixture and mixed well 2-3 times by pipetting. In case of rat primary neurons, the conditional medium was used. The whole content (600µl) was added on the cells and incubated for another 2 h. After that 2ml of medium with the serum was added on the cells and incubated for 15 h.

3.2.7.5 Cell toxicity assays

SH-SY5Y cells (15,000 cells/well) were plated on a 96 well plate and left it overnight in a CO_2 incubator. The cells were incubated with protein of interest for specific time periods and then used for toxicity assays. In all toxicity assays, the measurements were normalized to buffer control to evaluate the difference. Rat primary cortical and hippocampal neurons (15,000 cells/well in a 96 well plate and grown for 3 weeks) were treated similarly.

MTT assay

The assay is based on the cleavage of the tetrazolium salt MTT (3-(4,5-Dimethylthiazol-2-yl)-2,5-Diphenyltetrazolium bromide) in the presence of an electron-coupling reagent. The water-insoluble formazan salt produced must be solubilized in an additional step. Tetrazolium salts are cleaved to formazan by the succinate-tetrazolium reductase system which belongs to the respiratory chain of the mitochondria, and is only active in metabolically intact cells. This bio-reduction occurs in viable cells only, and is related to NAD(P)H production through glycolysis. Therefore, the amount of formazan dye formed directly correlates to the number of metabolically active cells (Vistica et al., 1991).

SH-SY5Y cells and rat primary neurons were treated with oligomers for certain time periods. After the incubation time, 10µl of MTT solution I (3-(4,5-Dimethylthiazol-2-yl)-2,5-Diphenyltetrazolium bromide) was added to the cells and incubated for 4 h at 37°C in a CO_2 incubator. After 4 h, 100µl solubilization solution (10% SDS in 0.01 M HCl) was added to the cells and incubated further overnight at 37°C in a CO_2 incubator. After the incubation time, the absorbance was recorded at 550 nm and the reference wavelength was 690 nm.

XTT assay

This assay is based on the cleavage of yellow tetrazolium salts XTT (2,3-Bis-(2-Methoxy-4-Nitro-5-Sulfophenyl)-2H-Tetrazolium-5-carboxanilide) to form an orange formazan dye by metabolically active cells. This conversion takes places only in the viable cells. This formazan dye formed is soluble in aqueous solutions and is directly quantifiable (Gerlier and Thomasset, 1986).

XTT solution: 2ml of XTT labelling reagent was mixed with 40µl of electron coupling reagent and mixed very well. SH-SY5Y cells and rat primary neurons were treated with oligomers for certain time periods. After incubation, 50µl of XTT solution was added to the cells and incubated overnight at 37°C in a CO2 incubator and then the absorbance was recorded at 450 nm with the reference wavelength of 690 nm.

Alamar blue assay

Alamar blue is a cell viability indicator that uses the natural reducing power of living cells to convert resazurin to the fluorescent molecule, resorufin. The active ingredient of alamarblue (resazurin) is a nontoxic, cell permeable compound that is blue in color and virtually nonfluorescent. Upon entering cells, resazurin is reduced to resorufin, which produces very bright red fluorescence. Viable cells continuously convert resazurin to resorufin, thereby generating a quantitative measure of viability and cytotoxicity (Page et al., 1993).

SH-SY5Y cells and rat primary neurons were treated with oligomers for certain time periods. After the incubation, 10µl of alamar blue solution was added to the well containing 100µl of medium and cells and incubated for 4 h at 37°C in a CO_2 incubator. The fluorescence intensity of resorufin was measured in a spectrophotometer using 560 nm excitation and 590 nm emission filter settings.

LDH release assay

Lactate dehydrogenase (LDH) is a soluble cytosolic enzyme that is released into the culture medium following loss of membrane integrity resulting from either apoptosis or necrosis and hence LDH activity can be used as an indicator of cell membrane integrity. The LDH kit (Roche) measures LDH activity in the culture medium using a coupled two-step reaction. In the first step, LDH catalyzes the reduction of NAD^+ to NADH and H^+ by oxidation of lactate to pyruvate. In the second step, diaphorase uses the newly-formed NADH and H^+ to catalyze the reduction of a tetrazolium salt (INT) to highly-colored formazan which absorbs strongly at 490 nm (Decker and Lohmann-Matthes, 1988).

45µl of dye solution was added to 1µl of catalyst solution and mixed well (ratio 45:1). Then 50µl medium from the wells were collected and 50µl of LDH reaction mixture was added to the medium and incubated at RT in the dark for 30 min. The reaction was stopped by the addition of 10µl of 1N HCl and incubated for another 1 h at 4°C. The absorbance was measured at 490 nm.

3.2.7.6 Functional assays

Calcium imaging: Intracellular calcium levels were measured using the Fura-2 ratiometric dye. Upon entering the cells Fura 2-AM is cleaved by cellular esterases. Fura-2 is free to interact with the calcium in the cells. Fura-2 is excited at two wavelengths (380 nm – free form; 340 nm – calcium bound form) and emits the light at 516 nm. Therefore the changes in the ratio of 340nm and 380 nm are calculated to measure the intracellular calcium level. The primary rat hippocampal neurons were grown on 96 well plates with the density of 15000 neurons per well. The conditional medium were collected and stored. The cells were incubated with 4µM Fura-2 and 2% F127 for 30 min at 37°C. After the incubation, the Fura 2 dye was removed and the cells were washed with 1X HBSS. The cells were filled with 80µl of calcium imaging solution and imaged on a fluorescence microscope (Cell Observer, Zeiss) at 20X magnification.Multiple acquisition mode was used to image in different wells simultaneously. The fileds were chosen and imaged for first 10 min. Then the required concentration of the sample (Buffer, $Tau^{RD\Delta}$ monomer and oligomers at different concentrations) was added to the calcium imaging buffer and the image acquisition was started immediately for another 30 min.

ROS Imaging: Reactive oxygen species levels were measured using the DCFDA dye. Carboxy-DCFDA can passively diffuse into cells and is colorless and nonfluorescent until the acetate groups are cleaved by intracellular esterases to yield the fluorescent fluorophore, 5-(and-6)-carboxy-2',7' –dichlorofluorescein (DCF). Upon the production of super oxide and peroxy radicals, this DCF is oxidized and shows an increase in the fluorescence intensity. 4µM of DCFDA dye was incubated along with 2% F127 (facilitates the solubilization of water insoluble dyes) for 30 min on rat primary hippocampal neurons. After the incubation, the fura 2 dye was removed and the cells were washed with 1X HBSS. The cells were filled with 80µl of calcium imaging solution and imaged by fluorescence microscopy as described above.

Confocal microscopy

Analysis of neurons, tissue cultures and slices was done by imaging on an LSM 700 confocal microscope using a 63X objective. Dendritic spines were counted at 30µm distance from the cell soma for the length of another 50µm. From each coverslip, a minimum of 10 neurons were imaged and counted for spine density analysis.

Flow cytometry (FACS)

Flow cytometry is a laser-based, biophysical technique in cell counting, by suspending cells in a stream of fluid and passing them through an electronic detection apparatus. Blue laser (488 nm laser) was used to excite ThS (Ex:440 nm/ Em:521 nm) and red laser (638 nm laser) was used to excite APC (Ex:633 nm/ Em:665 nm). The instrument was used according to the manufacturer's specifications.

Annexin V staining

Apoptosis is called programmed cell death where the loss of plasma membrane is one of the earliest features. In apoptotic cells, the membrane phospholipid phosphatidylserine (PS) is translocated from the inner to the outer leaflet of the plasma membrane. Annexin V is a 35-36 kDa Ca^{2+} dependent phospholipid-binding protein that has a high affinity for PS, and binds to cells with exposed PS. APC (Allophycocyanin) Annexin V staining can identify apoptosis at an earlier stage than assays based on nuclear changes such as DNA fragmentation.

SH-SY5Y cells were treated with the protein of interest for 15 h. The cells were trypsinized for 3 min at 37°C in a CO_2 incubator, collected in a tube and centrifuged at 1250 rpm for 5 min at RT. The supernatant was removed and the cells were suspended in 100µl of 1X annexin binding buffer. 5µl of annexin V dye was added to the cells and incubated in the dark for 30 min at RT. The cells were washed with 1X annexin binding buffer and collected in 1X annexin binding buffer in a flow cytometry tube. Cell counting was performed in Gallios Beckman-Coulter Flow cytometer. 20,000 cells were counted per sample without any gating. The excitation and emission of Annexin V APC dye used was 650nm and 660 nm respectively.

ThS staining

Thioflavin S binds to the ß-sheet structure of aggregates. SH-SY5Y cells were treated with the protein of our interest for 15 h. One hour before harvesting the cells, 0.0005% ThS was added to the cell culture medium and allowed them to enter the cells. The medium was collected and the cells were trypsinized for 3 min at 37°C and then cells were collected in a tube along with the pre collected medium. The cells were centrifuged at 1250 rpm for 5 min at room temperature. Then the supernatant was removed and the cells were resuspended in PBS buffer. The ThS positive cells were counted on flow cytometer without any gating. 20,000 cells were counted for each condition.

3.2.7.7 Immunocytochemistry

Rat primary neurons were treated with the protein of interest for different time intervals. After the incubation time, the cells were fixed with 4% sucrose and 3.7% formaldehyde in PBS solution for 30 min at 37°C, then washed with 1X PBS, 3 times. The cells were permeabilized and blocked using 5% BSA, 0.5% Triton X 100 in PBS for 6 min at RT and then washed thoroughly three times with 1X PBS. The primary antibody was diluted in 5% BSA and incubated on cells overnight at 4°C. Unbound antibodies were washed with 1X PBS three times. The secondary antibodies and dyes were incubated for 1 h at 37°C. The excess antibodies were washed three times with 1X PBS. 10µg/ml DAPI was incubated for 10 min at room temperature and washed once with 1X PBS. Finally the cells were mounted using poly mount solution and the coverslips were dried at 4°C overnight.

3.2.8 Tissue culture

Organotypic Hippocampal Slice Culture

Organotypic hippocampal slice cultures (OHSC) were prepared as described (Stoppini et al., 1991) with modifications. All the dissection materials were sterilized before the preparation. 8 days old wild type mice were sacrificed and the brain was quickly removed. The hippocampi were dissected out without destroying the architecture of hippocampus. The hippocampi were transferred to the filter paper and placed on the tissue chopper to prepare 400µm thick transverse slices. The slices were transferred to the medium quickly and the intact hippocampus slices were transferred to the semi-porous (0.4 µm) cell culture inserts. The inserts were equilibrated in the medium 1 h before the preparation and stored at 37°C in a CO_2 incubator. 8-10 slices were placed on one insert in a six well plate containing 1 ml slice culture media. Every third day the medium was replaced with the fresh media. The slices were maintained for 11 days *in vitro*. After 11 days, the slices were treated with respective protein of our interest for another 24 and 48 h.

3.2.8.1 Immunohistochemistry

After the treatment, the slice culture media was completely removed and the slices were fixed with 4% formaldehyde overnight at 4°C. The inserts were washed with 1X PBS 3 times, 10 min each at the room temperature on a shaker. The inserts were split into 3 pieces with 3-4 slices/ inserts and incubated with 0.1 M glycine for 20 min at room temperature. The slices were permeabilized with 0.5% triton X 100 in PBS overnight at 4°C, then washed 3 times with 1X PBS for 15 min each, at room temperature. Then the slices were blocked with 20% horse serum for at least 4 h at room temperature. The slices were incubated with primary antibody diluted in 5% horse serum and 0.05% triton-100 in PBS for at least 48 h and then the slices were washed with 1X PBS, 3 times with 10 min interval. Then the secondary antibody was also diluted in 5% horse serum and 0.05% triton X-100 and incubated for at least 24 h. The slices were washed with 1X PBS, 3 times, at 10 min interval and then the slices were mounted using poly mount solution.

3.2.9 Animal models

3.2.9.1 Brain homogenate preparation

Animals were sacrificed and the brains were removed and frozen in liquid nitrogen. Before the homogenate preparation, the brain sample was thawed by keeping it on ice. 800µl of 1x lysis buffer was added and the tissue was minced using a 1ml syringe attached with 18G needle and later with 24 G needle. The sample was placed on ice for 30 min. The sample was resuspended with a pipette and was centrifuged at 14,000 rpm at room temperature. The supernatant containing the proteins was collected and the protein concentration was estimated using BCA method.

3.2.9.2 Sarcosyl extraction of insoluble Tau

Three times more volume of buffer H was added to the brain tissue (w/v) (For ex: 57mg of cortex tissue was homogenized in 171 µl of buffer H). The sample should be kept on ice throughout the experiment. The sample was homogenized for 30 seconds and kept on ice for 1 minute. The same step was repeated once more. Later the sample was incubated on ice for 15 min and then centrifuged at 1000 rpm for 3 min at 4°C. The tissue was resuspended using pipettes and transferred to Beckman centrifugation tube and centrifuged for 26,000 rpm (TLA 100.3) for 20 min at 4°C. The supernatant (S1) was collected into another tube. To the pellet, buffer H was added again and the same step was repeated. The supernatant (S2) was collected and added to the same tube where supernatant (S1) was stored. The volume of supernatant S1 and S2 was measured and then 10% of N-lauroyl-sarcosinate and 10µg/ml ß-mercaptoethanol was added in a 9:1 ratio to the supernatant I and II mixture. This mixture was incubated at 37°C for 1.5 h – 2 h in a shaking condition and then centrifuged at 61,000 rpm (TLA, 100.3 rotor) for 35 min at 20°C. The pellet was very small but clearly visible. The supernatant was carefully collected (S3) and the pellet was rinsed in 100µl of 1X TBS and then the TBS was removed carefully without disturbing the pellet. The pellet was resuspended in 0.5µl of 1X TBS for each mg of brain tissue. The samples were run on SDS gel for further analysis.

3.2.9.3 Iodixanol gradient centrifugation

60% Optiprep Iodixanol was diluted in water and placed in a Sorvall centrifugation tube from top to bottom in an increasing concentration (5, 10, 20,25,30,40 and 50%).

On top of the 5% layer, 100µl of the brain homogenate was placed and centrifuged at 65,000 rpm (TV 865 rotor) at 4°C for 3 h. At the top of the centrifugation tube, a hole was made using a needle to let the air come in and from the bottom of a tube the fractions were collected by puncturing the tube at the bottom. 500µl fractions were collected and were run on an SDS gel and blotted with K9JA antibody for the detection of Tau protein.

3.2.10 Statistics

All experimental data were normalized with buffer controls. The statistics was done using graph pad prism software. The significance of differences was analyzed by one- way and two-way ANOVA test with Tukey´s post hoc test. In all the experiments the confidence interval was set at 95%. Hence a p value < 0.05 was considered to be statistically significant.

4 Results

As described in the Introduction section, it is known that the $Tau^{RD\Delta}$ mouse model shows pronounced neurodegeneration (Mocanu et al., 2008). However, switching off the expression of the soluble $Tau^{RD\Delta}$ reduces Tau pathology and improves memory (Sydow et al., 2011, Van der Jeugd et al., 2012). Recent reports have suggested that small oligomeric species are responsible for the toxicity of Tau (Lasagna-Reeves et al., 2010, Kumar et al., 2014, Flach et al., 2012). This provided the motivation for investigating the nature of $Tau^{RD\Delta}$ oligomers and their toxicity.

4.1 Oligomers interact via cys-cys bonding in ΔK280 transgenic mice

In order to characterize the oligomers of mutant repeat domain or full length Tau ($Tau^{RD\Delta}$ and $Tau^{FL\Delta}$) generated in the transgenic mouse models, mice aged > 18 months were sacrificed and the insoluble and soluble Tau protein was fractionated using the sarcosyl extraction procedure. The insoluble Tau was extracted in fractions P3 and contains both wild type mouse tau (Mr~55kDa in the SDS gel) and human $Tau^{RD\Delta}$ (Mr~14 kDa) (Figure 4.1 A). The soluble (S3) fractions were also run on a SDS gel and showed some oligomeric bands in the range of 80kDa (in case of $Tau^{RD\Delta}$ mouse brain homogenates (red arrow Figure 4.1 A) and ~ 100, 120 and 200 kDa (red arrows Figure 4.1 B) in the case of $Tau^{FL\Delta}$ mouse brain which indicate that the oligomeric species are present. These oligomeric bands did not appear in P3 fraction which suggests that these bands represent small soluble oligomeric species. We consider 2-10 molecules of Tau as low-n oligomers whereas the protein retained in the gel pockets are considered as high-n oligomers and/or pre-fibrillar or fibrillar aggregates. Since Tau-Tau interactions are promoted by disulfide crosslinks, a portion of the S3 samples were mixed with sample buffer without ßME (which breaks the disulfide bridges) and run on a gel. Interestingly, a smear of bands appeared on the western blot from 60 kDa to >200 kDa in case of S3 fraction of $Tau^{RD\Delta}$. Similar observations were made in case of $Tau^{FL\Delta}$ mouse brain homogenate. This suggests that there are higher order oligomeric species in both $Tau^{RD\Delta}$ and $Tau^{FL\Delta}$ mouse models connected via cys-cys bonding. However, it is not clear whether the smears contain only the exogenous human Tau and/or also endogenous mouse Tau.

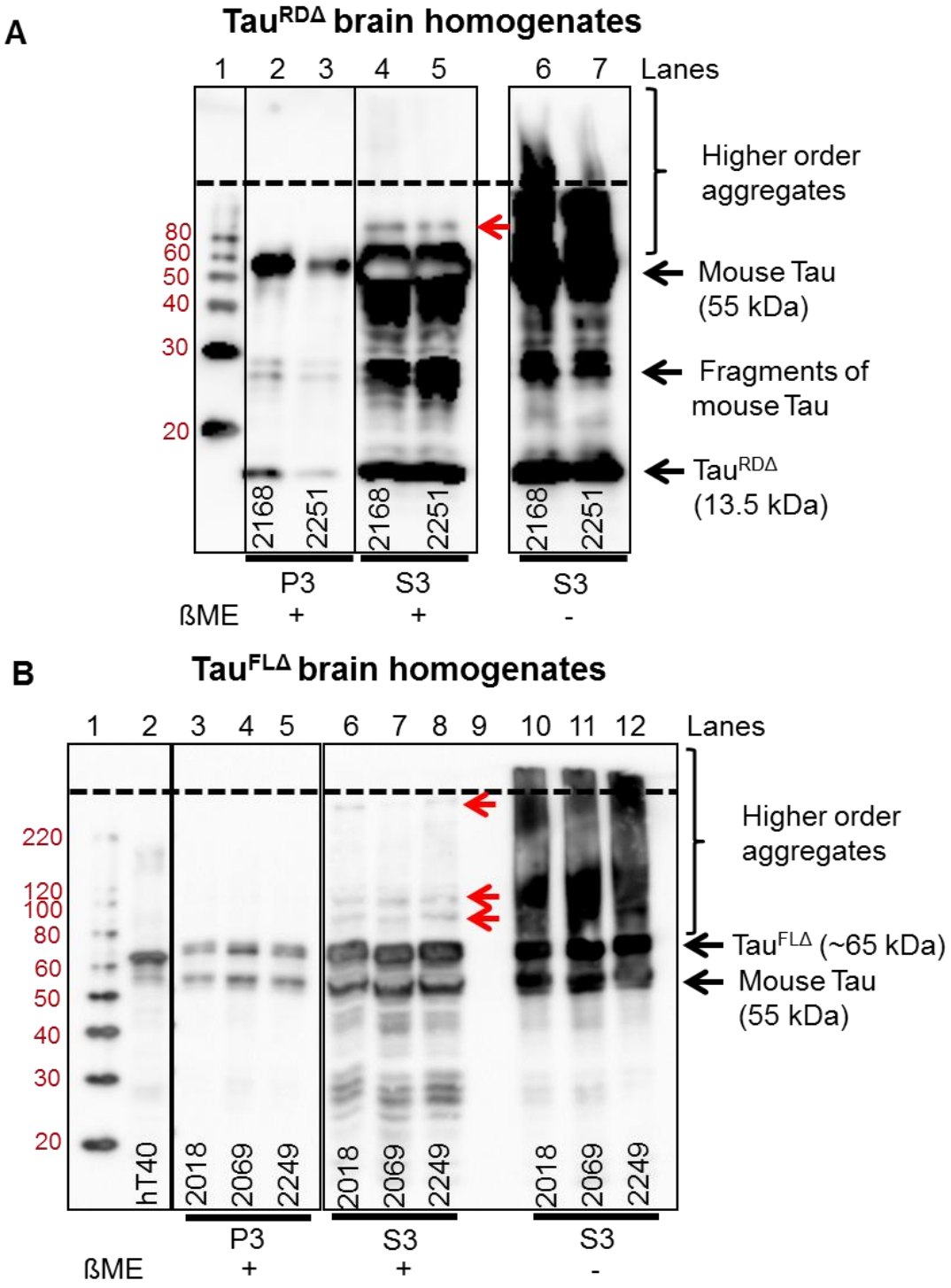

Figure 4.1 Tau oligomers in brains of transgenic mice.
Insoluble Tau and soluble Tau were separated from brain homogenates of cortex tissue from pro-aggregant full length (**B)** and repeat domain (**A)** transgenic mouse brains using the sarcosyl extraction method. P3 fractions contain the insoluble Tau and S3 fractions contain soluble Tau. The samples were run on a 17% and 10% SDS gel for $Tau^{RD\Delta}$ and $Tau^{FL\Delta}$ respectively and blotted with K9JA antibody (1:20,000 dilution). The blots display the smear of Tau proteins in the S3 fractions, in the absence of ßME suggesting the interaction of Tau-Tau via disulfide bridges (Fig A –Lanes 6,7; Fig B – Lanes 10,11,12). The red arrows on fig **A** and **B** show the SDS and DTT stable tau oligomers. The number on the bottom denotes the animal numbers. ßME – ß mercaptoethanol; hT40- purified recombinant full length tau protein; The dotted line separates the stacking gel from resolving gel.

4.2 Separation of Tau oligomers by iodixanol gradient centrifugation

To study the properties of the Tau oligomers, we applied iodixanol gradient centrifugation to separate the tau oligomers from the pool of other proteins. This method separates the molecules on the basis of their density. We used supernatant 3 from the sarcosyl extract, as it contains only the soluble protein with Tau monomers and oligomers. With this method it is possible to separate different forms of Tau protein in different gradient fractions. Figure 4.2 shows exogenous human Tau ($Tau^{RD\Delta}$) in 5-25% of iodixanol gradient fractions. Interestingly, at 40% iodixanol gradient, a faint band of SDS stable Tau oligomers at ~80 kDa is visible (red arrow). A similar observation was also made for S3 fractions of $Tau^{FL\Delta}$ mouse brain. The full length Tau protein (~65 kDa) was found in the fractions of 25 -35% iodixanol gradient. As shown in Figure 4.1B, there is also a faint additional band at ~100 kDa in the 35% iodixanol fraction (Figure 4.2 B; red arrow).

In both animal models, mouse Tau could not be separated from human Tau even though the molecular weights are different (mouse Tau - 55 kDa and human Tau ($Tau^{RD\Delta}$ - 14kDa; $Tau^{FL\Delta}$– 65kDa). One possibility is a strong interaction (coaggregation) between human and mouse Tau or that the oligomeric species contain a mixture of both endogenous mouse Tau and exogenous human Tau and become separated when treated with the sample buffer and SDS. This result suggests that separation of only the oligomeric form of exogenous human Tau from monomeric Tau and mouse Tau is not possible by iodixanol gradient.

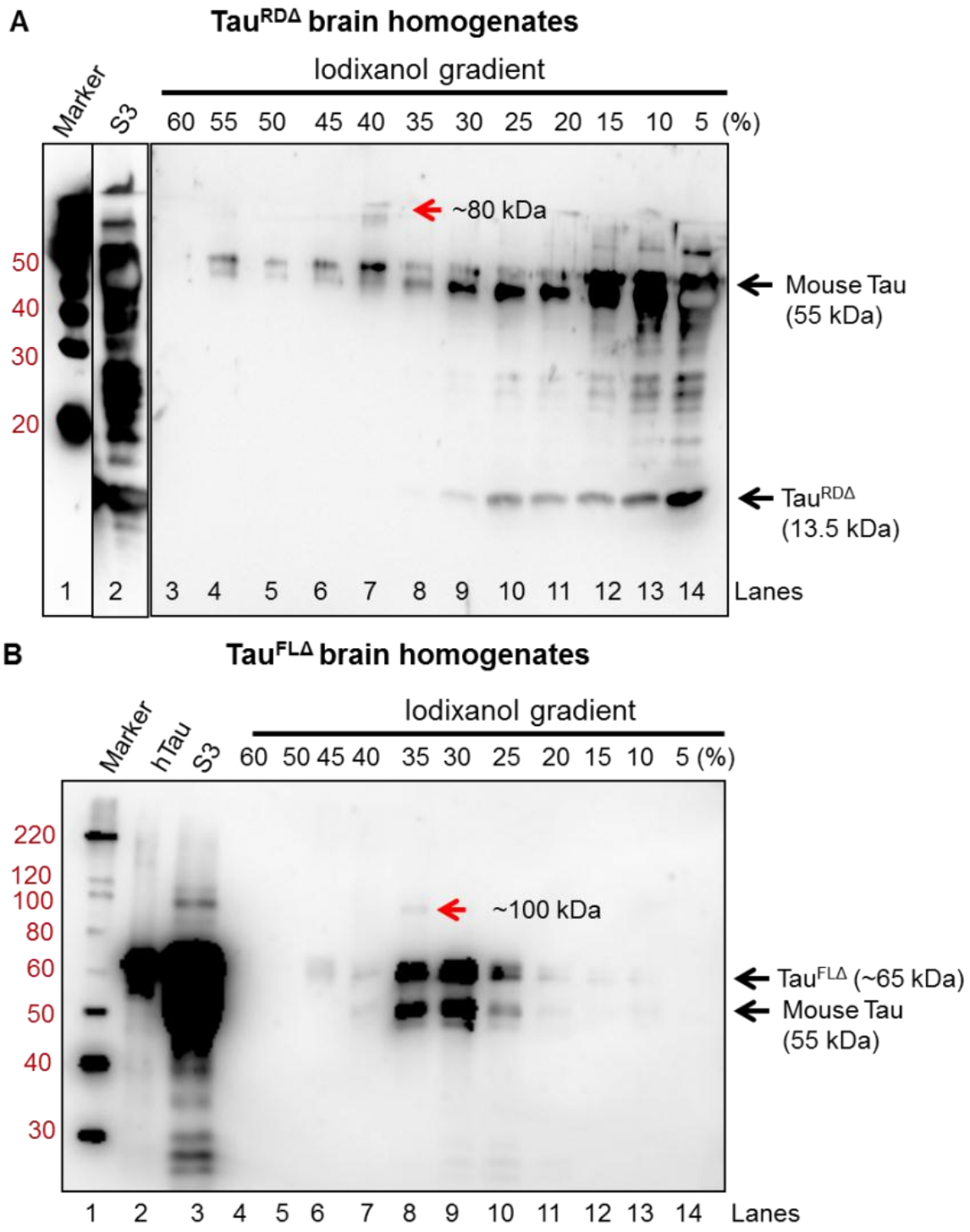

Figure 4.2 Separation of Tau oligomers by iodixanol gradient centrifugation.
100µl of S3 fraction from Tau$^{RD\Delta}$ **(A)** and Tau$^{FL\Delta}$ **(B)** mouse brain homogenates were applied on the bed of the iodixanol gradient and centrifuged at 65,000 rpm (TV 865 rotor) for 3 h. Western blot analysis (K9JA antibody, 1:20,000 dilution) of the fraction of iodixanol gradient shows that the proteins were separated. Oligomers are seen on the gel as faint bands at higher density (red arrow). In **(B)**, recombinant hTau40 protein was loaded as marker along with the mouse sample to differentiate the electrophoretic movement of mouse Tau from the human Tau. Note: Tau$^{RD\Delta}$ protein was fractionated at 5-25% of the gradient whereas Tau$^{FL\Delta}$ protein was fractionated at 25-35% suggesting the ability of the method to separate the protein based on density. S3 = Supernatant 3 sample used for iodixanol centrifugation.

4.3 Preparation of Tau$^{RD\Delta}$ protein *in vitro*

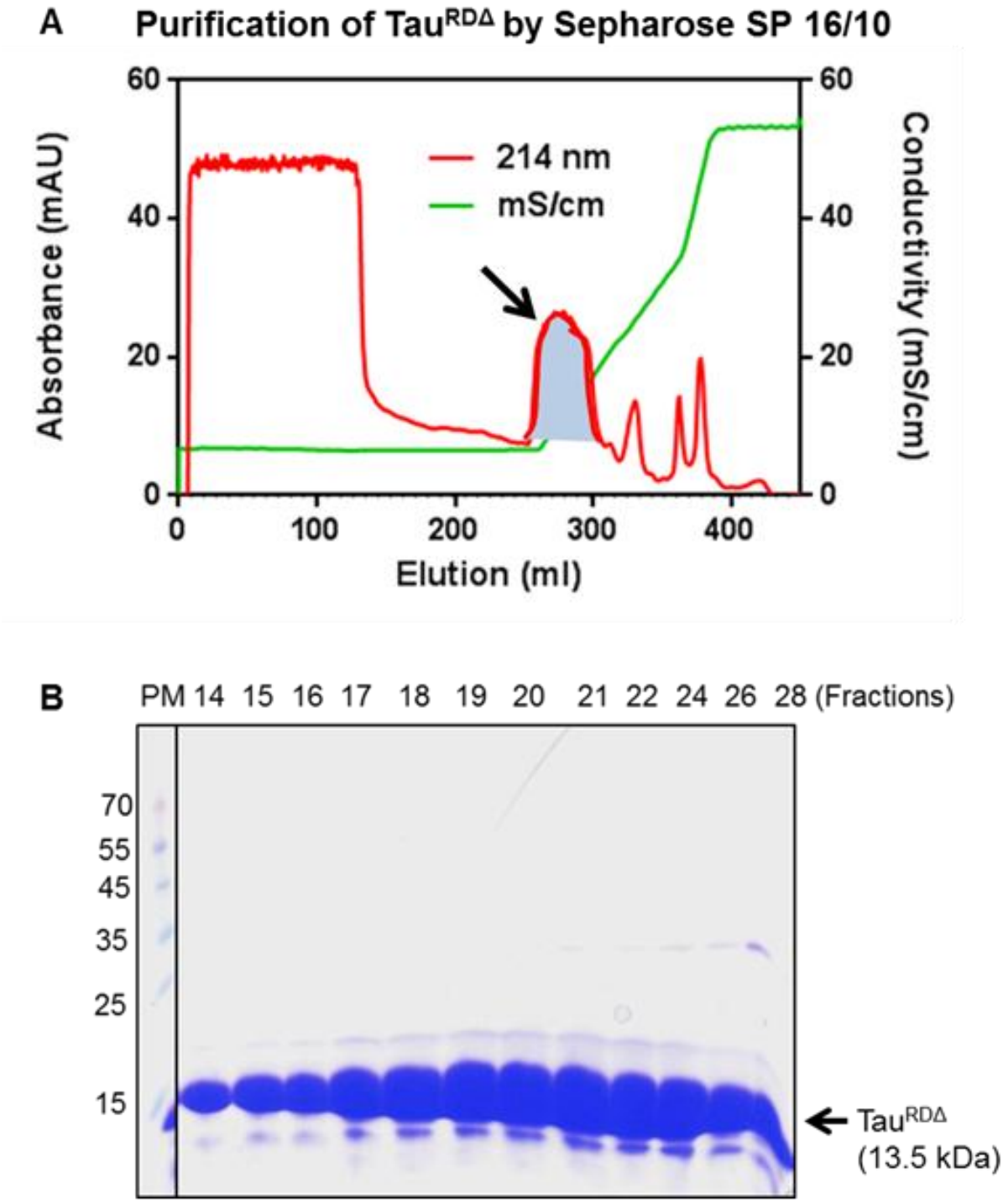

Figure 4.3 Preparation of Tau$^{RD\Delta}$ protein *in vitro*
A) Representative chromatogram of Tau$^{RD\Delta}$ protein prepared from 4 liters of bacterial culture and purified by Sepharose SP HP 16/10 cation exchange chromatography column. Note: The protein elutes early in the gradient (black arrow). The red curve represents absorbance of protein at 214nm. The green curve represents the concentration of Mono S B (high ionic strength) buffer. **B)** The protein (260-310 ml) was eluted as fractions in tubes (14-28) and was run on a 17% SDS gel and stained by Coomassie Blue.

The protein Tau$^{RD\Delta}$ was prepared in large quantity (~120 mg) and purified by Sepharose SP 16/10 cation exchange chromatography column as Tau protein is

positively charged. It binds to the negative ligand in the column and elutes later in the chromatogram whereas unbound protein is collected in the flow-through. A representative chromatogram is shown in Figure 4.3 A. The protein was eluted early in the elution gradient (black arrow) as the ionic strength (green curve) is increased in the buffer in a gradient fashion (Mono S A and Mono S B buffer). The purity of these fractions was analyzed by SDS gel and Coomassie Blue staining (Figure 4.3 B). The fractions show homogenous soluble monomeric protein without higher aggregates. This protein was used for further analysis.

4.4 Aggregation kinetics of Tau$^{RD\Delta}$

Under pathological conditions, Tau protein is aggregated to filaments and oligomeric precursors. As a model of Tau aggregation, we used Tau$^{RD\Delta}$ protein (von Bergen et al., 2000). The repeat domain of Tau aggregates more readily than full-length Tau into bona fide "paired helical filaments", and the "pro-aggregant" mutation (deletion of lysine at position 280) increases the propensity for ß-sheet structure even further (Barghorn et al., 2000). We therefore investigated the rate of aggregation of Tau$^{RD\Delta}$ protein *in vitro* under different buffer conditions by several methods in order to find the best conditions for oligomer preparation. The aggregation was carried out in the absence of heparin (an aggregation inducer), as Tau$^{RD\Delta}$ aggregates itself because of its strong ß-propensity.

4.4.1 Aggregation monitored by light scattering and fluorescence assays

50µM of Tau$^{RD\Delta}$ protein was diluted in PBS pH 7.4 and TBS pH 9.0. Prior to aggregation, the samples were heated with 1mM DTT for 20 min at 95°C in the presence of DTT to remove unwanted disulfide bridges (Schweers et al., 1995) and thus to monomerize the protein. After that the protein samples were incubated at 37°C for different time intervals.

The aggregation was monitored by assays of static UV light scattering at 350nm (which records particle size), Thioflavin S fluorescence (sensitive to amyloid like cross-ß-structure) and ANS fluorescence (reports on protein conformation). Under both buffer conditions (PBS pH 7.4 and TBS pH 9.0), Tau$^{RD\Delta}$ aggregates in a similar fashion with similar assembly rates and final levels (Figure 4.4 A). A similar observation was made for the case of static light scattering experiments, i.e. roughly comparable rates of assembly and final levels (Figure 4.4 B).

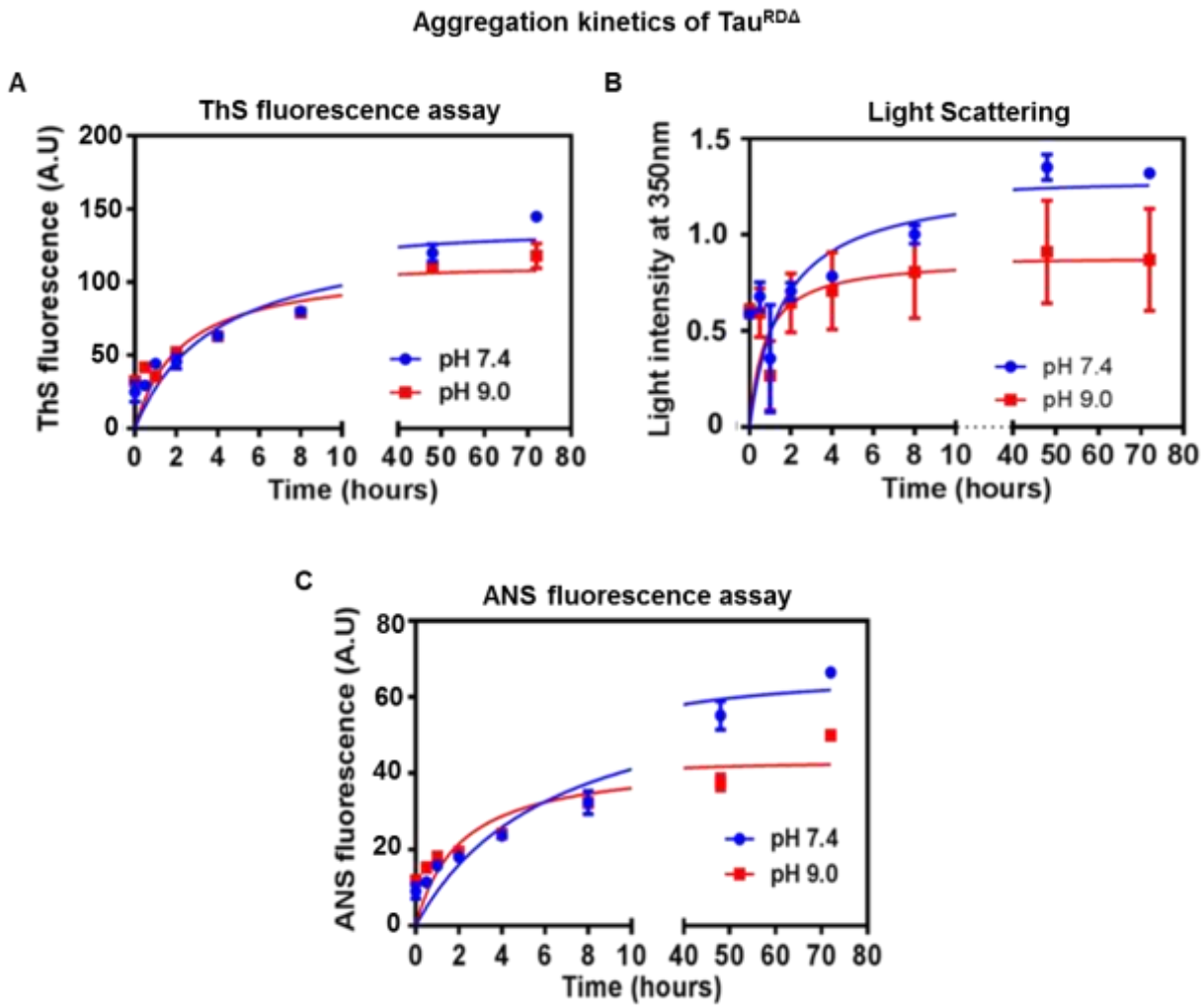

Figure 4.4 Aggregation of Tau$^{RD\Delta}$ by LS and fluoresence assays
Time course of aggregation of Tau$^{RD\Delta}$ protein was monitored by static UV light scattering, Thioflavin S and ANS fluorescence. **A)** ThS fluorescence intensity reached the maximum only after 8 h under both buffer conditions PBS pH 7.4 (blue lines) and TBS pH 9.0 (red lines). There is no significant change in the ThS fluorescence. **B)** Tau$^{RD\Delta}$ protein in TBS pH 9.0 was aggregated at the same rate as PBS pH 7.4. Hence no significant difference is observed. **C)** ANS fluorescence intensity reached the maximum only after 8 h under both buffer conditions PBS pH 7.4 (blue lines) and TBS pH 9.0 (red lines). There is no significant change in the ANS fluoresence.

ANS is a sensitive reporter of protein conformation. ANS binds to hydrophobic residues of a protein through its aromatic ring and positively charged amino acids through its sulfonate group. ANS fluorescence is increased during unfolding of a protein where the hydrophobic residues are available for binding. During aggregation, we observed an increase in the fluorescence intensity of ANS which reaches saturation after 8 hours in both buffer conditions (Figure 4.4 C) without a significant difference. This was contrary to expectations, since during aggregation Tau changes from a disordered state to an ordered ß-structured state. These assays suggest that conformational changes in the Tau$^{RD\Delta}$ take place under both buffer conditions.

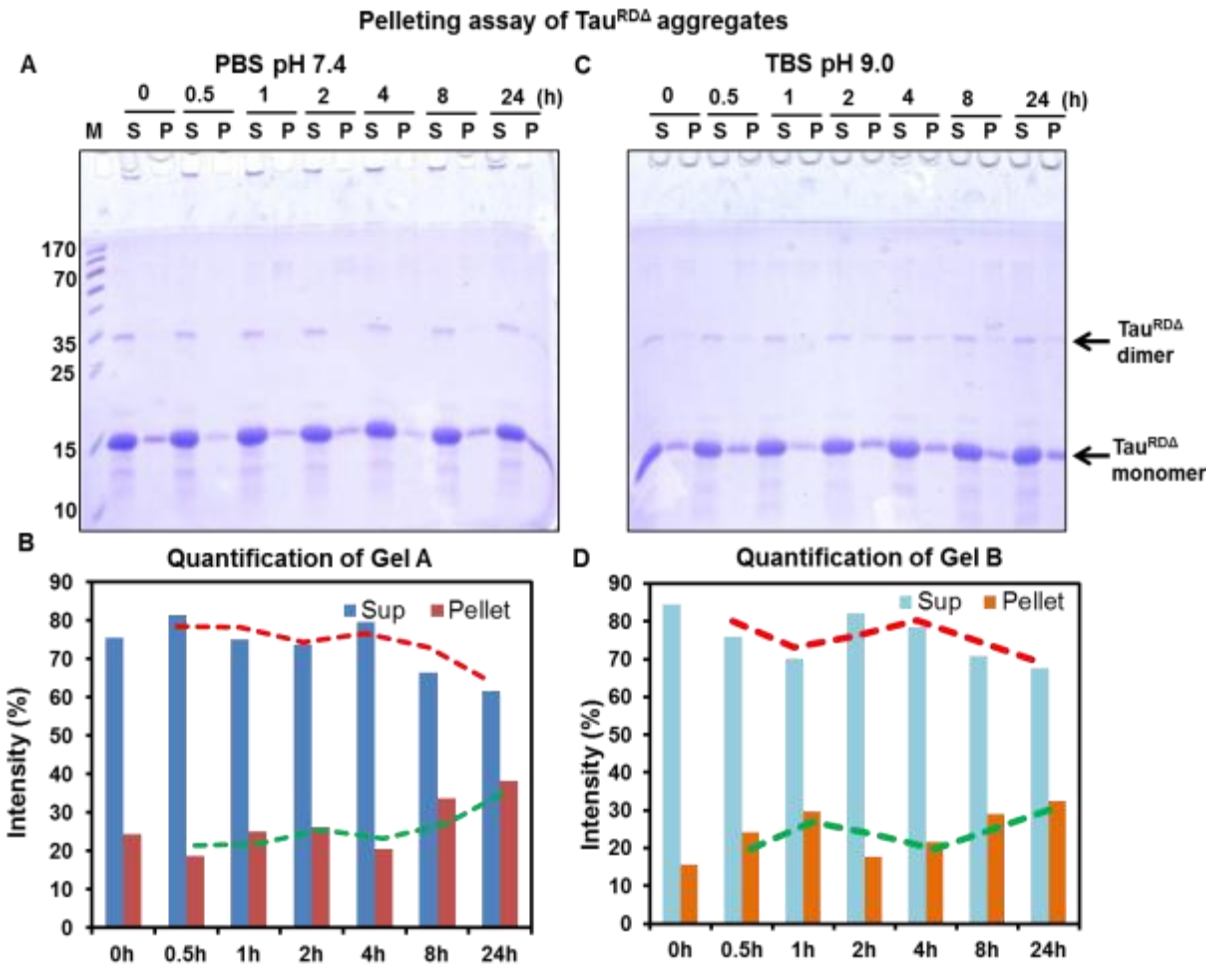

Figure 4.5 Sedimentation analysis of Tau$^{RD\Delta}$ aggregates.
The aggregates formed under both the buffer conditions (PBS pH 7.4 **(A)** and TBS pH 9.0 **(C)**) were sedimented by centrifugation (61,000 rpm; TLA 100.3 rotor). The supernatant and the pellet fractions were run on a 17% SDS gel and stained with Coomassie blue. Note: There is a time dependent increase in the protein amount in the pellet fraction in both buffer conditions, but the TBS buffer condition generates 10% less aggregates. **(B and D)** The intensity of Tau$^{RD\Delta}$ monomeric band was quantified by Image J software and plotted as a graph. S = Supernatant; P=Pellet; M=Marker and h= hours.

We also performed sedimentation analysis of these aggregated samples under both buffer conditions. At 0 hours, under both buffer conditions, we observed aggregates in the pellet fraction which is typical of this protein. Later during aggregation, Tau$^{RD\Delta}$ in TBS pH 9.0 and PBS pH 7.4 (Figure 4.5) showed significant increase in the protein aggregates in the pellet fraction. It appears that TBS, pH 9.0 condition has 10% less aggregates in the pellet fraction at 24 h compared to PBS,pH 7.4. This suggest that Tau$^{RD\Delta}$ protein in TBS pH 9.0 condition contains less aggregates and possibly favors oligomers.

4.4.2 EM and AFM reveal twisted fibrils and oligomeric structures

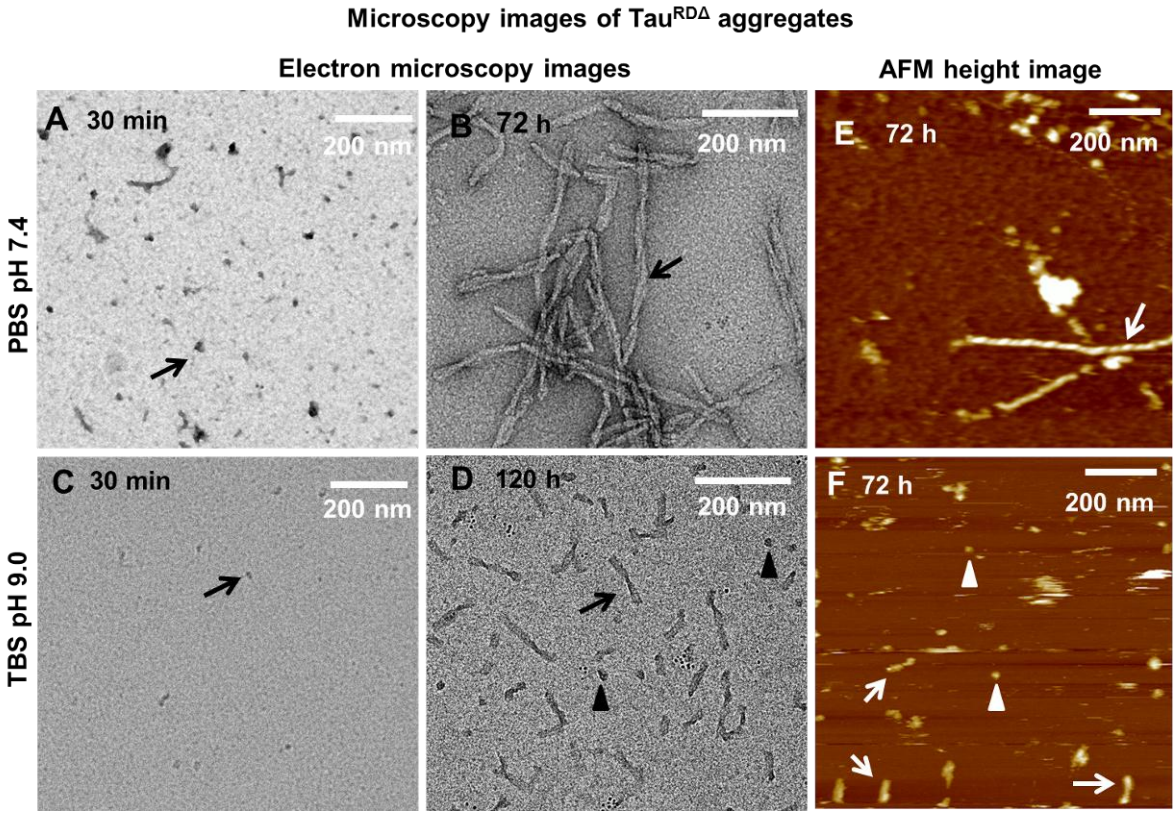

Figure 4.6 Analysis of Tau$^{RD\Delta}$ aggregates by EM and AFM
Electron micrographs of Tau$^{RD\Delta}$ at different time points of aggregation and in different buffer conditions. **A** and **B** show the aggregation of Tau$^{RD\Delta}$ in PBS pH 7.4. **(A)** At 30 min, Tau$^{RD\Delta}$ protein forms globular shaped aggregates (black arrow) and prefibrillar aggregates. **(B)** After 72 h of aggregation, Tau$^{RD\Delta}$ protein shows clear long twisted fibrils. **C** and **D** show the aggregation of Tau$^{RD\Delta}$ in TBS pH 9.0. At 30 min of aggregation, only few oligomers are present **(C)**. Even after 120 h, small oligomeric species were found along with bowtie shaped short fibrils. **E** and **F** show AFM images of the Tau$^{RD\Delta}$ aggregation at 72 h at pH 7.4 and pH 9.0 respectively.

The morphology of the aggregates formed by Tau$^{RD\Delta}$ under different buffer conditions was studied by EM and AFM. After 72 h (in PBS pH 7.4), there were long twisted fibrils typical of Alzheimer PHFs (Figure 4.6 B; black arrow and E; white arrow), but also a heterogeneous mixture of shorter fibrils and oligomeric aggregates. These intermediate prefibrillar aggregates were already observed 30 min after starting assembly (Figure 4.6 A arrow).

In contrast to PBS pH 7.4, we observed that at pH 9.0 the fibrils tend to be much shorter and have a bow-tie like shape (Figure 4.6 D), yet have a similar ThS signal. At 30 min of aggregation only few small oligomeric species were detectable by EM (Figure 4.6 C). The sensitivity of EM is poor for oligomers and hence it is possible that there are more oligomers in the pH 9.0 condition within 30 min of aggregation.

Interestingly the number of oligomeric species increased along with fibrils. Even after 120 h, we observed many small oligomeric species (arrowhead). AFM images of aggregates formed after 72 h at TBS pH 9.0 also displayed short fibrils (white arrows) and oligomers (white arrowhead) (Figure 4.6 F). This suggests that pH 9.0 favors the oligomers rather than fibrils and hence we chose TBS pH 9.0 conditions for oligomer preparation.

4.4.3 Purification of oligomers by size exclusion chromatography

The aggregation kinetics of $Tau^{RD\Delta}$ suggested that, at 30 min of aggregation there is an enrichment in small oligomers. Hence we chose the 30 min time point for the separation/purification of oligomers from the monomers and the prefibrillar forms of Tau aggregates. When testing gel filtration chromatography we observed that the initial aggregates are in a highly dynamic assembly/disassembly state and are therefore not separable on a superose PC 12 column. The protein eluted mostly as monomers in the chromatogram suggesting that the oligomers are not stable (Figure 4.7 C). But we also observed a smaller amount of higher aggregates at ~0.8 ml of elution volume which corresponds to the molecular weight of >2000 kDa. Thus it appears that smaller oligomeric species are not stable in PBS pH 7.4 conditions whereas aggregates >2000 kDa might be stable. The marker proteins were loaded on the same Superose PC 12 column and the elution profile of marker proteins were used to compare the size of the $Tau^{RD\Delta}$ aggregates (Figure 4.7 A).

We next checked $Tau^{RD\Delta}$ protein in the absence of DTT, because in the presence of DTT the oligomers might fall apart as DTT will reduce the disulfide bridges. Therefore, to prevent oligomer breakdown, we did not use DTT. Without DTT, higher molecular weight aggregates were pronounced in the elution profile. Monomers of $Tau^{RD\Delta}$ (13.6 kDa) were eluted at 1.6ml whereas higher molecular weight aggregates were eluted at 0.8ml corresponding to MW ~2000 kDa (or a multimers of ~150 monomers). This indicates that some aggregates were already present in the sample

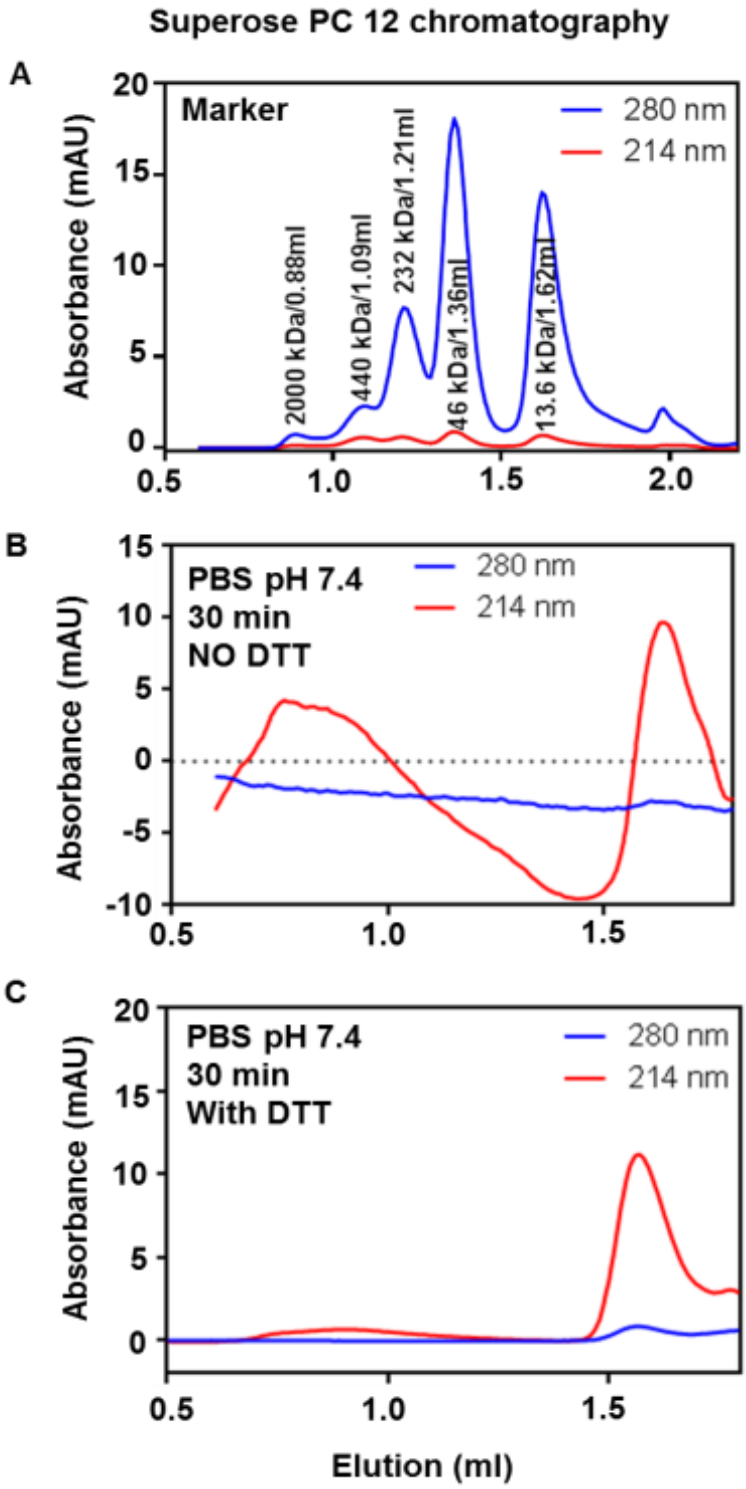

Figure 4.7 Separation of Tau$^{RD\Delta}$ oligomers.
A) Elution profile of the marker proteins on Superose PC 12 column. Mixture of blue dextran (2000 kDa), ferritin (440 kDa), catalase (232 kDa), ovalbumin (46 kDa), and ribonuclease A (13.6 kDa) were mixed at 10µg/ml concentration and run on Superose PC 12 column. The elution profile of these mixtures serves as a reference. **B)** Tau$^{RD\Delta}$ protein was incubated in PBS pH 7.4 for 30 min without DTT. The chromatogram displays monomers at 1.6 ml and the higher aggregates (multimers) at 0.8ml. **C)** Tau$^{RD\Delta}$ protein was incubated in PBS pH 7.4 for 30 min with 1mM DTT which caused the disappearance of the aggregates. No oligomers in the range of <200 kDa were observed in the chromatogram.

within 30 min of starting the aggregation (Figure 4.7 B). They could be considered as prefibrillar or amorphous aggregates since they do not show enhanced ThS fluorescence. We did not observe any peak in the range between 1 and 1.5 ml of elution in the chromatogram which suggests that the oligomers are not stable and are not separable by a superose PC 12 column.

4.5 Stabilization of Tau$^{RD\Delta}$ oligomers

Since the oligomers are not SDS stable and are not separable by chromatography columns, we next tried to stabilize the oligomers. It was shown earlier that the compound EGCG (a component of green tea) is able to induce the formation of off-pathway oligomers of α-synuclein protein and also inhibits its aggregation (Ehrnhoefer et al., 2008, Bieschke et al., 2010). Therefore we checked the ability of EGCG to inhibit the Tau aggregation and to preserve oligomers once they have formed.

4.5.1 Reduction of Tau aggregation by EGCG

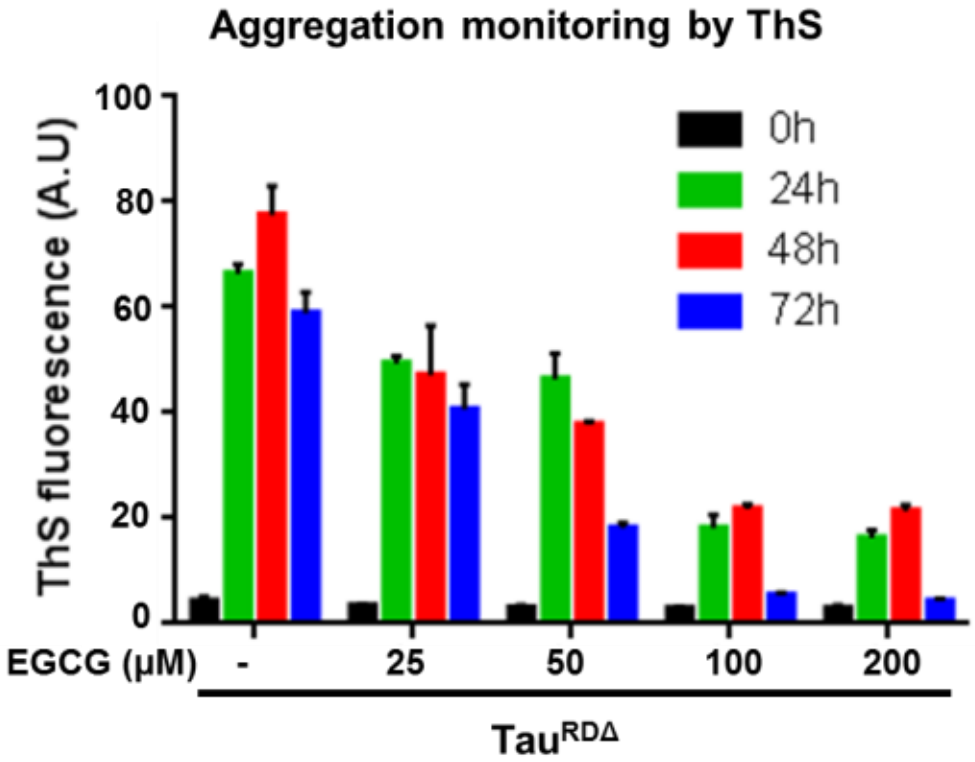

Figure 4.8 Reduction of aggregates of Tau$^{RD\Delta}$ protein by EGCG
Tau$^{RD\Delta}$ protein was incubated in PBS pH 7.4 for 24, 48 and 72 h at 37°C. In the absence of EGCG, Tau$^{RD\Delta}$ forms aggregates and shows increased ThS fluorescence intensity. With increasing concentration of EGCG, the ThS fluorescence intensity is greatly reduced.

We first performed the Thioflavin S assay to check whether the EGCG is able to inhibit the aggregation of $Tau^{RD\Delta}$ protein in vitro. In the absence of EGCG, $Tau^{RD\Delta}$ exhibits ThS fluorescence of 700 a.u. within 24 h of aggregation and thereafter remains steady (Figure 4.8). In the presence of EGCG, the aggregation is reduced in a concentration dependent manner for concentrations between 25µM to 200µM, judging by the reduction of ThS fluorescence (Figure 4.8). We also observed a time dependent decrease in the ThS fluorescence intensity. For example, at 50µM EGCG concentration there is a reduction of ThS positive aggregates in a time dependent manner.

4.5.2 EM reveals that EGCG reduces fibril length and increases oligomers

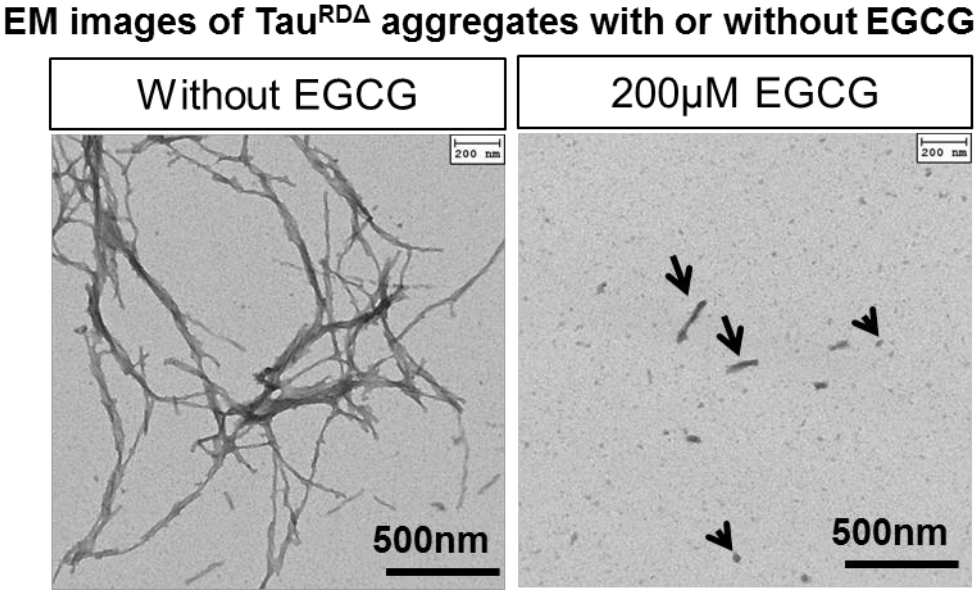

Figure 4.9 EGCG reduces fibril length and enhances oligomers of $Tau^{RD\Delta}$
$Tau^{RD\Delta}$ protein was incubated with and without 200µM EGCG for 72 h in PBS pH 7.4. **A)** $Tau^{RD\Delta}$ protein in the absence of EGCG shows twisted lengthy fibrils. **B)** $Tau^{RD\Delta}$ in the presence of EGCG displays reduced fibril length (black arrow) and more globular shaped oligomers or aggregates (arrow heads).

Electron microscopy was employed to study the structural changes caused by EGCG. In the absence of EGCG, $Tau^{RD\Delta}$ protein aggregates into long twisted fibrils similar to Alzheimer PHFs and contains only few smaller oligomeric species. By contrast, in the presence of EGCG (200µM, 72h) we observed short fibrils with varying lengths and many globular shaped oligomers or aggregates. Taken together, the ThS and EM data suggest that EGCG prevents the smaller aggregates or oligomers to become filaments.

4.5.3 EGCG increases SDS resistant soluble Tau$^{RD\Delta}$ oligomers

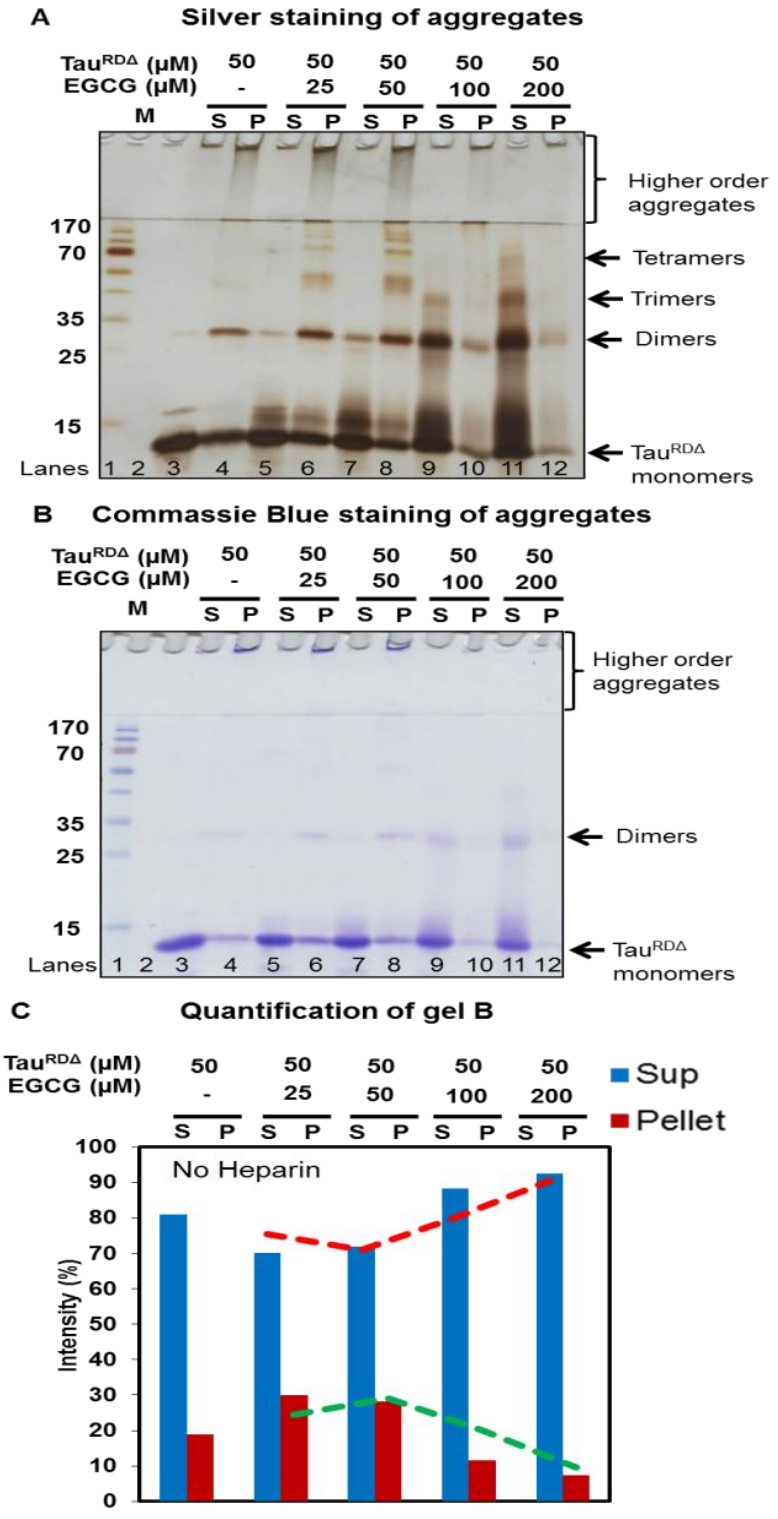

Figure 4.10 EGCG induces the formation of SDS stable soluble oligomers
Tau$^{RD\Delta}$ protein was incubated with and without EGCG at an increasing concentration for 72 h in PBS pH 7.4. The samples were centrifuged at 100,000Xg (TLA 100.3 rotor) for 1 h to separate pellet and supernatant and run on a 17% SDS gel. **A)** Silver stained gel of sedimentation assay samples in the presence of EGCG. **B)** Coomassie staining of sedimentation assay samples **C)** The quantification of the gel B using Image J. Note: Insoluble aggregates of Tau$^{RD\Delta}$ are reduced and SDS stable soluble Tau$^{RD\Delta}$ species are increased in an EGCG concentration dependent manner.

$Tau^{RD\Delta}$ protein was incubated in PBS pH 7.4, 1mM DTT at 37°C for 72 h with or without EGCG at an increasing concentration. After 72 h of incubation, the samples were pelleted down by centrifugation at 100,000xg. The supernatant and the pellet fractions were analyzed on 17% SDS gels and stained with silver and Coomassie Blue. The pellet fractions contained the higher molecular weight aggregates (above ~70 subunits) and the supernatant fractions contained smaller aggregates, oligomers and monomers.

By Coomassie staining ~20% of $Tau^{RD\Delta}$ was present in the pellet fraction in the control sample without EGCG decreasing to ~10% with EGCG, whereas the soluble supernatant fraction increased (Figure 4.10 B, C). The reduction of aggregates was also clearly visible in the gel pockets containing aggregates that did not move into the gel. A more detailed picture emerged when the samples were stained with silver (Figure 4.10 A), revealing that the majority of protein was in the supernatant fraction in the 200µM EGCG treated sample (Figure 4.10 A). The supernatant also revealed SDS stable soluble oligomers of low stoichiometry, mostly dimers and trimers of $Tau^{RD\Delta}$ which were not present without EGCG. Thus the sedimentation analysis suggests that EGCG promotes the formation of SDS-stable low-n oligomers.

EGCG stabilized oligomers are not separable from monomers by Superose PC 12 column (data not shown). In order to understand the oligomers in detail, a polyclonal antibody (by Eurogentec company, Belgium) was generated against the EGCG stabilized oligomers. Unfortunately, the generated antibody was not specific for oligomers analyzed by western and dot blot assays (data not shown). Therefore, we discontinued this approach and searched for alternative methods for stabilization of $Tau^{RD\Delta}$ oligomers. This lead us to test different methods of chemical cross-linking, focusing in particular on disuccinimidyl suberate (DSS) and glutaraldehyde (GA), as described in the following section.

4.6 Stabilization of $Tau^{RD\Delta}$ oligomers by chemical cross-linking

Glutaraldehyde is a common cross-linker used in biological microscopy. It has homo-bifunctional reactive groups at both ends which can react with amine groups of proteins, mainly lysine (Migneault et al., 2004).

DSS is a noncleavable and membrane permeable cross-linker that contains an amine-reactive N-hydroxysuccinimide (NHS) ester at each end of an 8-carbon spacer

arm. NHS esters react with primary amines at pH 7-9 to form stable amide bonds, accompanied by the release of the N-hydroxysuccinimide leaving group (Mattson et al., 1993). Proteins, including antibodies, generally have several primary amines in the side chain of lysine (K) residues and the N-terminus of each polypeptide that are available as targets for NHS-ester cross-linking reagents.

$Tau^{RD\Delta}$ protein was incubated in PBS pH 7.4 for 30 min to allow limited aggregation and then cross-linked with different concentrations of DSS and GA. At 0.125% concentration, glutaraldehyde cross-linked the protein after 5 min of incubation at 37°C (Figure 4.11 A), without further increase in the band intensity at later times. The cross-linked protein contained low-n oligomers (dimers, trimers, tetramers at ~28 – 42 kDa Mr values) and some higher order species visible as a smear in the stacking gel. We analyzed the potency of GA as a cross-linker and found that concentrations below 0.01% were not effective in cross-linking the protein. Between 0.01% and 0.125% of GA there were no significant changes (Figure 4.11 B). These results suggest that GA cross-links the aggregates which are already present in the solution, and that a low level of 0.01% GA and 5 min of incubation is enough to cross-link the aggregates.

Similarly, we tested the cross-linker DSS which had been used to cross-link Tau protein previously (Guttmann et al., 1995) The stabilization of Tau-Tau interactions with DSS indicated that intermolecular disulfide bonds likely play a predominant role in dimer formation, but the formation of higher order oligomers of Tau cannot be attributed to these bonds alone.

DSS at concentrations as low as 0.1mM and at 30 min incubation at 37°C was able to cross-link mainly the higher order aggregates, as we did not observe any low-n oligomers in the SDS gel (Figure 4.11 C). As a control, to confirm the presence of low-n oligomers, we also loaded GA cross-linked oligomers on a gel. The sample without any cross-linker did not show any intermediate bands, as the oligomers were not SDS stable. However, there were higher order aggregates in the stacking gel which could be SDS stable aggregates (Figure 4.11 C).

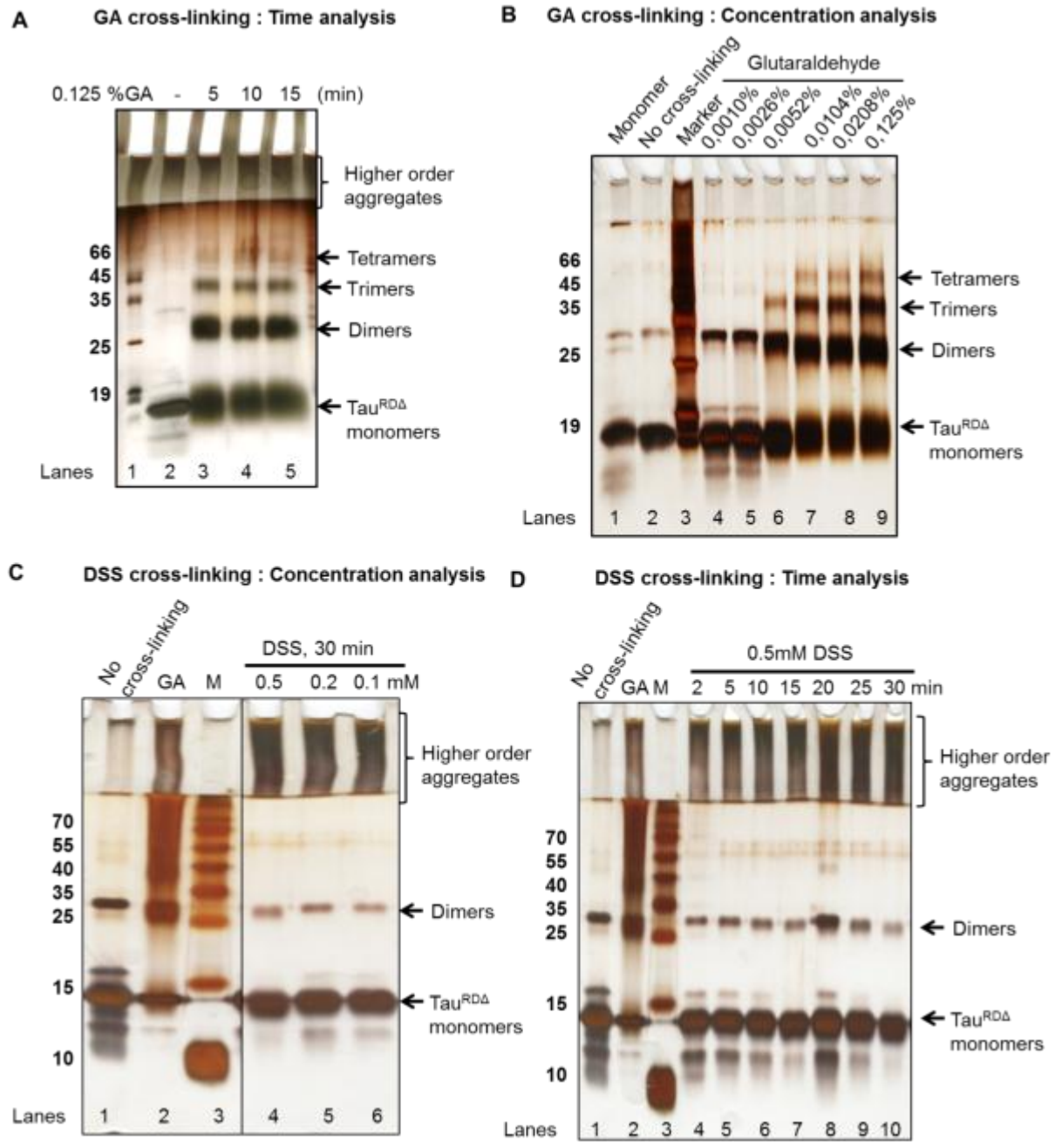

Figure 4.11 Stabilization of Tau$^{RD\Delta}$ oligomers by chemical cross-linking
Tau$^{RD\Delta}$ protein was incubated in PBS pH 7.4 for 30 min at 37°C. **A)** Glutaraldehyde cross-linker at 0.125% concentration was incubated for different time intervals up to 15 min. **B)** Incubation of Tau$^{RD\Delta}$ with increasing concentrations of glutaraldehyde for 10 min at 37°C. **C)** Incubation of Tau$^{RD\Delta}$ oligomers with decreasing concentrations of DSS (0.5-0.1 mM) for 30 min. **D)** Incubation of Tau$^{RD\Delta}$ oligomers formed during 30 min of aggregation with 0.5mM DSS for different time intervals (2-30 min). In figure C and D, GA sample is used as a control to show different aggregates present in the same sample used for DSS cross-linking. GA -Glutaraldehyde, M -marker proteins.

We next asked whether the DSS cross-linker forces the low-n oligomers into the higher-n aggregates during the incubation time. We incubated DSS cross-linker with the protein for short time periods and observed that within 2 min of incubation, DSS

cross-linked the protein aggregates, but not the low-n oligomers which were already present. At extended times, the cross-linker reacted with $Tau^{RD\Delta}$ more strongly and generated an intense higher molecular weight smear at 30 minutes of incubation (Figure 4.11 D). In conclusion, since DSS did not cross-link all the species of aggregates, we chose to use GA for further experiments.

4.6.1 Separation of GA stabilized oligomers

A major tasks of this project was to separate the oligomers from the monomers and fibrils. To achieve this, we incubated $Tau^{RD\Delta}$ protein at 50µM concentration in PBS pH 7.4 and TBS pH 9.0 for 30 min without DTT at 37°C. (TBS buffer at pH 9.0 conditions reduced the fibril length and increased the oligomers and polymers which led us to choose this condition for oligomer preparation (Figure 4.6 D). The half-life of DTT is 9 h in PBS/TBS buffer. DTT breaks the disulfide bridge links between tau molecules. In order to avoid the disintegration of oligomers into monomers by DTT, we omitted DTT in our experiments; (Figure 4.7 C). The aggregated samples were cross-linked using 0.01% GA for another 10 min at 37°C and run on analytical Superose PC 12 column.

We observed low-n oligomers of $Tau^{RD\Delta}$ already at 0 h which are formed during the sample preparation before the beginning of aggregation (Figure 4.12 A; arrow). When $Tau^{RD\Delta}$ protein was incubated for 30 min in PBS pH 7.4, we observed low-n oligomers and higher aggregates in a chromatogram (Figure 4.12 B; arrows). However, there was little difference in the oligomer content but more aggregates. A different picture emerged in conditions of TBS pH 9.0. There was an increase in the oligomer content compared to the conditions of PBS, pH 7.4 (Figure 4.12 D; arrow). This was confirmed by the gel analysis (Figure 4.12 E).

The results suggest that the oligomers are highly stable in TBS pH 9.0. The fractions of FPLC (elution volume 0.8 to 1ml – Lane 3 & 4 and 1.2 to 1.6ml – Lane 5 to 14) were run on a 17% gel which shows the separation of oligomers from the monomers. Although the separation is not complete, we were able to separate more than 60% of the oligomeric protein from the monomers (Figure 4.12 E). These chromatography results together with aggregation kinetics results (especially light scattering and ANS (Figure 4.4) provided the rationale for generating oligomers of the

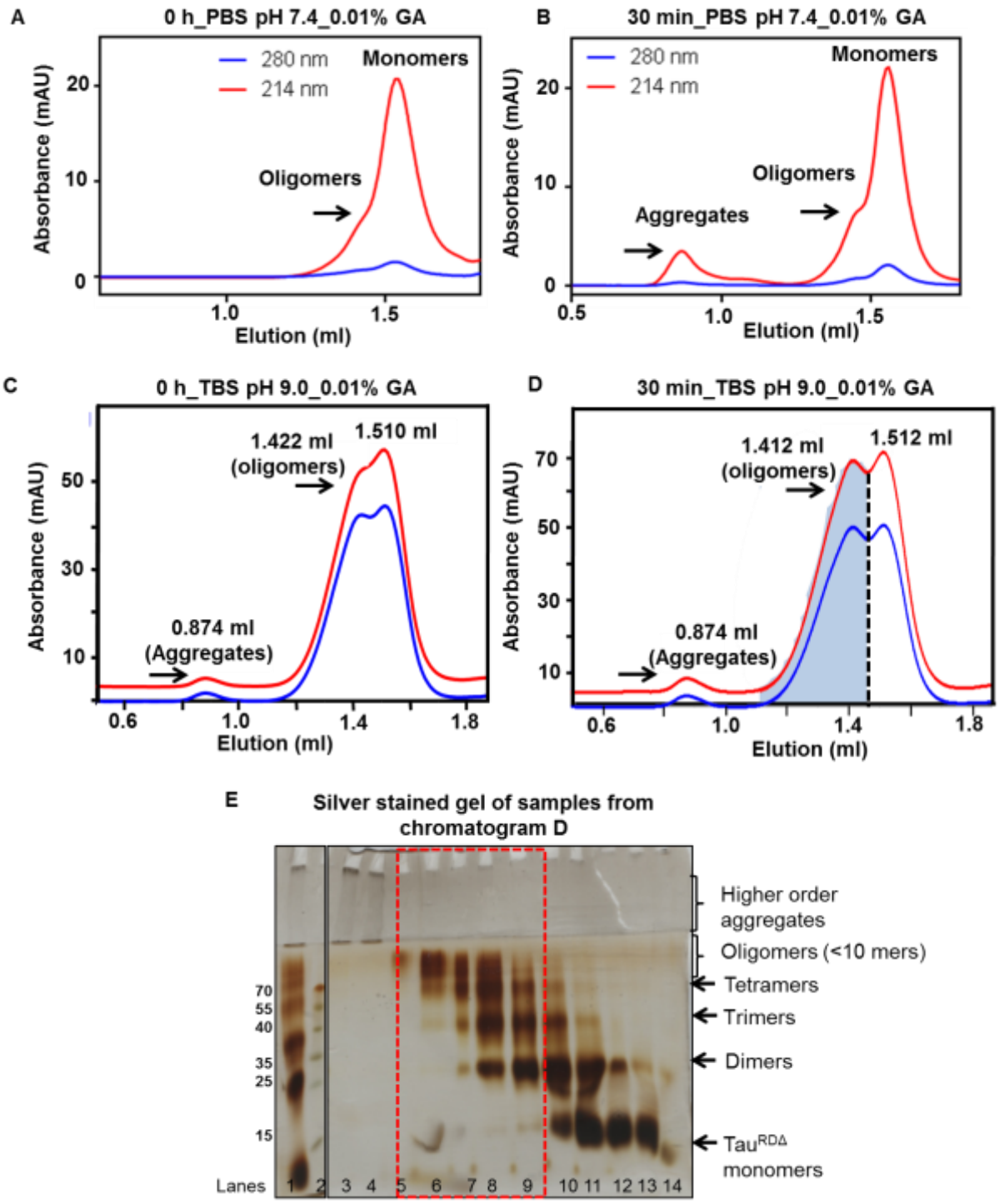

Figure 4.12 Separation of oligomers stabilized by glutaraldehyde
Tau$^{RD\Delta}$ protein was incubated in PBS pH 7.4 or TBS pH 9.0 buffer for 30 min at 37°C, then the sample was cross-linked with 0.01% GA for 10 min and run on a Superose PC 12 column. **A)** At 0 h, oligomers are observed at a low level (mostly dimers, trimers, and tetramers). **B)** At 30 min, oligomers and higher aggregates are present when incubated in PBS pH 7.4. **C)** 0 h sample cross-linked in TBS pH 9.0 buffer contains monomers, low-n oligomers and higher aggregates. **D)** Oligomers and aggregates increased after 30 min of aggregation. The peak filled with blue color represents the oligomeric fraction without monomers. The peak right to the dotted line represents monomers with little oligomers. **E)** Representative silver stained SDS gel picture of fractions (Figure D) shows the separation of oligomers from monomers (Red box; lanes – 5 to 9). Lane 1 – Sample before HPLC; Lane 2 – Marker; Lane 3 & 4 – fractions with higher aggregates.

protein in TBS pH 9.0 without DTT. The next task was to upscale the production of $Tau^{RD\Delta}$ oligomers, as described below.

4.6.2 Large scale purification of $Tau^{RD\Delta}$ oligomers by G200 column

2 ml of $Tau^{RD\Delta}$ oligomers prepared in TBS pH 9.0 were injected into a Superdex G 200 column for purification. The elution profile of this sample shows a merge of two peaks around 90 and 100 ml of elution. There was also a small peak at 40ml representing higher aggregates. From the chromatogram it is not evident whether the oligomers are separated from monomers (Figure 4.13 A and B). However, analysis on 17% SDS gels (silver stained) demonstrates that fractions eluted between 70-90 ml contain primarily low-n oligomers; fractions between 90-100 ml contain both monomers and oligomers (Figure 4.13 C). The oligomers-only and mixed fractions were collected separately, concentrated, and analyzed on 17% SDS gels to check the stability of the oligomers. This showed that the oligomers are stable and GA cross-linking was intact (data not shown). These G200 purified $Tau^{RD\Delta}$ oligomers were used for further studies.

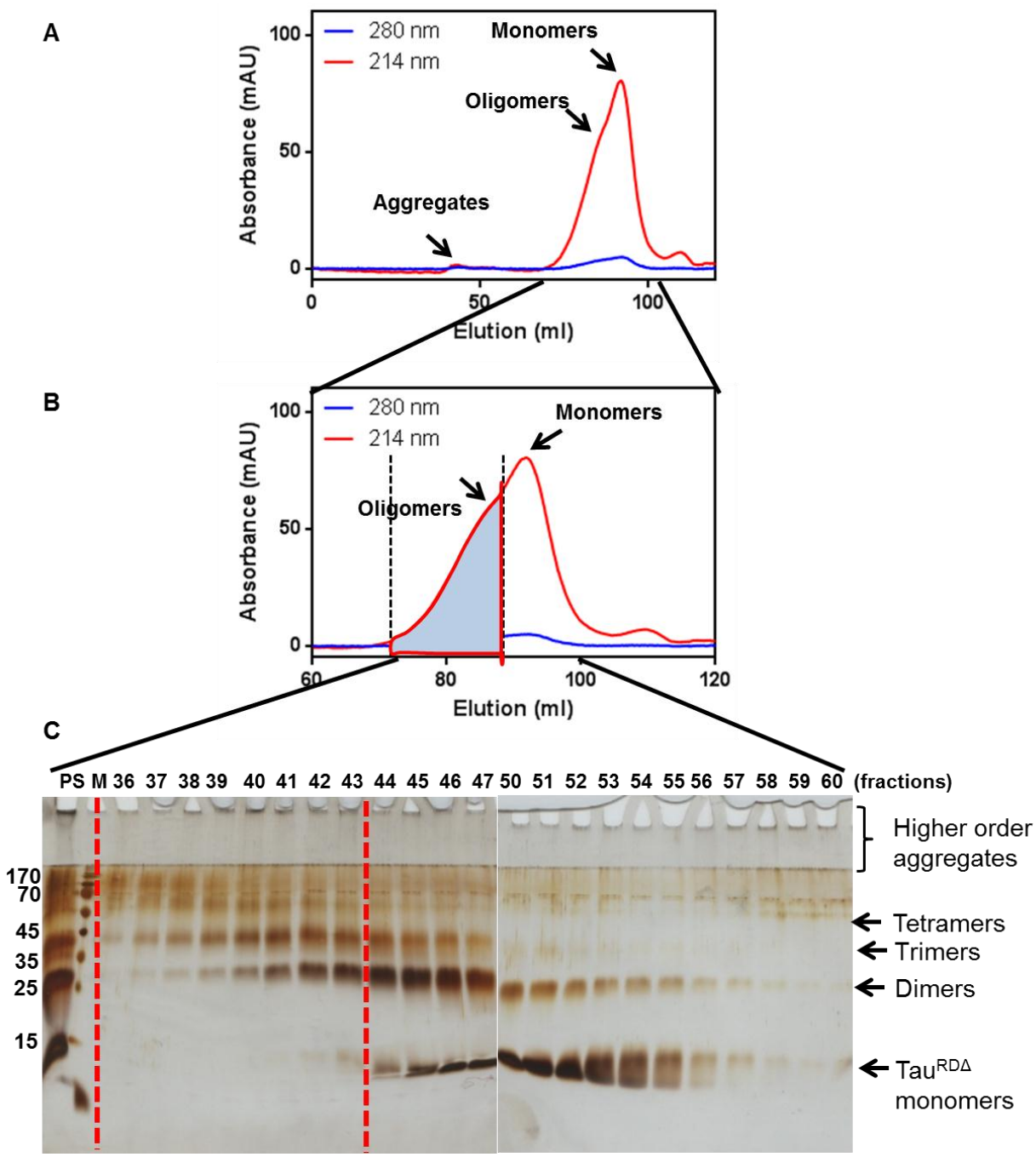

Figure 4.13 Large scale production of oligomers using a G200 column
$Tau^{RD\Delta}$ oligomers were run on a Superdex G 200 column to separate the oligomers from monomers. **A)** Representative chromatogram displaying the elution profile of $Tau^{RD\Delta}$ protein aggregated for 30 min and cross-linked with 0.01% GA. **B)** Magnification of the main peak from the chromatogram (A). The fractions from 70 to 100 ml (between dotted lines; shaded blue; fractions 36-43) contain only oligomers without monomer contaminations. **C)** The fractions were eluted and run on a 17% SDS gel and stained with silver. PS – Sample before FPLC, M – Marker, number denotes tube number of collected fractions.

4.6.3 Characterization of GA-stabilized oligomers purified by G200 column

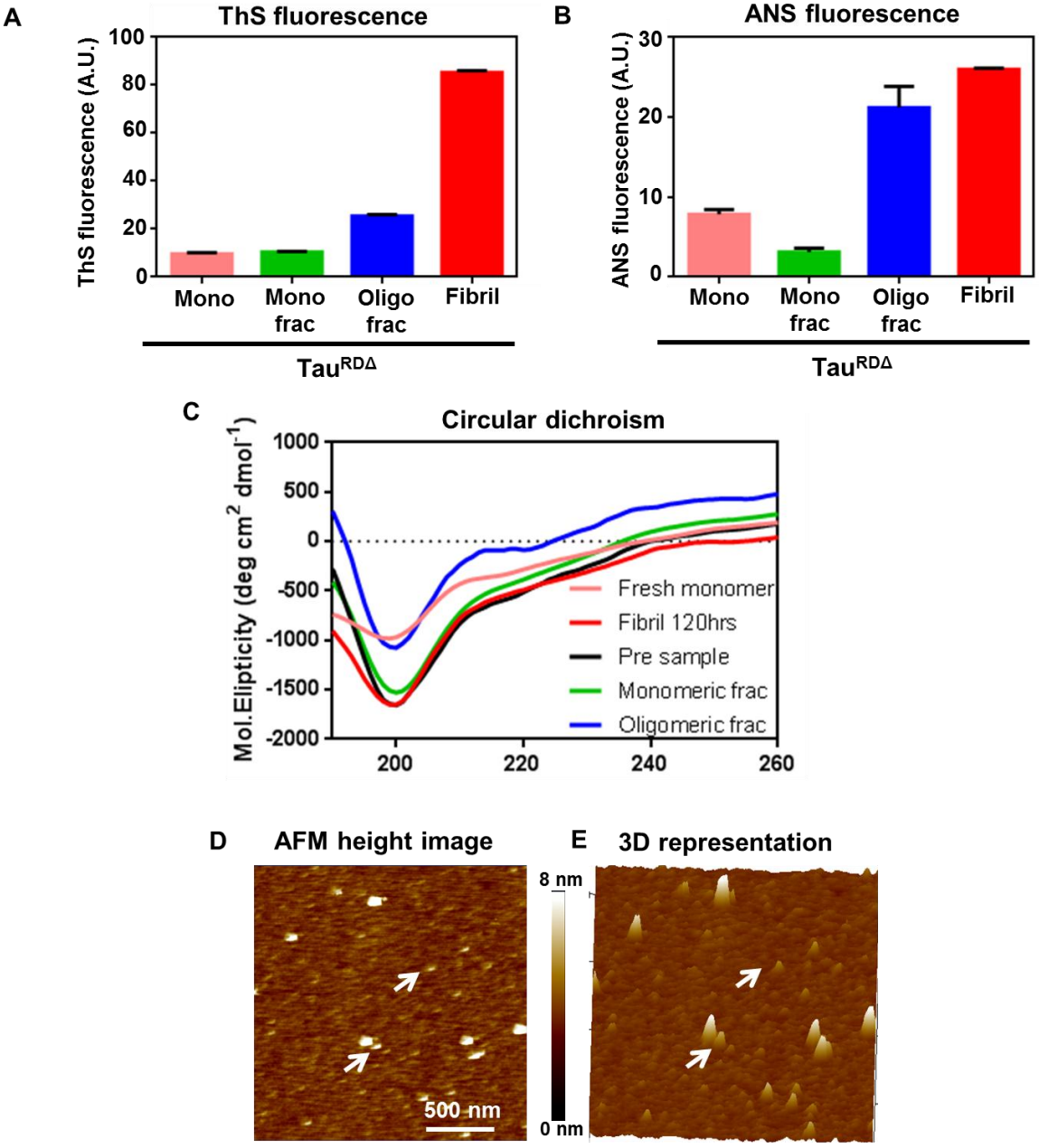

Figure 4.14 Characterization of oligomers purified by G200 column
A) The oligomeric fractions of the sample show a moderate (~2-fold) increase in ThS intensity compared to the monomer fraction, but a much larger increase (~9-fold) for the fibril sample. **B)** ANS fluorescence shows a pronounced increase (~4-fold) both for the oligomeric fractions and fibrillar fractions. **C)** Circular dichroism spectra display negative maxima at ~200 nm (indicative of natively unfolded structure) for monomer, oligomer and fibril samples. **D)** AFM height image and **(E)** its 3D-representation revealed oligomers corresponding roughly to 5-6nm (arrows).

The biophysical and structural analysis included spectroscopic methods like CD and fluorescence. For example, the dye ThS binds to extended ß-sheet structures and responds by an increase in fluorescence. $Tau^{RD\Delta}$ monomers showed only minimal

fluorescence, oligomers showed only a slight increase, but both were negligible compared to the ThS response of fibrils. This suggests that there is only minimal ß-sheet structure in the oligomeric fractions (Figure 4.14 A). Circular dichroism spectra confirmed that there is only minimal ß-sheet structure in oligomers, as the negative maximum was at ~200 nm, characteristic of random coiled structure. A similar pattern occurred in the fibrillar sample, indicating that the major part of the protein is unstructured. This could be due to the fact that $Tau^{RD\Delta}$ protein has only a few amino acids around the hexapeptide motifs in the R2 and R3 region to form ß-sheet structure (Figure 4.14 C). Whereas ThS reports on ß-sheet structure of a protein locally, CD is sensitive to the protein structure as a whole, which would explain the difference in the outcome by these two methods. Contrary to ThS, the dye ANS displayed a 4-5 fold increase in the fluorescence intensity in the oligomeric fraction compared to monomers, suggesting hydrophobic patches and/or cationic residues on the surface of the oligomers exposed by conformational changes (Figure 4.14 B). A similar increase occurred in the fibril sample. The dyes ThS and ANS show markedly different reactions with regard to oligomers and polymers of Tau. Finally, AFM demonstrates that the oligomers are roughly globular in shape, with a height less than 8nm (~7-8 monomers), consistent with low-n oligomers. (Figure 4.14 D and E; arrows).

4.6.4 Selection of the hydrophobic interaction chromatography column

After the preliminary characterization of the oligomers, the major concern was to enhance the amount of oligomers, as the G200 column was able to purifiy only ~50% of the total oligomeric protein. The reason is that substantial amounts of oligomers were needed for further characterization and for antibody generation. Therefore we searched for other methods to purifiy oligomers.

One hint was provided by the observation that $Tau^{RD\Delta}$ oligomers contain exposed hydrophobic microdomains as suggested by the increase in ANS fluorescence. This prompted us to apply hydrophobic interaction chromatography (HIC) to separate the oligomeric species from the monomers. We used the HIC selection kit (GE Healthcare) to identify a suitable column for oligomer separation. The selection kit comprises seven columns with different hydrophobicities. During the HPLC run, the hydrophilic molecules do not bind to the column and elute earlier in the flow-through whereas the bound hydrophobic proteins elute later. 1M ammonium sulfate

$(NH_4)_2SO_4$ buffer was used as an adsorption buffer which improves the binding of the hydrophobic protein to the column. A gradient of TBS pH 9.0 /water was used as an elution buffer. A decreasing concentration of salt reduces the interaction of the protein with the hydrophobic column matrix and thus allows detachment of the protein from the column.

The tests showed that the Butyl FF HiTrap 1ml column is able to separate the oligomers with high purity. The strongly hydrophilic $Tau^{RD\Delta}$ monomers did not bind to the column and eluted in the flow-through, whereas the more hydrophobic oligomers eluted later in the middle of the gradient (Figure 4.15 C). The silver stained gel picture illustrates that the flow-through contains only the monomer (Figure 4.15 D; red arrow). The quantification of the silver gel revealed that ~5% monomers were still present in the fractions so that oligomers (only low-n) were separated with a purity of ~95%. Similarly, other columns, e.g. the Phenyl Sepharose HP column was able to separate the oligomers with high purity, except that the recovery was lower (< 70%) (Figure 4.15 E). The Butyl Sepharose HP column was also able to separate the oligomers, but a fraction of oligomers eluted in the flow-through which made this column unsuitable for the oligomer preparation (Figure 4.15 A; red oval box). Similar results were obtained with the Phenyl FF column (Figure 4.15 H; red oval box). Three further columns were also tested but did not separate the oligomers from the monomers. The characteristics of the columns used and the results of the experiments are summarized in Table 4.1. For further work we used the Butyl FF column for purification of $Tau^{RD\Delta}$ oligomers.

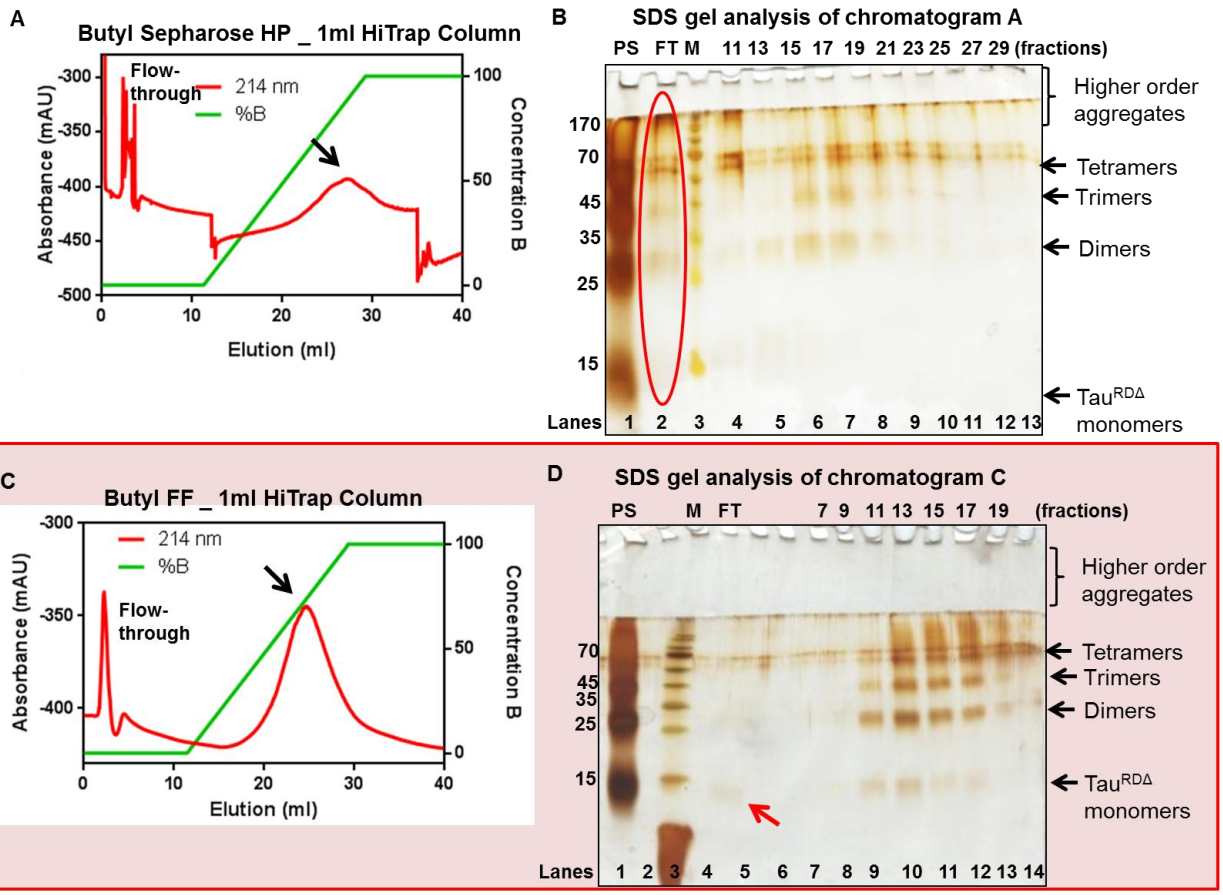
A
Butyl Sepharose HP _ 1ml HiTrap Column
Flow-through
214 nm
%B
Absorbance (mAU)
Concentration B
Elution (ml)
B
SDS gel analysis of chromatogram A
PS FT M 11 13 15 17 19 21 23 25 27 29 (fractions)
Higher order aggregates
Tetramers
Trimers
Dimers
Tau^RDΔ monomers
Lanes 1 2 3 4 5 6 7 8 9 10 11 12 13
C
Butyl FF _ 1ml HiTrap Column
214 nm
%B
Flow-through
Absorbance (mAU)
Concentration B
Elution (ml)
D
SDS gel analysis of chromatogram C
PS M FT 7 9 11 13 15 17 19 (fractions)
Higher order aggregates
Tetramers
Trimers
Dimers
Tau^RDΔ monomers
Lanes 1 2 3 4 5 6 7 8 9 10 11 12 13 14
E
Phenyl sepharose HP _ 1ml HiTrap Column
214 nm
%B
Absorbance (mAU)
Concentration B (%)
Elution (ml)
F
SDS gel analysis of chromatogram E
PS M FT 15 17 19 21 23 25 27 (fractions)
Higher order aggregates
Tetramers
Trimers
Dimers
Tau^RDΔ monomers
Lanes 1 2 3 4 5 6 7 8 9 10 11 12 13 14
G
Phenyl sepharose FF _ 1ml HiTrap Column
214 nm
%B
Absorbance (mAU)
Concentration B (%)
Elution (ml)
H
SDS gel analysis of chromatogram G
PS FT M 13 15 17 19 21 23 25 27 29 (fractions)
Higher order aggregates
Tetramers
Trimers
Dimers
Tau^RDΔ monomers
Lanes 1 2 3 4 5 6 7 8 9 10 11 12 13

Figure 4.15 Selection of the hydrophobic interaction chromatography column
Tau$^{RD\Delta}$ protein was incubated at 37°C for 30 min in TBS pH 9.0 and cross-linked with 0.01% GA for 10 min. The reaction was stopped by 10mM Tris HCl pH 8.8. The samples were run on the 1ml HiTrap HIC columns to select the suitable column for oligomer purification. The samples were adsorbed in the column by 1M $NH_4(SO_4)_2$ and eluted in 20 column volume of buffer with an increasing concentration of buffer B (H_2O) and reducing concentration of buffer A (TBS pH 9.0). The black arrows on the chromatogram show the oligomeric peak. The oligomeric peak fractions were run on a 17% SDS gel along with the flow-through sample and stained with silver. **(A)** The chromatogram of Butyl Sepharose HP column and **(B)** the respective silver stained SDS gel picture. **(C)** The chromatogram of Butyl FF column and **(D)** the respective silver stained SDS gel picture. **(E)** The chromatogram of Phenyl Sepharose HP column and **(F)** the respective silver stained SDS gel picture. **(G)** The chromatogram of Phenyl Sepharose FF column and **(H)** the respective silver stained SDS gel picture. PS – Sample before the HPLC run; FT – Flowthrough (red arrows on the gels); M – Marker; numbers on the top of the gels denote the fraction tube numbers in which the proteins were collected.

Column	Butyl FF	Butyl-S-FF	Butyl-S-HP	Phenyl S-FF (LS)	Phenyl-S-FF (HS)	Phenyl-S-HP	Octyl
Hydrophobic ligand	Butyl	Butyl-S	Butyl	Phenyl	Phenyl	Phenyl	Octyl
Ligand density	40µM/ml	10µM/ml	50µM/ml	25µM/ml	40µM/ml	25µM/ml	5µM/ml
Average particle size	90µm	90µm	34µm	90µm	90µm	34µm	90µm
Separation	Yes	No	Yes	Yes	No	Yes	No
Quality of separation	Good	-	Poor	Poor	-	Medium	-
Efficiency (approximately)	95%	-	70%	32%	-	68%	-

Table 4.1 Purification of Tau$^{RD\Delta}$ oligomers by hydrophobic interaction chromatography (HIC)

4.7 In vitro Characterization of Tau$^{RD\Delta}$ oligomers

4.7.1 Large scale preparation of Tau$^{RD\Delta}$ oligomers

Tau$^{RD\Delta}$ monomers (0 h) were diluted in TBS pH 9.0 and ran on a Butyl FF 16/10 column. The protein did not bind to the column although a high salt buffer was present as an adsorption buffer. Since Tau$^{RD\Delta}$ monomers are highly hydrophilic they did not bind to the column and hence the protein was collected as flow-through (Figure 4.16 A).

The next experiment shows $Tau^{RD\Delta}$ protein incubated in TBS pH 9.0 buffer at 37°C for 30 min and then cross-linked with 0.01% GA (oligomer sample) and run on the Butyl FF 16/10 column. As shown in Figure 4.16 B, the hydrophilic monomers eluted in the flow-through fractions, oligomers eluted in the middle of the gradient using the gradient buffer of TBS pH 9.0 / water. Decreasing the salt concentration by water released the oligomers from butyl ligand of the column. When using 1M $(NH_4)_2SO_4$ and TBS pH 9.0 as elution buffer it was not possible to elute the oligomers in the middle of the gradient, indicating a strong interaction of $Tau^{RD\Delta}$ oligomers with the butyl ligand of the column (data not shown). Finally we also checked whether a low concentration of adsorption buffer reduces the binding of the oligomers to the column. However, reducing the concentration of $(NH_4)_2SO_4$ to 0.5M in the adsorption buffer caused no binding of oligomers to the column (Figure 4.16 C). Therefore we conclude that the $Tau^{RD\Delta}$ oligomers can be separated by Butyl FF 16/10 column only with a high concentration of $(NH_4)_2SO_4$ as an adsorption buffer followed by TBS pH 9.0 + water gradient as an elution buffer. This experiment further confirms the presence of hydrophobic residues on the surface of $Tau^{RD\Delta}$ oligomers.

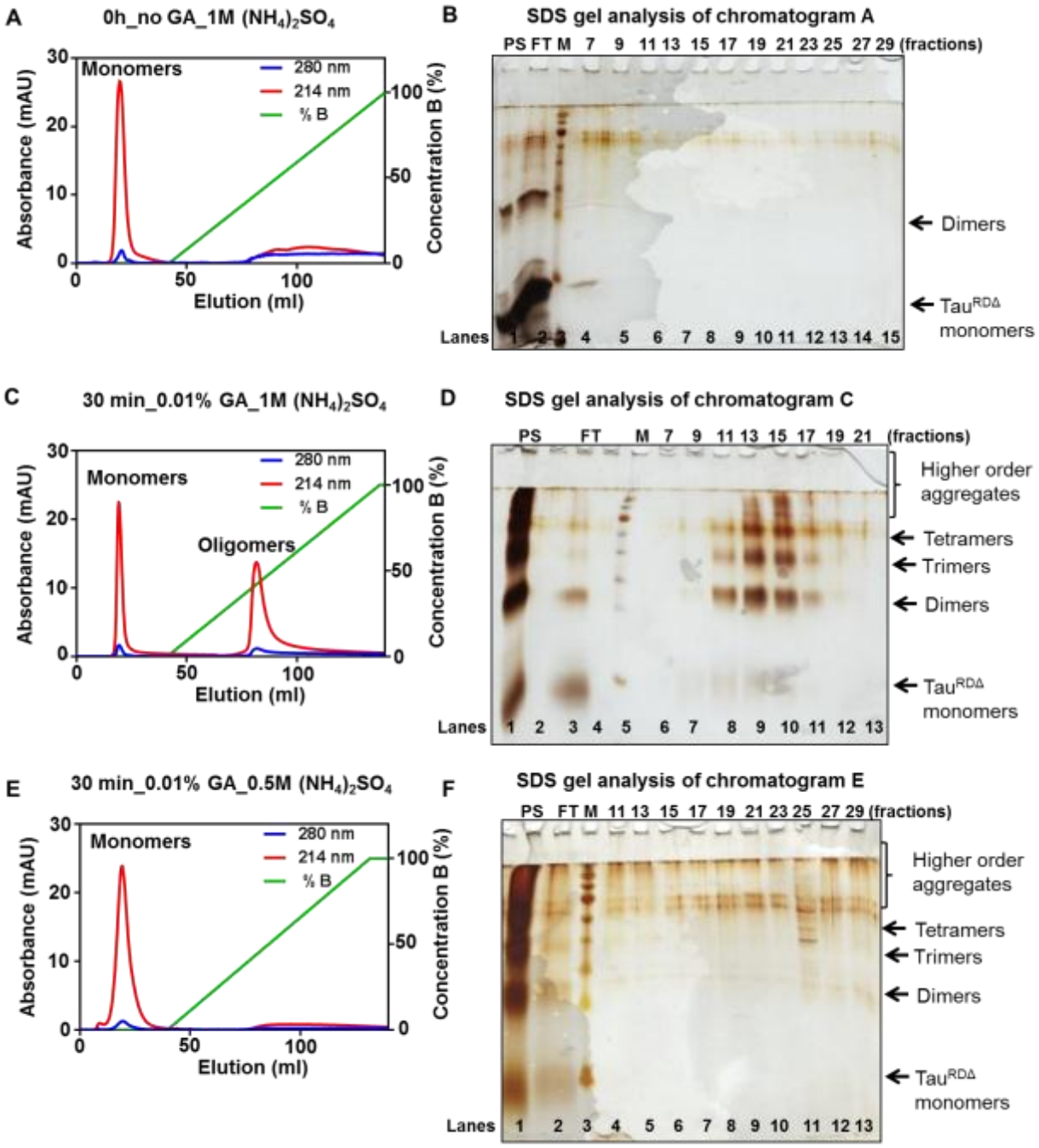

Figure 4.16 Large scale preparation of Tau$^{RD\Delta}$ oligomers by Butyl FF 16/10 column
1M $NH_4(SO_4)_2$ was used as an adsorption buffer and a TBS pH 9.0 / water gradient was used as an elution buffer. **A)** Tau$^{RD\Delta}$ monomers were run on Butyl FF 16/10 column. The hydrophilic monomers did not bind to the column and get eluted in the flow-through. **B)** The fractions were analyzed by SDS gel and stained with silver. **C)** Cross-linked Tau$^{RD\Delta}$ oligomers (30 min aggregation at 37°C and cross-linked) bound to the column and eluted in the TBS/ water gradient (in the middle of the gradient). **D)** The fractions were analyzed by SDS gel and stained with silver. **E)** Cross-linked Tau$^{RD\Delta}$ oligomers were run through the column with 0.5M $(NH_4)_2SO_4$ adsorption buffer. The chromatogram shows that the oligomers did not bind to the column. **F)** The fractions were analyzed by SDS gel and stained with silver. Note: Tau$^{RD\Delta}$ oligomers can be separated by Butyl FF 16/10 column only with a high concentration of $(NH_4)_2SO_4$ as an adsorption buffer followed by TBS pH 9.0 + water gradient as an elution buffer.

4.7.2 Tau$^{RD\Delta}$ oligomers undergo structural changes without ß-structure

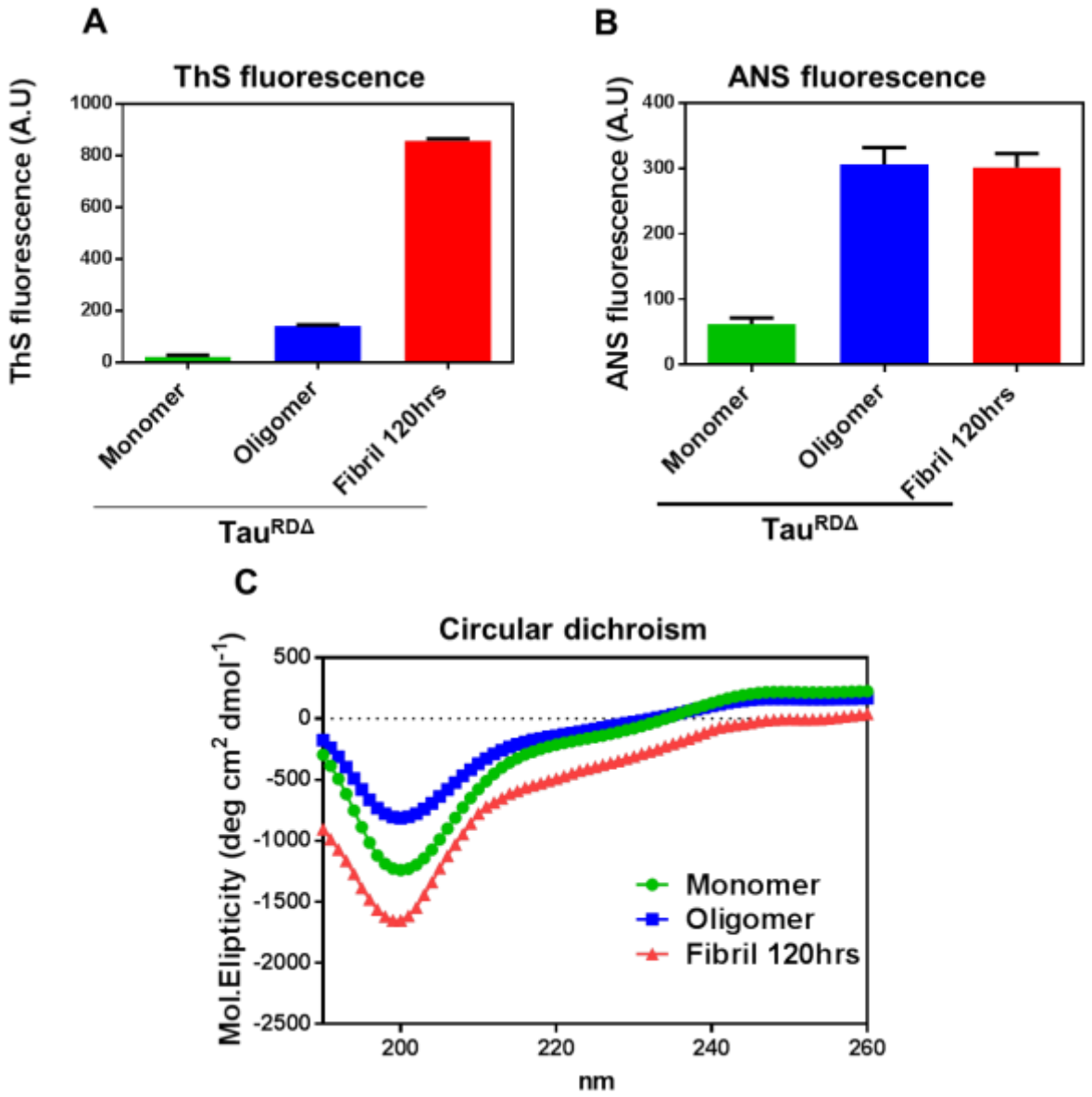

Figure 4.17 Biophysical characterization of purified Tau$^{RD\Delta}$ oligomers
Purified Tau$^{RD\Delta}$ oligomers were concentrated and buffer exchanged to PBS pH 7.4. **A)** Oligomers do not enhance ThS fluorescence, indicating a low content of ß-sheet structure. **B)** ANS fluorescence shows that the purified oligomers display an increase in ANS fluorescence due to surface exposed hydrophobic microdomains, confirming a conformational change in Tau$^{RD\Delta}$ during oligomerization. **C)** CD spectroscopy shows that monomers, oligomers and fibrils are all dominated by random coil structure (negative maximum at ~200 nm).

The Tau$^{RD\Delta}$ oligomers were concentrated by centrifugation using 3000 MWCO filters and the buffer was exchanged to PBS pH 7.4. Next we used ANS fluorescence to assess whether Tau$^{RD\Delta}$ oligomers underwent a structural rearrangement. Since monomers are hydrophilic, they do not bind to the ANS dye strongly. Tau$^{RD\Delta}$ oligomerization leads to an increase in ANS fluorescence up to 4-5 fold. A similar

increase occurred in the fibril sample of $Tau^{RD\Delta}$ (Figure 4.17 B) indicating that fibrils also have similar level of hydrophobicities as oligomers.

In order to investigate the contribution of ß-sheet structure which has been shown to be necessary to cause toxicity in the $Tau^{RD\Delta}$ cell and animal models, thioflavin S (ThS) and circular dichroism (CD) measurements were performed. We observed that there was a slight increase in the ThS intensity in the fractions containing pure oligomers compared to the monomer. However, when compared to fibril sample, the ThS intensity observed in oligomers was insignificant (Figure 4.17 A).

Changes in the secondary structure of oligomers were measured by CD analysis. $Tau^{RD\Delta}$ monomers showed the spectral minimum at 198 nm which is the typical absorption spectrum of a randomly coiled and natively unfolded protein structure. At the same wavelength (198 nm) $Tau^{RD\Delta}$ oligomers and $Tau^{RD\Delta}$ fibril also absorbed the maximum of circularly polarized light (Figure 4.17 C). The data obtained from ThS fluorescence and CD analyses suggest that $Tau^{RD\Delta}$ oligomers have a low content of beta sheet structure. In summary, the $Tau^{RD\Delta}$ oligomers undergo structural rearrangements without adopting ß-sheet conformation. The above data also confirm that the properties of $Tau^{RD\Delta}$ oligomers were not altered by Butyl FF 16/10 column.

4.7.3 Atomic force microscopy reveals globular $Tau^{RD\Delta}$ oligomers

The biophysical and biochemical characterization reveal that the protein undergoes structural rearrangements during oligomerization. The morphology of the $Tau^{RD\Delta}$ oligomers was analyzed by atomic force microscopy. $Tau^{RD\Delta}$ oligomers appear as punctate structures in height images (Figure 4.18 A). The amplitude images clearly distinguish the edges from the surface of the mica, arguing that the oligomers have a roughly globular shape (Figure 4.18 C). The 3-dimensional view of the height image precisely demonstrates the height of the oligomers (Figure 4.18 B). The observed height of the oligomers ranges from 1.6 nm to 15 nm (Figure 4.18 D) with an average of 3.7±1.9 nm. The majority of the oligomers (approximately 90%), have heights between 1.6 nm to 5.4 nm (corresponding to dimers up to hexamers), and only a few were >10nm (corresponding to 15-20 tau molecules).

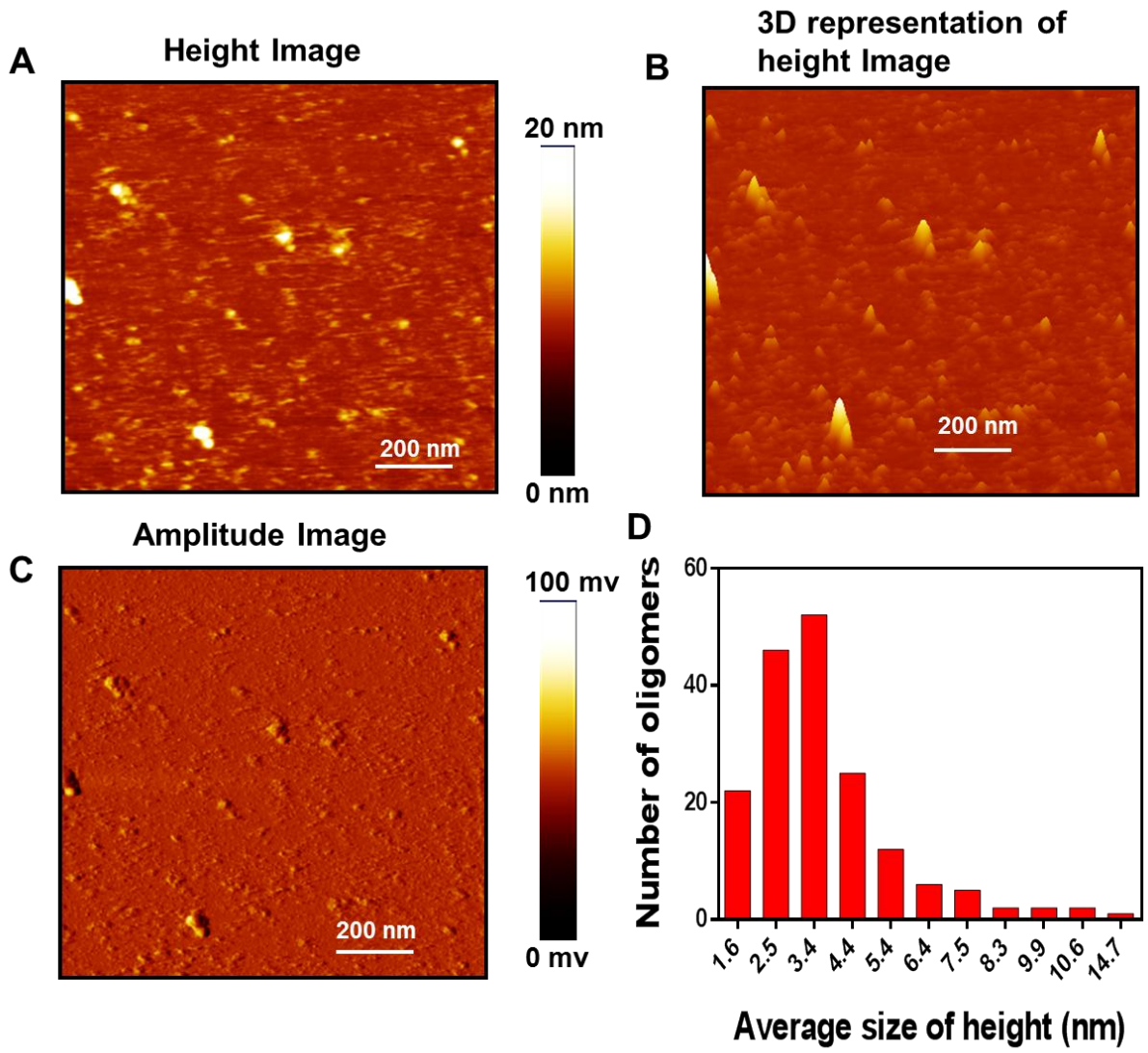

Figure 4.18 AFM characterization of globular Tau$^{RD\Delta}$ oligomers
Tau$^{RD\Delta}$ oligomers purified by the Butyl FF 16/10 column were imaged by atomic force microscopy in oscillation mode of imaging. **A)** Height image shows punctate structures ranging from 2 nm to 15 nm. **B)** 3D representation of the height image displays the height of the oligomers. **C)** Amplitude image shows globular shaped oligomers. **D)** Quantification of height of the Tau$^{RD\Delta}$ oligomers by nanoscope III software.

The average height of the monomer of Tau$^{RD\Delta}$ is not accurately known, as this protein does not stay in the monomeric state and also Tau$^{RD\Delta}$ monomers do not have a specific conformation. At early time points of oligomerization the average height is about 3.2±0.1 nm. For monomeric TauRD the height was reported as 1-2 nm (Kumar S.et.al 2014). Hence comparing with the TauRD monomers, the average size of the Tau$^{RD\Delta}$ oligomers appears to contain approximately 4-5 molecules of Tau$^{RD\Delta}$. This is broadly consistent with the SDS gel analysis showing predominantly dimers, trimers

and tetramers of Tau$^{RD\Delta}$ (Figure 4.16 B). These observations confirm that the oligomers formed by this specific preparation method are primarily low-n oligomers.

4.7.4 Hydrodynamic radius of oligomers

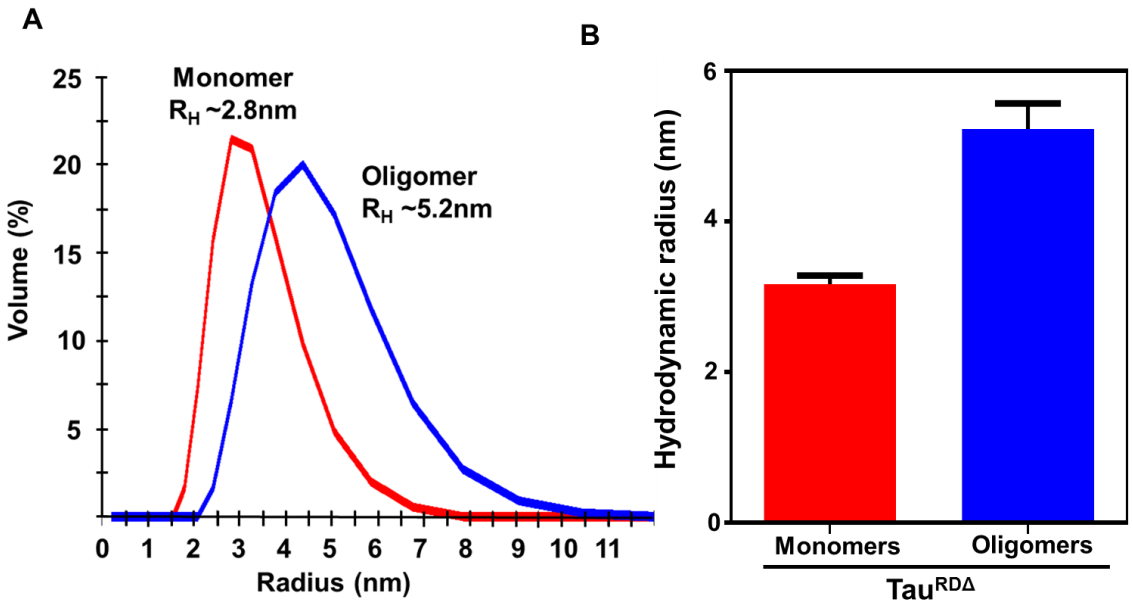

Figure 4.19 Hydrodynamic radius of Tau$^{RD\Delta}$ oligomers
The hydrodynamic radius of Tau$^{RD\Delta}$ monomers and oligomers were measured by dynamic light scattering. The samples were thermally equilibrated for 2 min before measurements were taken. **A)** Tau$^{RD\Delta}$ monomers and oligomers displayed the hydrodynamic radius of ~3nm and ~5-6 nm respectively. **(B)** The histogram shows that average of hydrodynamic radius of multiple experiments.

Next, we analyzed Tau$^{RD\Delta}$ oligomers by dynamic light scattering (DLS) which yields the effective hydrodynamic radius deduced from the fluctuations of scattered light. The average hydrodynamic radius of Tau$^{RD\Delta}$ monomers is 3.17±0.19 nm, in the case of oligomers it increases about 2-fold to 5.23±1.03 (Figure 4.19 A, B). This average value corresponds effectively to a stoichiometry of n=4, consistent with the mixture observed in SDS gels.

4.8 Functional characterization (extracellular effects) of Tau$^{RD\Delta}$ oligomers

A major question in the field of Tauopathies is whether Tau oligomers are toxic. In case of other amyloidogenic oligomers like Aß oligomers the toxic effects were shown to be strongly assay dependent (Wogulis et al., 2005) and the mechanism of toxicity and the nature of the toxic species are still a matter of debate. Thus, to make results comparable and to avoid false positive results, we first standardized the

methods to analyze the toxicity of the oligomers. $Tau^{RD\Delta}$ oligomers do not cause cell death in neuronal cell culture

4.8.1 $Tau^{RD\Delta}$ oligomers do not cause cell death in cell culture models

We tested 4 different assay systems to analyze the toxic properties of oligomers. In order to standardize the assay, the monomers and oligomers of $Tau^{RD\Delta}$ were incubated for different time intervals (24 h and 48 h), at different concentrations (1µM, 5µM and 10µM), using both SH-SY5Y human neuroblastoma cells and primary cortical neurons.

(1) The lactate dehydrogenase (LDH) assay of cell viability measures the LDH level in the cell culture medium, as the affected cells will lose their membrane integrity and increase the LDH level in the medium. Thus the amount of LDH in the medium is directly proportional to the amount of dead cells. The positive control (rupturing of membranes by Triton X-100) showed a clear increase of LDH, but samples treated with $Tau^{RD\Delta}$ for different periods and concentrations showed no release of LDH above background. Thus, judging by the standard LDH release assay $Tau^{RD\Delta}$ monomers and oligomers do not affect the membrane integrity of the cell and therefore show no detectable toxicity (Figure 4.20 A and B).

(2) A second parameter of toxicity is metabolic activity of the cells which can be measured by the reduction of MTT which is achieved by metabolically active cells and is therefore indirectly proportional to the dead cells. As controls, there was a pronounced loss of cell viability in cells treated with Triton X-100 (disrupting membranes). However, there was no change in cells treated with $Tau^{RD\Delta}$ monomers or oligomers (Figure 4.20 C and D). A variant of it is the XTT assay which measures the pyridine nucleotide redox status of cells controlled by the mitochondrial oxidoreductase. Consistent with the MTT assay, there was no change in the monomer and oligomer treated cells for both SH-SY5Y cells and rat primary cortical neurons (Figure 4.20 E and F).

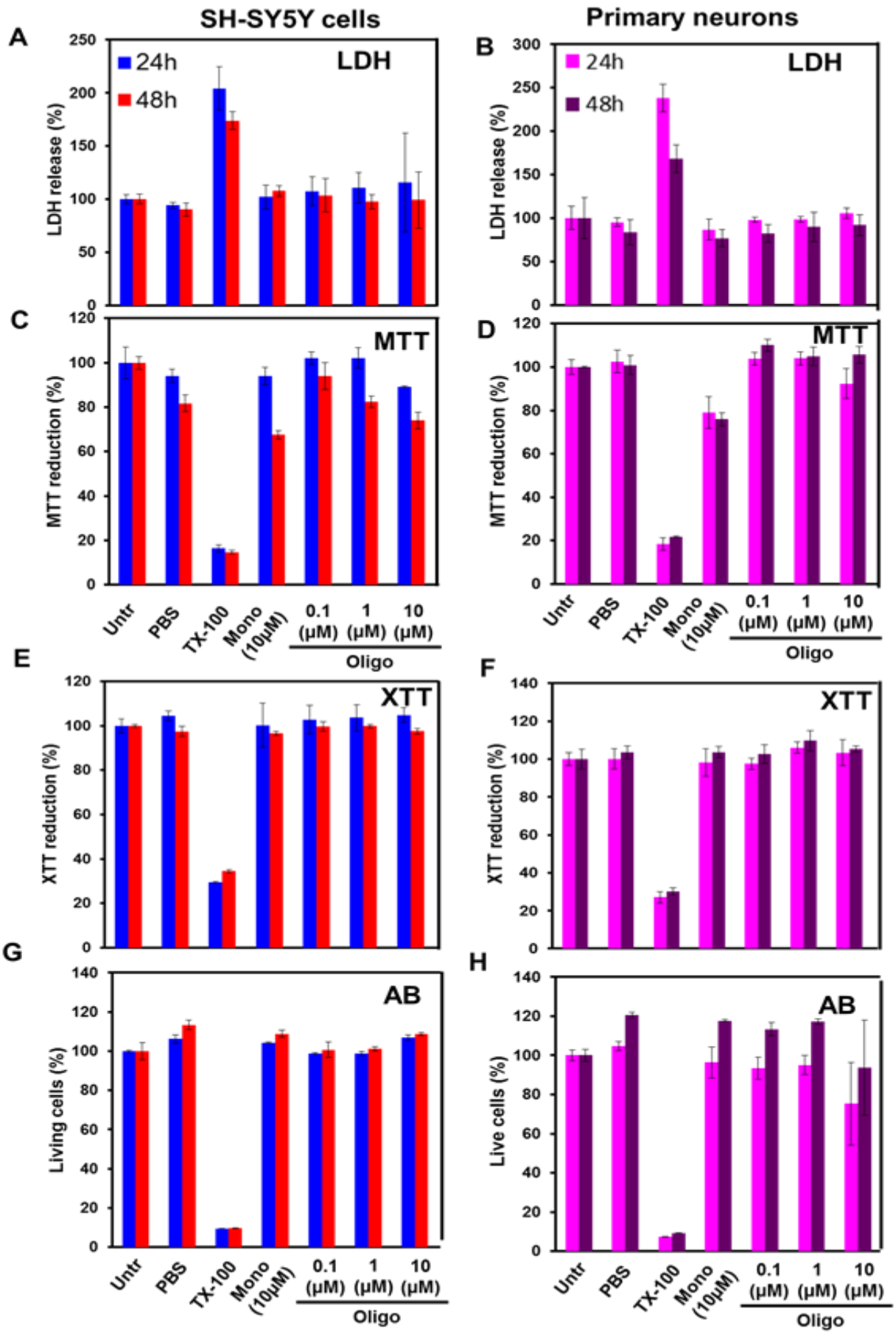
SH-SY5Y cells
Primary neurons
A
B
C
D
E
F
G
H
LDH
MTT
XTT
AB
24h
48h
LDH release (%)
MTT reduction (%)
XTT reduction (%)
Living cells (%)
Live cells (%)
Untr
PBS
TX-100
Mono (10μM)
0.1 (μM)
1 (μM)
10 (μM)
Oligo

Figure 4.20 Selection of assays for Tau-induced cell toxicity
The monomers and oligomers of $Tau^{RD\Delta}$ were incubated for different time intervals (24 h and 48 h), at different concentrations (1µM, 5µM and 10µM) with both SH-SY5Y cells (left panels) and rat primary cortical neurons (right panels). The toxic effects were monitored by LDH, MTT, XTT and Alamar blue (AB) assays. (**A-B)** LDH release assay, **(C-D)** MTT assay, **(E-F)** XTT assay, **(G-H)** Alamar Blue assay. Note that there is no difference between the untreated cells and $Tau^{RD\Delta}$ oligomer treated cells in all the assays. The MTT and LDH assays were chosen to measure toxicity in cell culture systems. Untr – Untreated; Tx-100 – Triton X-100 (2%).

(3) As a further criterion we used the Alamar Blue assay of cell viability. Upon entering cells, resazurin is reduced to resorufin, which produces a bright red fluorescence when it reacts with Alamar Blue. Viable cells continuously convert resazurin to resorufin, thereby generating a quantitative measure of viability or conversely, cytotoxicity. Consistent with the other methods, the Alamar Blue assay illustrates that monomers and oligomers are not toxic to the cells. (Figure 4.20 G and H). In summary, because of the differences in the responses to XTT and Alamar Blue, we decided to follow the MTT and LDH as a measure of toxicity.

Since the $Tau^{RD\Delta}$ oligomers are cross-linked, we also looked at the viability of the cells when treated with unpurified $Tau^{RD\Delta}$ oligomers which are formed from monomers after 30 minutes of incubation at 37°C without and with GA cross-linking. These unpurified oligomers in the non-cross-linked state or cross-linked state are also not toxic to rat primary neuronal cells analyzed by MTT and LDH assays (Figure 4.21 A, B). Similarly, the effects of non-cross-linked oligomers prepared in PBS pH 7.4 buffer were analyzed in SH-SY5Y cells without revealing toxicity by MTT assay (Kumar et al., 2014).

We also used several other controls (buffer from column, BSA, BSA cross-linked) to prove that GA neither induces toxicity nor blocks the toxic effects of a protein. We cross-linked bovine serum albumin (BSA, whose amino acid composition resembles that of Tau protein) at similar concentrations and applied it to SH-SY5Y cells. We did not observe any toxicity in cells treated with BSA or crosslinked BSA (Figure 4.21 C).

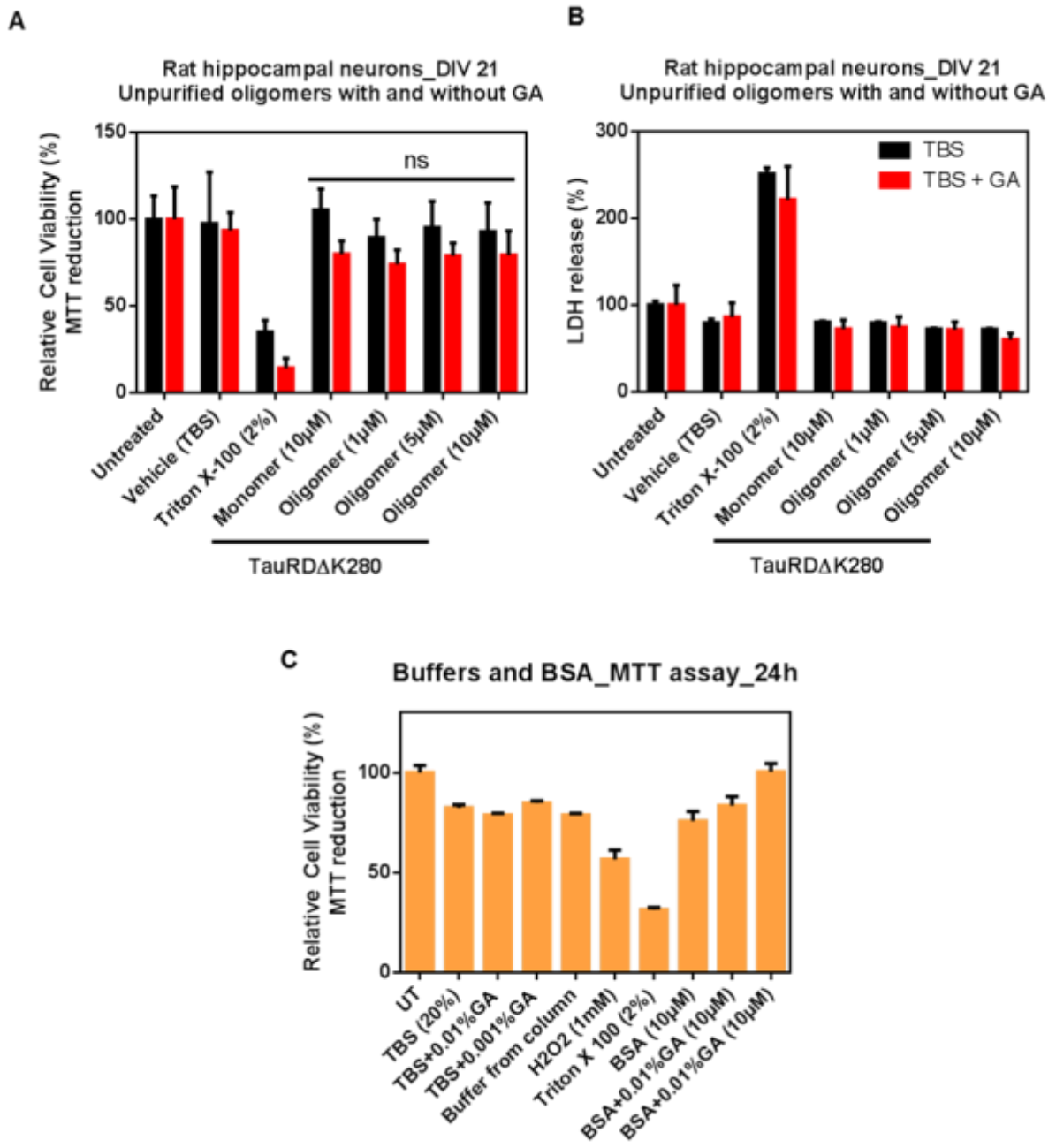

Figure 4.21 GA does not block the Tau$^{RD\Delta}$ mediated toxicity
Tau$^{RD\Delta}$ protein was incubated in TBS buffer, pH 9.0 for 30 min at 37°C. The sample was cross-linked with 0.01%GA and some portion was not cross-linked. The unpurified non-cross-linked and cross-linked oligomers were applied to rat primary hippocampal neurons for 24 h and the toxicity was analyzed by MTT **(A)** and LDH **(B)** assays. Results show that the non-cross-linked and cross-linked oligomers are not toxic to the neurons. **(C)** GA neither induces nor blocks the toxicity which was analyzed by MTT assay using other proteins like BSA and several buffer controls

In summary, all these results suggest that Tau$^{RD\Delta}$ oligomers are not toxic to the neuronal cell culture models and that crosslinking of Tau$^{RD\Delta}$ by GA does not alter the response of cells to Tau$^{RD\Delta}$.

4.8.2 Tau$^{RD\Delta}$ oligomers do not cause cell death in OHSC model

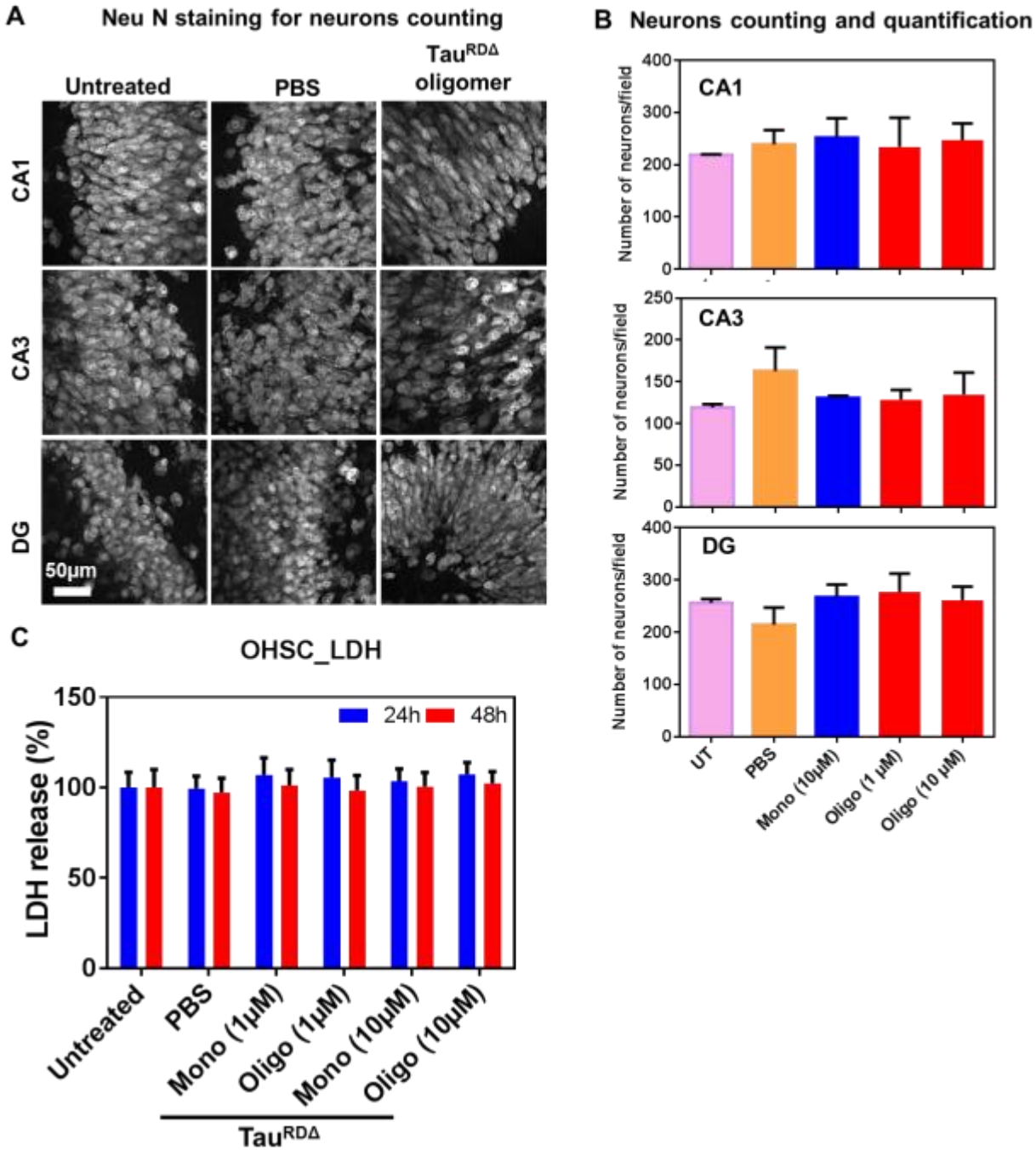

Figure 4.22 Tau$^{RD\Delta}$ oligomers do not cause cell death in the OHSC model
Hippocampal slices were prepared from 8 days old wild type mice and cultured for 11 days *in vitro*. Tau$^{RD\Delta}$ monomers and oligomers (1µM and 10µM) were incubated with the slices for 48 h. **A)** NeuN staining revealed that there was no neuronal loss in CA1, CA3 and DG of the hippocampus. **B)** There was no change in the neuronal number in all regions of the hippocampus (CA1, CA3 and DG). **C)** There was no increase in the LDH release in the oligomer and monomer treated slices compared to untreated slices.

Organotypic hippocampal slice cultures (OHSCs) represent an ex vivo method to examine mechanisms of neuronal injury. The advantage of OHSCs is that the basic

architecture and composition of the hippocampus is relatively well preserved. It was shown earlier that the $Tau^{RD\Delta}$ expressing mice display loss of neurons in the CA3 and other regions of the hippocampus (Mocanu et al., 2008, Messing et al., 2013). We reasoned that microglia and other cell types in the hippocampus might act as mediators for the cytotoxicity caused by $Tau^{RD\Delta}$ protein, which could explain why cytotoxicity was not observed in the cell culture system, and hence we utilized the OHSC model. OHSCs were prepared from p8 wild type mice and cultured for 11 days. $Tau^{RD\Delta}$ oligomers were applied on slices for 48 hours and the toxicity was measured by LDH release and total neuron counting. The LDH release assay showed that $Tau^{RD\Delta}$ oligomers did not cause any significant toxicity or cell death in slices even at higher concentrations (10µM) compared to monomer and buffer treated slices (Figure 4.22 C). Consistent with this, NeuN staining of the slices fixed after 48 hours of treatment with $Tau^{RD\Delta}$ oligomers revealed that there was no reduction in the neuronal number in all regions of the hippocampus (CA1, CA3 and DG) (Figure 4.22 A, B), suggesting that $Tau^{RD\Delta}$ oligomers do not cause cell death in the OHSC model as well.

4.8.3 Aggregation intermediates of full length Tau are not toxic

In the literature there have been claims that Tau oligomers prepared from full length Tau protein by different methods are highly toxic to the SH-SY5Y cell system (Lasagna-Reeves et al., 2010, Flach et al., 2012). We therefore checked the toxicity of aggregates of recombinant human full length Tau protein (ht40 wt) formed under different buffer conditions in the presence of heparin 16,000 at different time points. The presence of aggregates was confirmed by ThS and ANS fluorescence measurements (data not shown). In our hands, these aggregated Tau species formed in different conditions did not show any significant release of LDH when applied on the differentiated SH-SY5Y cells (Figure 4.23 B), and they did not show a significant reduction in cell viability by the MTT assay (Figure 4.23 A). This argues that wild type full-length Tau monomers and aggregates are not toxic to SH-SY5Y cells when present in the extracellular medium and suggests that the toxicity is not dependent on the domains of Tau.

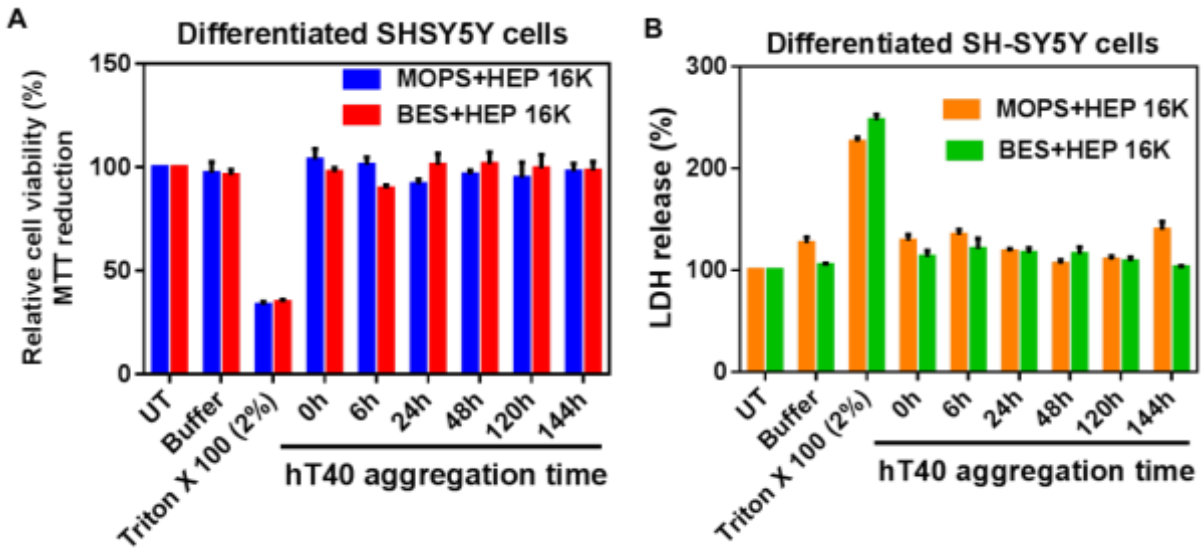

Figure 4.23 Tau^{FL} aggregation intermediates are not toxic to SH-SY5Y cells
Full length wild type recombinant Tau protein (2N4R) was aggregated in MOPS pH 7.0 and BES pH 7.0 buffers in the presence of heparin 16000 (protein to heparin ratio = 4:1). The aggregates formed at different time points were applied to the cell culture medium (7.5 µM for 48 h) on SH-SY5Y cells and the cytotoxicity was measured by LDH **(B)** and MTT **(A)** assays. No significant amount of LDH release or MTT reduction was observed after exposure of cells with full-length Tau aggregates

4.8.4 Tau$^{RD\Delta}$ oligomers cause loss of spines and postsynaptic proteins

Since Tau$^{RD\Delta}$ oligomers did not cause cell death to the neuronal cell culture and OHSC models, we focused on morphological changes in rat primary hippocampal neurons. We incubated Tau$^{RD\Delta}$ (monomers or oligomers) at 1µM concentration with rat primary hippocampal neurons (DIV 21) for 3 h. After 3 hours the cells were fixed and stained with phalloidin red which stains the actin filaments, a marker of spines, projecting away from dendritic shafts. Dendritic spines serve as a storage site for synaptic strength and help transmit electrical signals to the neuron's cell body. Most spines have a bulbous head (the spine head), and a thin neck that connects the head of the spine to the shaft of the dendrite. The most notable classes of spine shape are "thin", "stubby" and "mushroom". Spines with strong synaptic contacts typically have a large spine head (mushroom spines), which connects to the dendrite via a membranous neck. We observed up to 50% loss of spines in Tau$^{RD\Delta}$ oligomer treated cells compared to monomer treated cells. Moreover the majority of spines in the oligomer treated cells were of the "stubby" type (Figure 4.24 A arrow), whereas the PBS and monomer treated cells show mixture of thin, stubby and mushroom head spines. For quantification, the lateral projections of dendrites were counted as spines

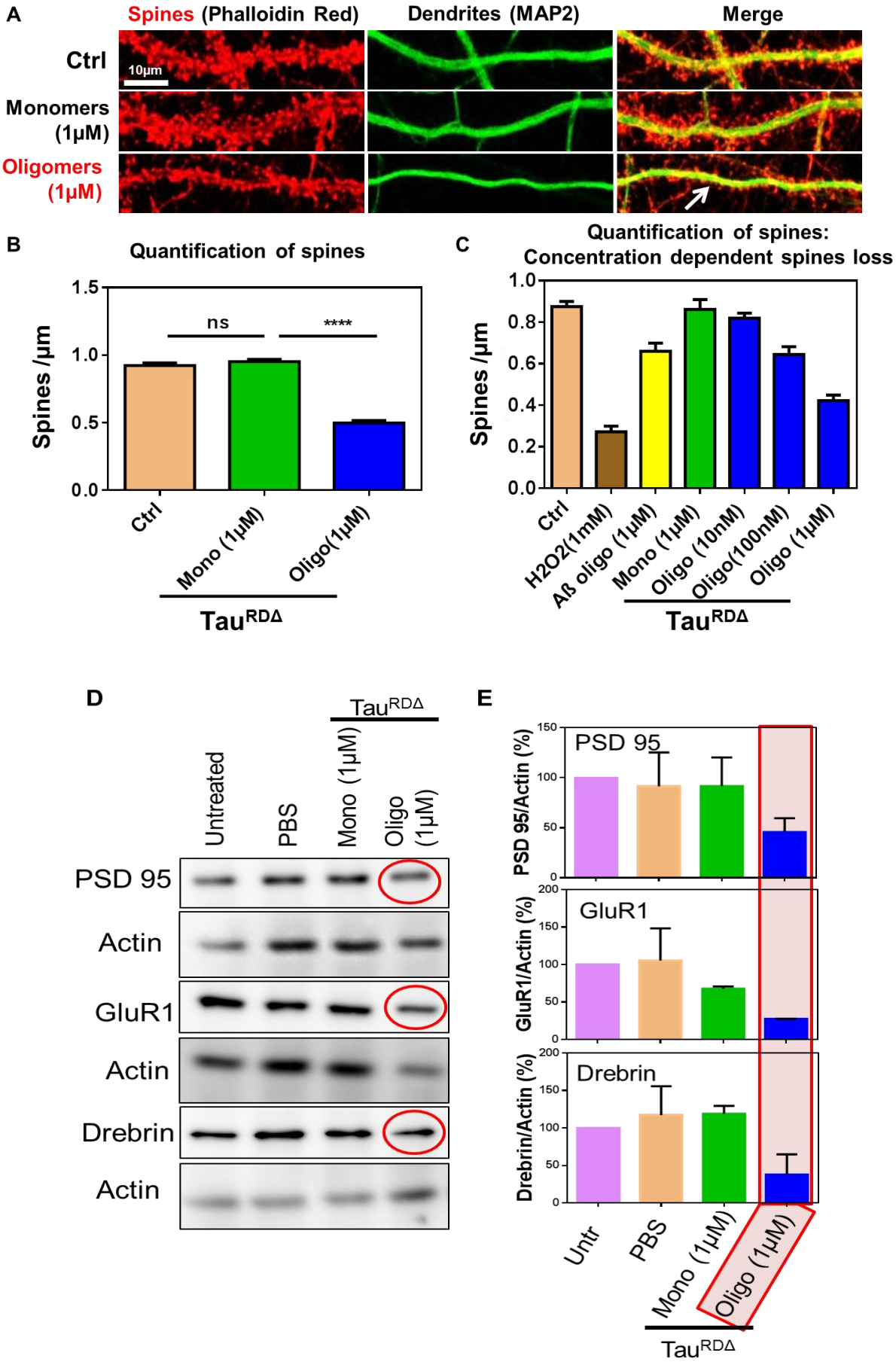
A
Spines (Phalloidin Red)
Dendrites (MAP2)
Merge
Ctrl
Monomers (1µM)
Oligomers (1µM)
10µm
B
Quantification of spines
Spines /µm
ns
****
Ctrl
Mono (1µM)
Oligo(1µM)
TauRDΔ
C
Quantification of spines:
Concentration dependent spines loss
Spines /µm
Ctrl
H2O2(1mM)
Aß oligo (1µM)
Mono (1µM)
Oligo (10nM)
Oligo(100nM)
Oligo (1µM)
TauRDΔ
D
TauRDΔ
Untreated
PBS
Mono (1µM)
Oligo (1µM)
PSD 95
Actin
GluR1
Actin
Drebrin
Actin
E
PSD 95
PSD 95/Actin (%)
GluR1
GluR1/Actin (%)
Drebrin
Drebrin/Actin (%)
Untr
PBS
Mono (1µM)
Oligo (1µM)
TauRDΔ

Figure 4.24 Tau$^{RD\Delta}$ oligomers reduce spine number and postsynaptic proteins
Rat primary hippocampal neurons (DIV 21) were treated with Tau$^{RD\Delta}$ oligomers (1µM) for 3 h. The cells were fixed and stained with phalloidin red which stains the actin filaments a major component of spines. **A)** A representative image shows the presence of spines; Cultures treated with PBS buffer and Tau$^{RD\Delta}$ monomers reveal no changes in the spine density whereas Tau$^{RD\Delta}$ oligomer treatment reduces the spine density up to 50%. Note that the Tau$^{RD\Delta}$ oligomer treated samples displayed more stubby spines (arrow). **B)** Quantification of spine density; **** p value <0.0001. **C)** Tau$^{RD\Delta}$ oligomers dependent loss of spines; **** p value <0.0001. **D)** Western blot analysis of postsynaptic proteins in the Tau$^{RD\Delta}$ oligomer treated samples (red circle). **E)** Quantification of D shows a significant reduction of post synaptic proteins PSD 95, GluR1 and Drebrin (pink shaded box).

whose head diameter was >1µm. Normal dendrites contain 1 spine/µm length. (Figure 4.24 A and B). Finally as shown earlier, there was no reduction in the spine numbers in the fibril treated samples (data not shown; See (Kumar et al., 2014).

Tau$^{RD\Delta}$ oligomers cause loss of spines at concentrations as low as 100nM. For comparison, 1µM Aß oligomers caused a spine reduction of ~30% (Zempel et al., 2010), comparable to that observed with 100nM of Tau$^{RD\Delta}$ oligomers. Lower concentrations (e.g. 10nM of Tau$^{RD\Delta}$ oligomers) did not lead to statistically significant changes (Figure 4.24 C).

To corroborate the findings we investigated the level of postsynaptic proteins in oligomer treated cells. PSD-95, a marker of postsynaptic spines, decreased up to 50% in the Tau$^{RD\Delta}$ oligomer treated cells, compared to buffer and monomer treated cells. Similarly, the GluR1 subunits of AMPA receptors decreased in the oligomer treated samples up to 70%; they are characteristic of mature spines and necessary for LTP and calcium signaling. Drebrin, a neuronal actin-binding protein involved in spinogenesis and synaptogenesis, was decreased by up to 50% consistent with the reduced number of spines (Figure 4.24 D and E).

4.8.5 Tau$^{RD\Delta}$ oligomers increase intracellular reactive oxygen levels

There are several reasons for selective spine loss in the absence of overt cell death, one of them being increased stress conditions (Chen et al., 2008) (Zempel et al., 2010). To test this, we determined the levels of reactive oxygen species as a measure of stress in the rat primary hippocampal neurons upon addition of Tau$^{RD\Delta}$ oligomers. If the level of ROS is increased the dye DCFDA becomes oxidized and converted to DCF which serves as a reporter of ROS.

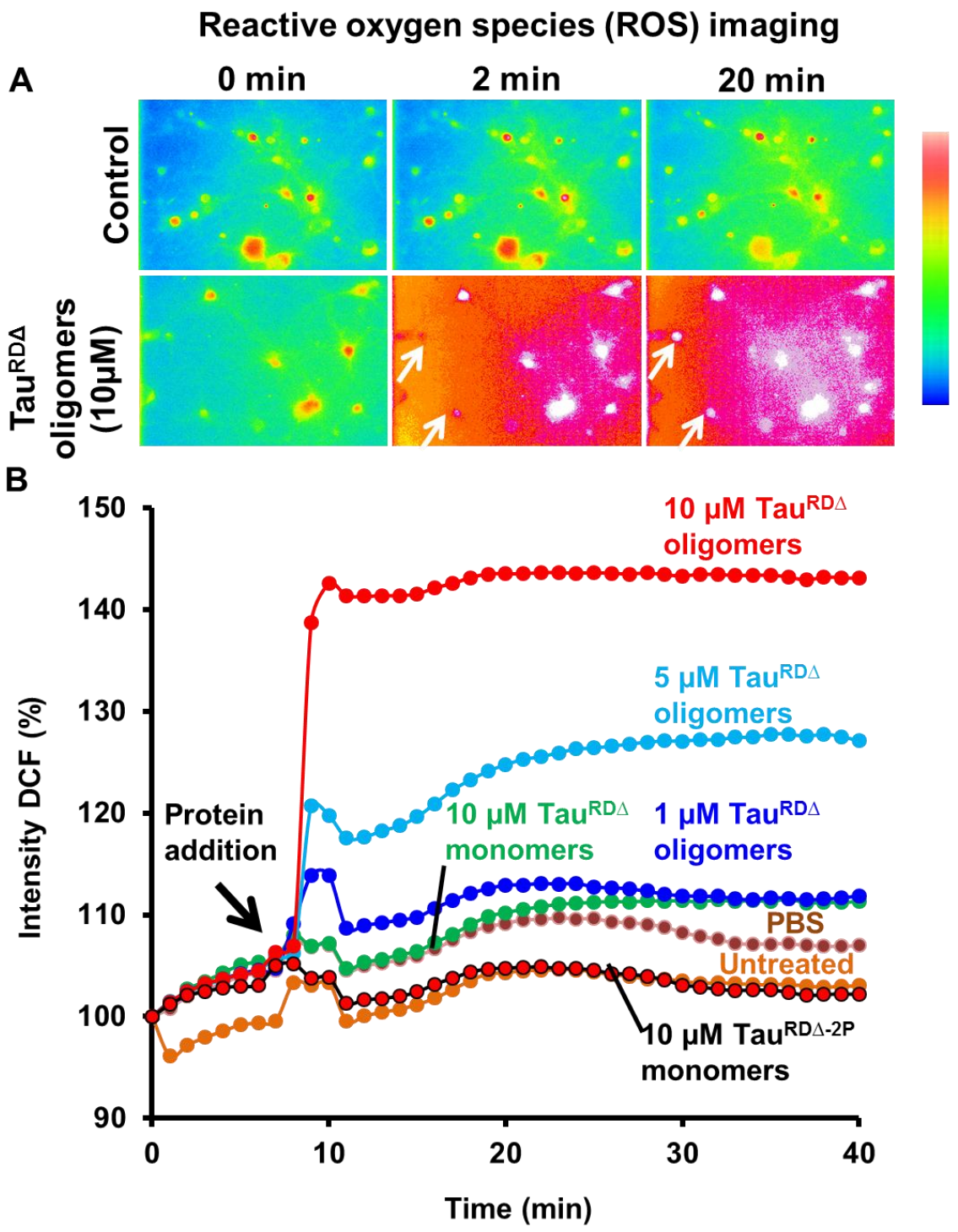

Figure 4.25 Tau$^{RD\Delta}$ oligomers increase the intracellular ROS production
Rat primary hippocampal neurons of 3-4 weeks old cultures were treated with Tau$^{RD\Delta}$ oligomers at different concentrations. Changes in the intracellular ROS level was monitored by live imaging using the DCFDA dye (the fluorimetric ROS sensor dye). **A)** Image displayed the ROS level at 0 time point or basal level which increases within 2 minutes of Tau$^{RD\Delta}$ oligomer addition and extends up to 20 minutes. The white arrows show the same cells at 2 minutes and 20 minutes time points which show time dependent increase in ROS. **(B)** Quantification of ROS level in a complete field, as the increase in the ROS level was observed in the whole culture including dendrites and axons. Note: There was a Tau$^{RD\Delta}$ oligomer concentration dependent increase in the ROS level in mature rat primary hippocampal neurons. The transitory hump immediately after protein addition could be due to slight mechanical disturbance of the sample.

We observed that there was $Tau^{RD\Delta}$ oligomer concentration dependent increase in the ROS production in the mature rat primary hippocampal neurons (Figure 4.25 B). Oligomers as low as 1µM were able to increase the DCF fluorescence up to 15%, rising up to 50% at 10µM oligomers. By contrast, monomers of $Tau^{RD\Delta}$ even at 10µM concentration did not cause any significant increase. The maximum fluorescence intensity of DCF within 2 minutes of incubation occurred in all cell compartments. These observations argue that $Tau^{RD\Delta}$ oligomers cause the production of ROS in rat primary hippocampal neurons.

Although overall, the ROS level reaches a maximum in 2 min, there are a few cells that show a time dependent increase in the ROS level reaching a maximum in ~20 min of incubation (Figure 4.25 A; white arrows). By contrast there was no or only a minor increase in the ROS level in the buffer control and monomer control treated cells. We conclude that $Tau^{RD\Delta}$ oligomers cause the production of ROS in rat primary hippocampal neurons.

4.8.6 $Tau^{RD\Delta}$ oligomers increase intracellular calcium levels

Calcium homeostasis is important to regulate the signaling in a cell. Therefore we next checked the calcium homeostasis of rat primary hippocampal neurons treated with $Tau^{RD\Delta}$ oligomers using the ratiometric dye fura-2 by live imaging. Fura-2 in its free form absorbs light at 380 nm and emits at 516nm. The excitation wavelength will be shorter (340 nm) when the dye binds to calcium. The ratio of 340 to 380 nm in $Tau^{RD\Delta}$ oligomer treated cells showed a steady concentration dependent increase in the intracellular calcium. The maximum signal was reached at 20 minutes of incubation with oligomers (10µM) and occurred in all cell compartments (Figure 4.26 A arrow). By contrast, there was no significant increase in the calcium level in the $Tau^{RD\Delta}$ monomer incubated cells even at higher concentration (10µM) (Figure 4.26 B). Interestingly, we saw up to 40% increase in the fura-2 calcium bound form in the cell body alone and the remaining percentage of increase must be from other compartments of a cell (Figure 4.26 C). These observations suggest that $Tau^{RD\Delta}$ oligomers increase the intracellular calcium level in the rat primary hippocampal neurons.

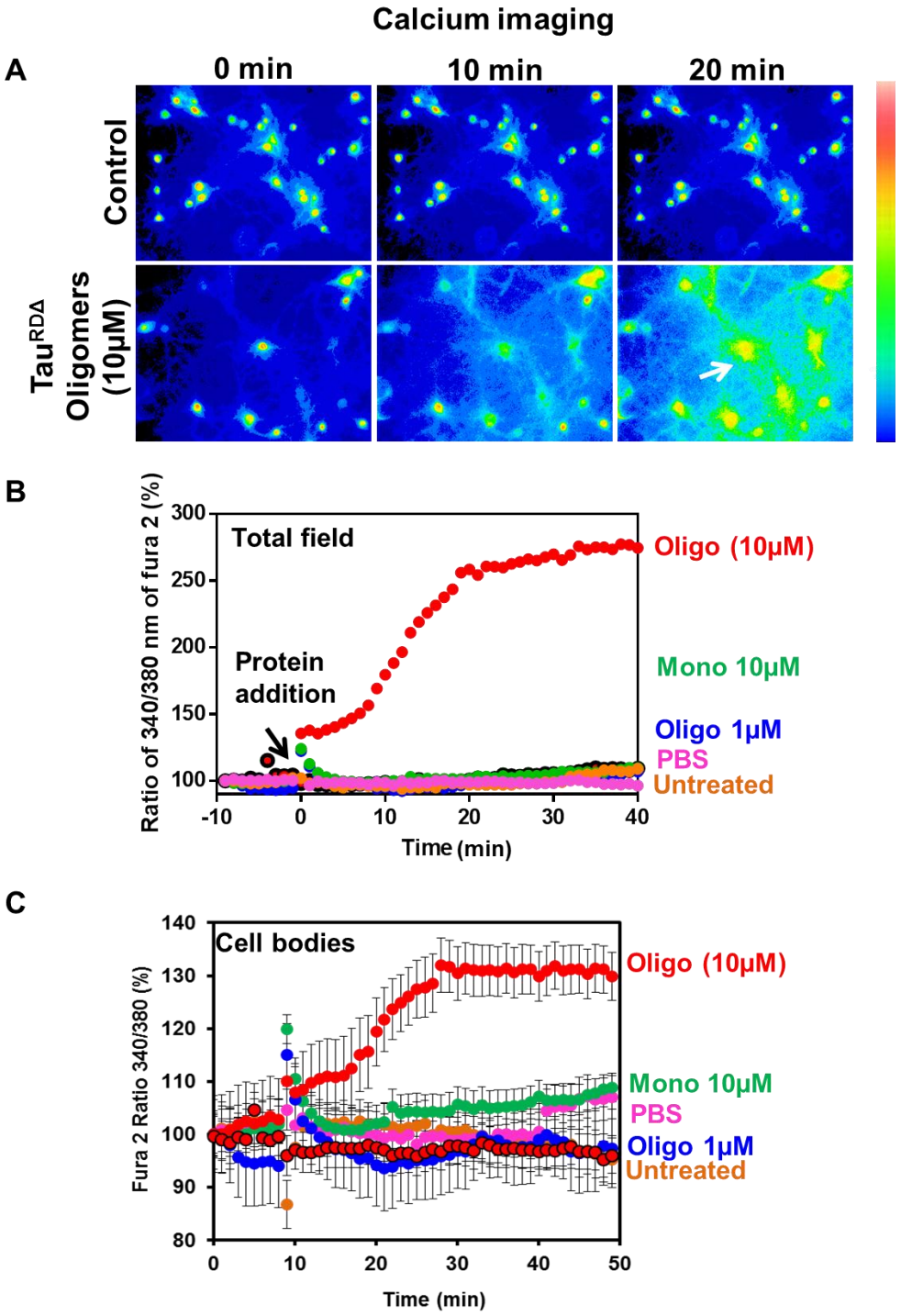

Figure 4.26 Tau$^{RD\Delta}$ oligomers increase the intracellular calcium level
Rat primary hippocampal neurons of 3-4 weeks old cultures were treated with Tau$^{RD\Delta}$ oligomers at different concentration and changes in the intracellular calcium level were monitored by Fura 2 ratiometric dye by live imaging. **A)** Image displays the calcium level at 0 time point or basal level which increased gradually and saturated in 20 minutes when Tau$^{RD\Delta}$ oligomers were applied. The white arrow at 10 minutes shows the increase of calcium in the dendrites and calcium and the white arrow at 20 minutes show that the cell bodies of Tau$^{RD\Delta}$ treated cells are filled with calcium **B)** Quantification of intracellular calcium level in a complete field, as the increase in the ROS level was observed in the whole culture including dendrites and axons. Note: There is a Tau$^{RD\Delta}$ oligomer concentration dependent increase in the ROS level in mature rat primary hippocampal neurons. **C)** Quantification of calcium solely in the cell bodies also showed an increase in the intracellular calcium level.

4.8.7 Tau$^{RD\Delta}$ oligomers do not cause phosphorylation and missorting of Tau

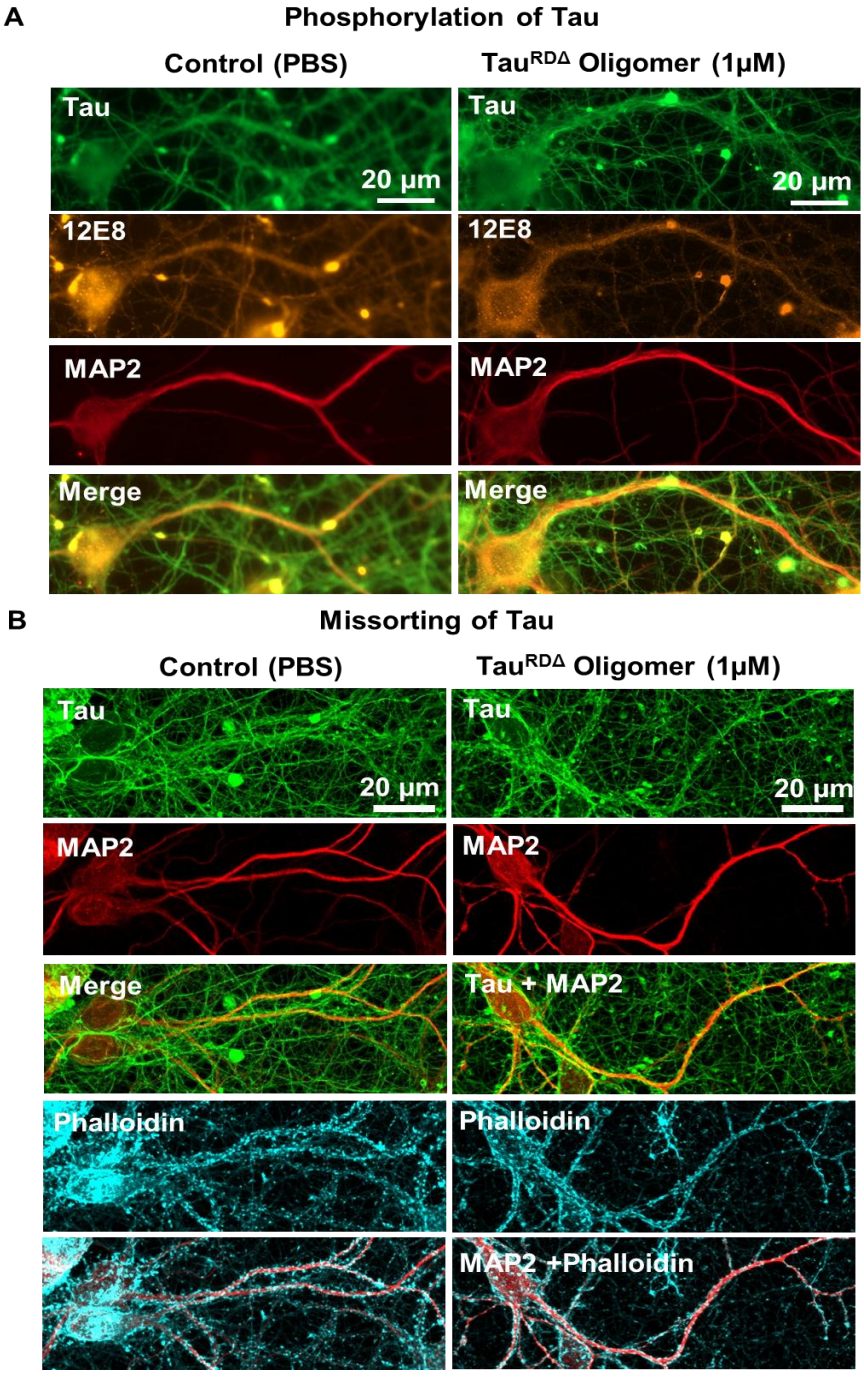

Figure 4.27 Tau$^{RD\Delta}$ oligomers do not cause phosphorylation and missorting of endogenous Tau
Tau$^{RD\Delta}$ oligomers were incubated with primary rat hippocampal neurons (DIV 21) for 3 hours and then the cells were fixed and immunostained for the following antibodies K9JA (detects total Tau), 12E8 (detects the phosphorylation of Tau at KXGS motifs), Phalloidin CF405 (dye binds to actin) and MAP2 antibody (dendritic marker). **A)** There is no increase in the intensity of 12E8 antibody signal in oligomer treated cells compared to buffer control **B)** There is no missorting of Tau cells treated with buffer or oligomers (Tau+MAP2). Missorting of endogenous Tau is not necessary for reduction in spine density. However, severe spine loss occurs in oligomer treated cells and those dendrites do not reveal increased levels of endogenous Tau.

Tau protein is primarily an axonal protein. During disease and stress conditions, it can become missorted into the dendrites of a neuron and phosphorylated at several

sites (Zempel et al., 2010, Zempel et al., 2013). We therefore investigated whether $Tau^{RD\Delta}$ oligomers also cause the phosphorylation and missorting of endogenous Tau. $Tau^{RD\Delta}$ oligomers were incubated with primary rat hippocampal neurons (DIV 21) for 3 hours and then the cells were fixed and immuno stained for 12E8 (KXGS motifs phospho tau antibody), K9JA (total Tau antibody) and MAP2 antibody (marker for dendrites). We did not observe any significant increase in the intensity of 12E8 antibody in the $Tau^{RD\Delta}$ oligomer treated sample suggesting that there is no phosphorylation of Tau at KXGS motifs (Figure 4.27 A). We also checked the phosphorylation of Tau at other sites (e.g. using the antibody AT8) and did not observe an increase in the phosphorylation (data not shown).

We next performed double immunostaining with MAP2 and K9JA antibody to test the missorting of Tau, but this was not observed, as we did not observe co-localization of K9JA antibody (Tau) and MAP2 antibody (dendrites). Tau protein was present only in the axons, not in the cell body and dendrites. (Figure 4.27 B), even though there was a reduction in the spine density in the oligomer treated samples (Figure 4.27 B) compared to buffer control. This observation suggests that missorting of endogenous Tau is not essential for the spine loss in $Tau^{RD\Delta}$ oligomer treated cells.

4.8.8 $Tau^{RD\Delta}$ oligomers act as seeds for intracellular Tau aggregation

It is an open question whether $Tau^{RD\Delta}$ oligomers present in the extracellular medium induce the aggregation of intracellular Tau. Therefore, we applied the $Tau^{RD\Delta}$ protein (monomers and oligomers) directly on the cell culture medium of SH-SY5Y cells at different concentrations for 15 h and the aggregation of Tau was monitored by ThS positive cells using flow cytometry. As shown in Figure 4.28 f, $Tau^{RD\Delta}$ oligomers treated cells displayed a very low percentage of ThS positive cells (0.115%) when applied extracellularly. We also observed that there is a 2 fold increase in the ThS positive cells in the $Tau^{RD\Delta}$ oligomers treated cells (0.115%) compared to monomer treated cells (0.055%) (Figure 4.28 c and f). The fact that the anti-aggregant mutant $Tau^{RD\Delta\text{-}PP}$ monomers did not show any increase in the ThS positive cells compared to untreated samples confirms that anti-aggregant mutant does not aggregate and does

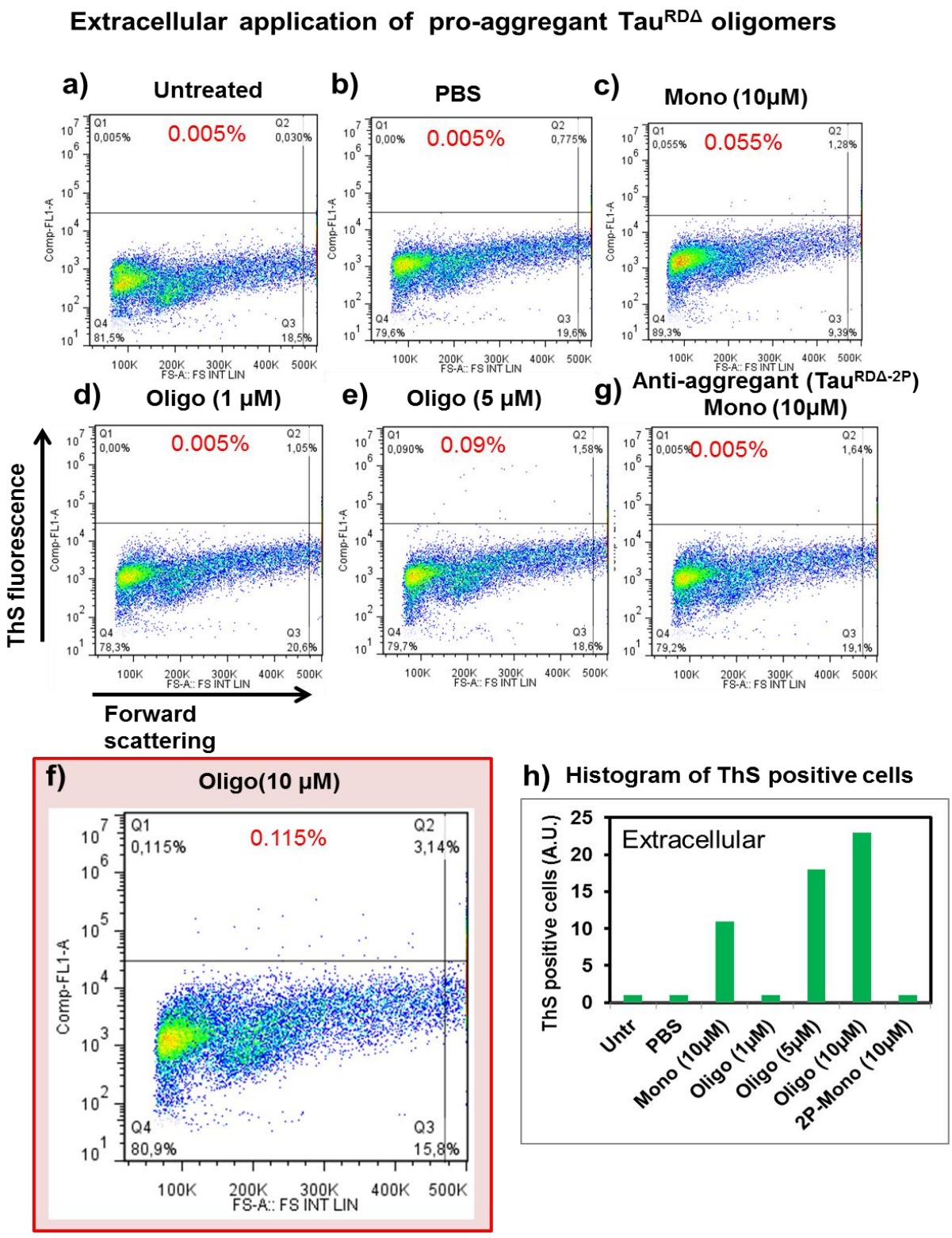

Figure 4.28 Extracellular Tau^{RDΔ} oligomers act as seeds
Tau^{RDΔ} proteins were applied directly on the SH-SY5Y cells for 15 hours. 1 h prior to the 15 h of incubation, 0.0005% ThS dye was added for 1 h and then ThS positive cells were counted using flow cytometry. Oligomers at 5 and 10µM concentration **(e and f)** showed very small percentage of ThS positive cells but higher than the monomer treated cells **(c)**. There was a ~2-fold increase in the ThS positive cells in oligomer treated cells (0.115%) (Red box) compared to monomer treated cells (0.055%). Note: Anti-aggregant Tau **(g)** does not show ThS positive cells, similar to untreated cells. **(h)** Histogram summarizing ThS positive fractions in the different conditions.

not induce the aggregation of endogenous Tau protein. Hence this result suggests that extracellular $Tau^{RD\Delta}$ oligomers can act as seeds to some extent.

4.9 Intracellular effects of $Tau^{RD\Delta}$ oligomers

4.9.1 $Tau^{RD\Delta}$ oligomers aggregate into filaments after transfection into SH-SY5Y cells

Since Tau is an intracellular protein and the aggregation of Tau occurs inside the cells during disease conditions, we delivered the $Tau^{RD\Delta}$ oligomers directly inside the cells (SH-SY5Y and rat primary hippocampal neurons) using Xfect protein transfection reagent.

The aim was to understand the toxic properties of $Tau^{RD\Delta}$ oligomers when present inside the cells. 15 hours after delivery of protein inside SH-SY5Y cells, $Tau^{RD\Delta}$ oligomers were able to induce Tau aggregation inside the cells. The aggregation was analyzed by counting ThS positive cells using flow cytometry.

The number of ThS positive cells after treatment (delivered inside the cells) with $Tau^{RD\Delta}$ monomer (10µM) (0.515%; Figure 4.29 d) increased significantly compared to control (Figure 4.29 a, b and c). However, the number of ThS positive cells in $Tau^{RD\Delta}$ oligomer (10µM) transfected cells (5.99%; Figure 4.29 g) was increased to 12-fold higher than the level achieved by monomers. $Tau^{RD\Delta}$ oligomers showed a concentration dependent increase in the ThS positive cells (Figure 4.29 e,f and g). We also used anti-aggregant mutant ($Tau^{RD\Delta\text{-}PP}$) monomeric protein which generated 5-fold less ThS positive cells (0.11%) (Figure 4.29 h) compared to pro-aggregant $Tau^{RD\Delta}$ monomers (0.515%) and 50 fold less ThS positive cells compared to $Tau^{RD\Delta}$ oligomers delivered cells (5.99%) (Figure 4.29). This result demonstrates that $Tau^{RD\Delta}$ oligomers could act as seeds and assemble to ThS positive Tau aggregates. The likely explanation for the increase in the ThS positive cells in $Tau^{RD\Delta}$ monomers transfected cells could be the presence of small oligomeric species in the monomer sample when delivered to the cells.

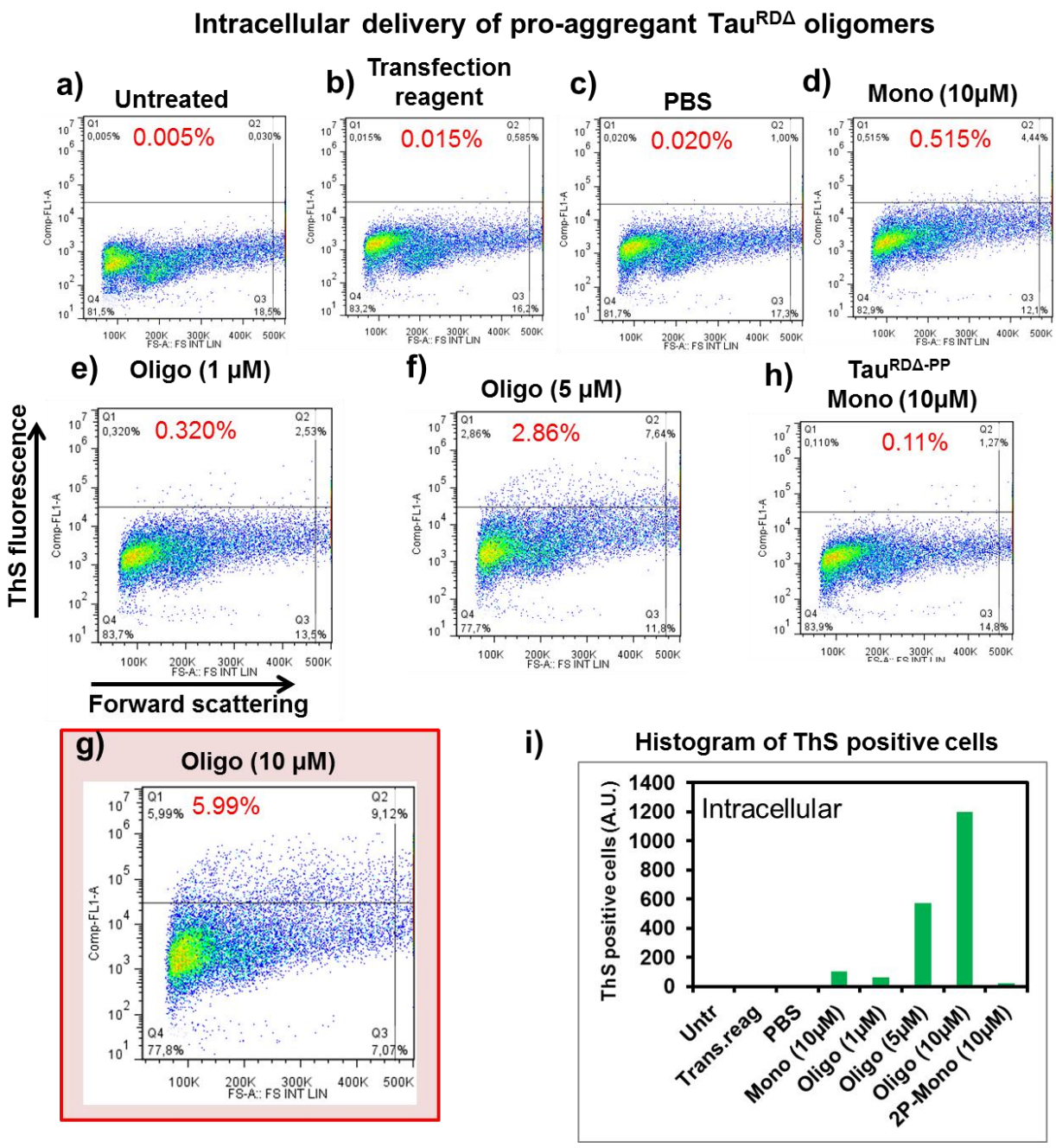

Figure 4.29 Intracellular delivery of Tau$^{RD\Delta}$ oligomers causes aggregation of Tau
SH-SY5Y cells were treated with Tau$^{RD\Delta}$ monomers or oligomers (intracellular delivery using Xfect transfection reagent kit) for 15 h. 1 h prior to the 15 h of incubation, 0.0005% ThS dye was added for 1 h and then ThS positive cells were counted using flow cytometry. Increased fractions of ThS positive cells were observed in an oligomer concentration dependent manner (up to ~6%) **(e, f, g),** compared with only low numbers of ThS positive cells in monomer transfected cells (~0.5%) **(d)**. **(i)** Histogram summarizing ThS positive fractions in the different conditions.

4.9.2 Tau$^{RD\Delta}$ oligomers recruit endogenous Tau into filaments

We next investigated the composition of aggregates in the oligomer treated cells. As Tau$^{RD\Delta}$ oligomer treated cells showed more ThS positive cells, it is important to demonstrate the composition of aggregates. We delivered Tau$^{RD\Delta}$ oligomers inside SH-SY5Y cells (by Xfect) and incubated them for 15 hours. The lysates of SH-SY5Y

cells were separated as soluble and insoluble fractions by centrifugation at 100,000x g. Analysis of these lysates by immunoblotting with pan Tau antibody K9JA demonstrated a large amount of aggregates in the pellet fraction of $Tau^{RD\Delta}$ monomer and oligomer delivered cells. By contrast, there were no aggregates in the pellet fraction of the untreated, PBS treated or $Tau^{RD\Delta\text{-}PP}$ monomer delivered cells. As observed in flow cytometry, we also observed a concentration dependent increase in the aggregates in the pellet fractions of $Tau^{RD\Delta}$ oligomers delivered cells. Remarkably we observed a large amount of aggregates in the monomer sample (Figure 4.30 A) but a reduced number of ThS positive cells (Figure 4.29 d). One possible explanation is that $Tau^{RD\Delta}$ monomers induced aggregates do not attain ß-sheet conformation detected by ThS dye within 15 hours of delivery.

We also analyzed whether the endogenous human full length Tau was recruited to the growing fibrils. We probed the blot with CP27 (Tau N-terminal specific) antibody. As $Tau^{RD\Delta}$ oligomers do not contain the N-terminal sequence, $Tau^{RD\Delta}$ protein is not detected by the CP27 antibody. Surprisingly, $Tau^{RD\Delta}$ oligomer-delivered cells showed CP27 positive aggregates in the pellet fractions which were absent in the $Tau^{RD\Delta}$ monomer-delivered cells (Figure 4.30 B). This suggests that only $Tau^{RD\Delta}$ oligomers could act as seeds to recruit the endogenous full-length Tau into the aggregates in SH-SY5Y cells. We also observed the increase in ThS positive cells in $Tau^{RD\Delta}$ oligomer-delivered cells in N2a cells expressing $Tau^{RD\Delta}$ protein (data not shown), confirming that the results are not cell dependent.

We next checked the ability of $Tau^{RD\Delta}$ oligomers to induce the aggregation of Tau in rat primary hippocampal neurons. As expected, we observed a concentration dependent increase in the aggregates in the lysates of $Tau^{RD\Delta}$ oligomer delivered cells compared to monomers analyzed by immunoblotting with the K9JA antibody. Interestingly we observed less aggregates in the $Tau^{RD\Delta}$ monomer delivered cells unlike in SH-SY5Y cells (Figure 4.30 C).

We also checked the ability of fibrils to induce aggregation. $Tau^{RD\Delta}$ fibrils generated in vitro and delivered into cells generated less aggregates compared to the $Tau^{RD\Delta}$ oligomer treated cells, as analyzed by blots of cell extracts. However, it is not known, whether the aggregates observed in the gel pockets are the transfected fibrils or

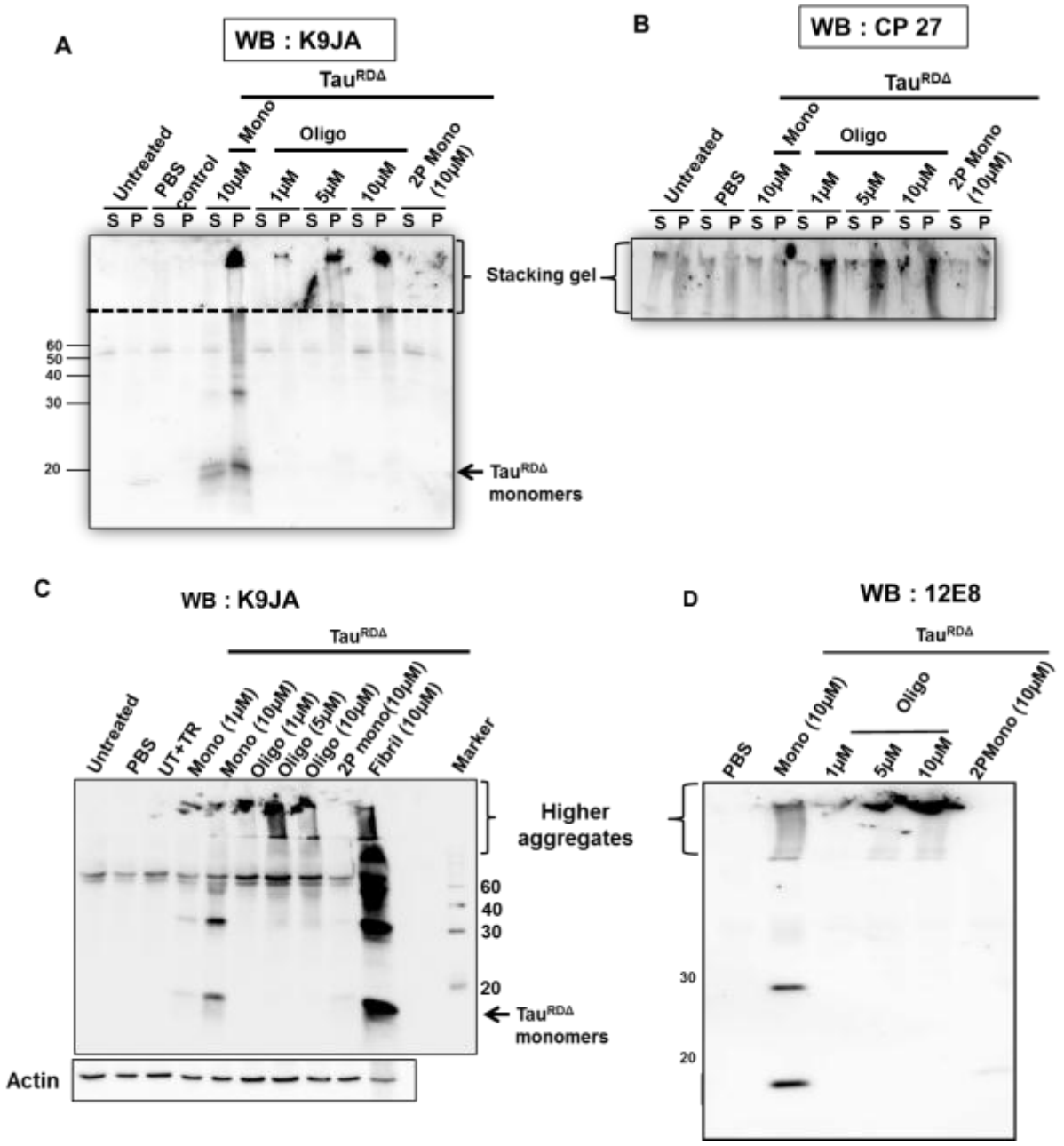

Figure 4.30Tau$^{RD\Delta}$ oligomers recruit endogenous Tau into filaments
Tau$^{RD\Delta}$ protein was transfected into SH-SY5Y cells and rat primary hippocampal neurons. **A)** Sedimentation of lysates of SH-SY5Y cells showed that there is an oligomer concentration dependent aggregation of Tau confirmed by western blotting using K9JA antibody. S – Supernatant; P – Pellet. **B)** The same blot was re-probed with CP27 antibody (N-terminal specific antibody). It showed that the endogenous full length Tau was aggregated along with the transfected oligomers. **C)** Primary rat hippocampal cell (DIV 21) lysates also revealed that the aggregation of Tau is concentration dependent. Tau$^{RD\Delta\text{-}PP}$ monomers did not aggregate in SH-SY5Y and rat primary hippocampal neurons. **(D)** Tau$^{RD\Delta}$ oligomer transfected primary hippocampal neuronal lysates displayed 12E8 positive phosphorylated Tau in the gel pockets, confirming that the aggregates are phosphorylated which was absent in the anti-aggregant transfected cell lysates.

newly formed aggregates. As expected, $Tau^{RD\Delta-PP}$ monomers delivered into cells did not cause aggregation at all, as there was no protein detected in the gel pockets (Figure 4.30C).

We next investigated whether the aggregates formed are phosphorylated. We observed a concentration dependent increase in the 12E8 positive aggregates in the gel pockets of lysates delivered with $Tau^{RD\Delta}$ oligomers (Figure 4.30 D). There was less 12E8 positive aggregates in the $Tau^{RD\Delta}$ monomer delivered cells and no 12E8 positive aggregates in the $Tau^{RD\Delta-PP}$ delivered cells (Figure 4.30 D) suggesting that $Tau^{RD\Delta}$ oligomers induce the aggregation in rat primary hippocampal neurons, and the aggregates are phosphorylated at KXGS motifs

4.9.3 $Tau^{RD\Delta}$ oligomers cause early apoptosis to the SH-SY5Y cells

The preceding experiments showed that $Tau^{RD\Delta}$ oligomers delivered into cells can cause the aggregation of endogenous Tau. An open question was whether this aggregation could compromise the health of the cell. In order to understand the toxic properties induced by the $Tau^{RD\Delta}$ oligomers, we determined the fraction of annexin V positive cells (an early apoptotic marker) in the $Tau^{RD\Delta}$ oligomer, monomer and buffer treated cells. $Tau^{RD\Delta}$ oligomers delivered into cells caused early signs of apoptosis in a $Tau^{RD\Delta}$-oligomer-dependent manner within 15 hours. The fraction (~28%) was ~7-fold higher in $Tau^{RD\Delta}$ oligomer-delivered cells, compared with transfection of $Tau^{RD\Delta}$ monomers (~4%) (Figure 4.31), or with monomers of the anti-aggregant $Tau^{RD\Delta-PP}$. This data suggest that $Tau^{RD\Delta}$ oligomers induce early apoptosis when present inside the neurons.

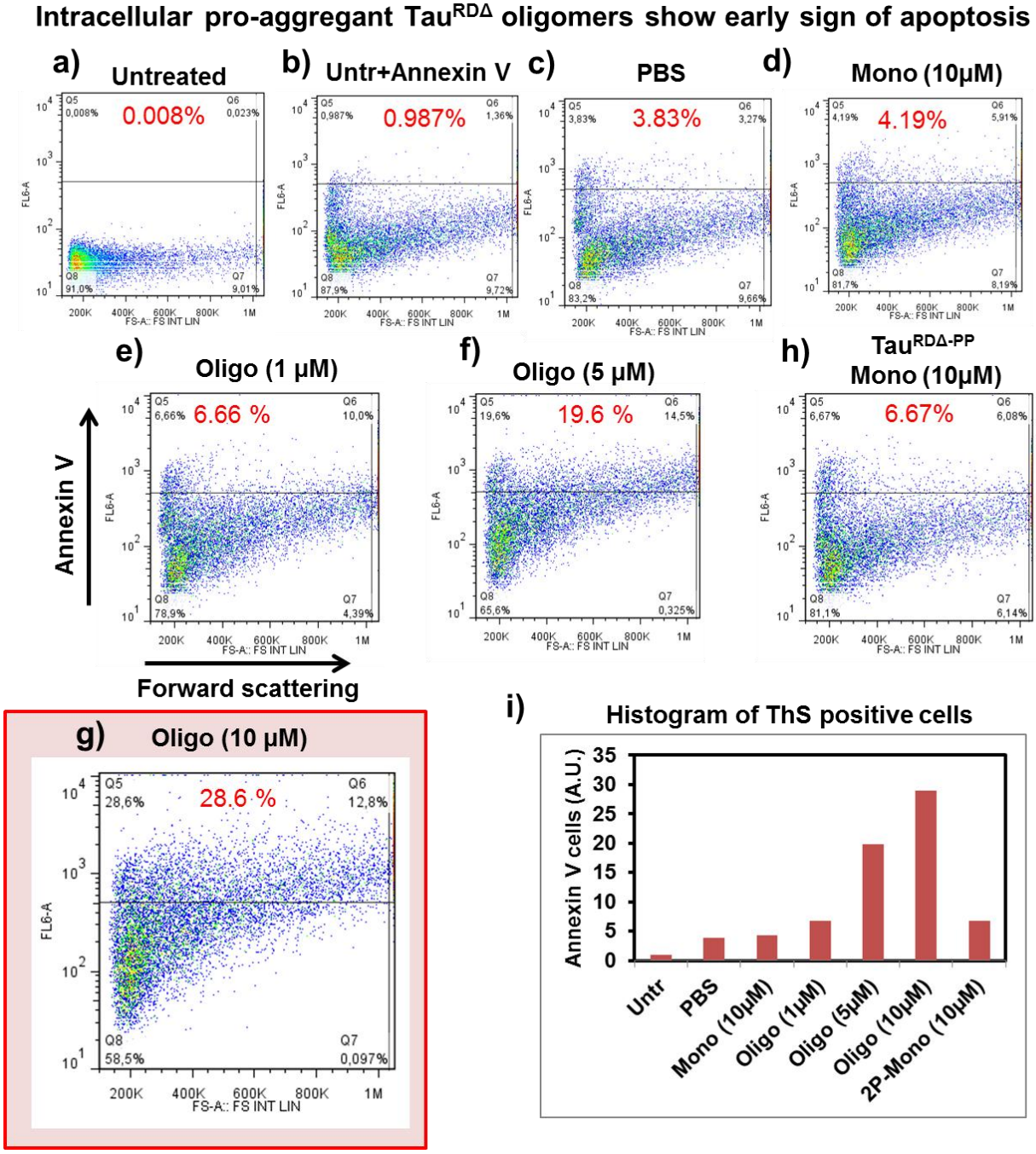

Figure 4.31 Tau$^{RD\Delta}$ oligomers promote apoptosis in cells
Tau$^{RD\Delta}$ protein was delivered directly into SH-SY5Y cells using Xfect transfection reagent kit and the samples were analyzed using annexin V (an early apoptotic marker) by flow cytometry. Note that there is a shift in the annexin V positive cells in an oligomer concentration dependent manner. The toxicity caused by Tau$^{RD\Delta}$ monomers was not significant compared with Tau$^{RD\Delta}$ oligomers.

5 Discussion

Tau protein is a natively unfolded protein because of its hydrophilic aminoacid composition (Lee et al., 1988). A major role of Tau is the stabilizion of microtubules, thereby maintaining the architecture of neurons and enabling axonal transport. There are several brain diseases where Tau is pathologically altered, leading to hyperphosphorylation, detachment from microtubules, missorting into the somatodendritic compartment, aggregation into fibers, synaptic decay, neuronal loss and further changes. These diseases are collectively termed "tauopathies" and include Alzheimer disease, Frontotemporal dementia, Pick disease, and others (Mandelkow and Mandelkow, 2012). It was initially suspected that the fibrillar form of Tau ("paired helical filaments") is the toxic species. However, in recent years the emphasis shifted to pre-fibrillar forms as the toxic agents. Evidence from mouse models (Santacruz et al., 2005, Andorfer et al., 2005, Yoshiyama et al., 2007, Berger et al., 2007, Eckermann et al., 2007, Van der Jeugd et al., 2012) and human studies (Gomez-Isla et al., 1997, Maeda et al., 2006) suggested that the toxic species could be some intermediate oligomeric forms of Tau assembly. However, the nature of the oligomeric species remained a matter of debate.

Earlier, our group demonstrated that the aggregation of Tau protein into fibers is based on beta-structure forming hexapeptide motifs (von Bergen et al., 2000). This knowledge was exploited in cell and animal models which enhances the beta propensity or delete it (pro-aggregant or anti-aggregant tau) which proved that tau pathology is closely linked to aggregation (Khlistunova et al., 2006, Eckermann et al., 2007, Mocanu et al., 2008). The $Tau^{RD\Delta}$ transgenic mice show strong aggregation of Tau, memory impairment and pronounced loss of long term potentiation. However, when the $Tau^{RD\Delta}$ protein expression was switched on for 14 months and then off for 1 to 4 months, memory and LTP was recovered, synapse loss was largely rescued, but the aggregates decreased only moderately. Surprisingly, the composition of the aggregates changed from a mixture of mouse Tau plus human $Tau^{RD\Delta}$ to mouse Tau only. These mouse models suggested that soluble oligomeric mutant forms of Tau might be the toxic species rather than larger fibrillar aggregates. Moreover, the early forms of Tau aggregation are likely heterogeneous and do not necessarily have beta structure (detectable by ThS), hence there was a need for other markers. Therefore,

this work was focussed on preparing homogeneous low-n oligomers and then probing their properties and toxic effects with different methods.

5.1 Stabilization and purification of Tau$^{RD\Delta}$ protein *in vitro*

Several other groups have reported on the generation of Tau oligomers. In most of the cases, Tau oligomers are prepared with the aid of inducers like heparin (Sahara et al., 2007), arachidonic acid (Patterson et al., 2011), metal ions (Bader et al., 2011) and by cross-seeding using other amyloidogenic proteins (Aß and α-Syn) (Lasagna-Reeves et al., 2010). The oligomers prepared by these methods, probably do not exist in AD brains. The advantage of our preparation method is that Tau$^{RD\Delta}$ protein readily forms oligomers without the aid of any inducers due to its enhanced ß-sheet propensity. Therefore, these oligomers would be expected to be a better approximation to the physiological situation.

The aggregation kinetics of Tau$^{RD\Delta}$ protein under different buffer conditions (PBS pH 7.4 and TBS pH 9.0) was performed in vitro in order to determine optimal conditions for oligomer preparation. It was shown earlier in our lab that Tau$^{RD\Delta}$ protein under PBS pH 7.4 conditions aggregates rapidly (Kumar et al., 2014). Similarly, the condition TBS, pH 9.0 is also favorable for formation of PHFs of full length Tau protein (Goux, 2002). Consistent with these earlier data (Kumar et al., 2014), we observed that under both buffer conditions (PBS and TBS) aggregation occurs in a similar fashion. i.e., the aggregation reaches a maximum at 8 hours and stays stationary till 72 hours. There was no significant difference in the ThS positive aggregates in both buffer conditions (Figure 4.4 A). However, EM and AFM revealed short fibrils and many oligomers in the TBS, pH 9.0 condition whereas long twisted fibrils were formed in the PBS pH 7.4 condition (4.6 B and E), suggesting that TBS, pH 9.0 condition favors the oligomer formation and thus we prepared our oligomers in TBS, pH 9.0 buffer.

As the oligomers prepared in TBS pH 9.0 were not SDS stable, they could not be separated by size exclution chromatography (SEC) (Figure 4.7 B, C). Thus we searched for alternative methods to stabilize the Tau$^{RD\Delta}$ oligomers. It was reported that ECGC inhibits the aggregation of α-synuclein and induces the formation of off-pathway oligomers which are not toxic (Ehrnhoefer et al., 2008). EGCG has also been shown to inhibit the aggregation of His-Tau$^{RD\Delta}$ (Wobst et al., 2015) and more

specifically SDS stable insoluble oligomers. We used EGCG to inhibit the aggregation of $Tau^{RD\Delta}$ protein (without His tag). Unlike the His-$Tau^{RD\Delta}$, $Tau^{RD\Delta}$ readily forms filamentous aggregates within 72 hours. The presence of EGCG reduces the length of the fibrils and increases the oligomers (Figure 4.9) . Thus it appears that the assembly competence of $Tau^{RD\Delta}$ was reduced by the N-terminal His tag. We observed that the EGCG increases the formation of SDS stable low-n oligomers and reduces the aggregates and SDS stable insoluble oligomers (Figure 4.8, Figure 4.10). However, the SDS stable soluble oligomers induced by EGCG were not separable by SEC due to the small difference in the molecular weight of monomers, dimers and trimers. We therefore turned to a cross-linking approach to stabilize the $Tau^{RD\Delta}$ oligomers.

We used glutaraldehyde to cross-link the $Tau^{RD\Delta}$ oligomers. As low as 0.01% GA was sufficient to cross-link the $Tau^{RD\Delta}$ oligomers and achieved stable dimers, trimers and tetramers in SDS denaturing gels. We observed that indeed the TBS pH 9.0 condition favors the oligomer formation better than PBS pH 7.4, as we observed more oligomers in the chromatogram (Figure 4.12). The purified oligomers were stable at 4°C for more than a month, as analyzed by SEC and AFM (data not shown).

The stabilized $Tau^{RD\Delta}$ oligomers (TBS pH 9.0, GA fixed) were SDS stable and were separable by size exclusion chromatography. However, only half of the fractions contained only oligomers, the remaining half contained a mixture of monomers and oligomers (Figure 4.13). The purified oligomers display a 4-fold increase in ANS fluoresence intensity confirming that the oligomers are structurally modified. ANS is a sensitive marker of protein conformation and is often used to study protein folding (Semisotnov et al., 1991). It binds to exposed hydrophobic residues as well as cationic side chains (Arg, Lys) (Gasymov and Glasgow, 2007) which are numerous in $Tau^{RD\Delta}$ (20 out of 129 aa or ~15%). Thus the increase in ANS fluorescence during oligomerization could be explained by a conformational change exposing more Arg and Lys residues (Figure 4.14 B). Although conformational changes are evident in the oligomers, they do not attain ß-sheet structure, as judged by the low ThS fluorescence (Figure 4.14 A) and CD measurements (Figure 4.14 C). Most of the oligomers are less than 6nm in AFM height images suggesting that they are low-n $Tau^{RD\Delta}$ oligomers.

Since we observed an increase in the intensity of ANS in Tau$^{RD\Delta}$ oligomers, hinting at an increased exposure of hydrophobic residues, we tested hydrophobic interaction chromatography to purify the oligomers. This proved to be successful, in particular the Butyl FF 16/10 column separated the Tau$^{RD\Delta}$ oligomers from Tau$^{RD\Delta}$ monomers with high purity (>90%). These purified oligomers were SDS stable, with increased ANS intensity, yet a random coiled secondary structure (as judged by CD), and lacking pronounced beta structure, as seen by the low ThS intensity.

5.2 Structural properties of purified low-n Tau$^{RD\Delta}$ oligomers

The structural morphology of Tau$^{RD\Delta}$ oligomers was analyzed by atomic force microscopy and dynamic light scattering. The purified Tau$^{RD\Delta}$ oligomers demonstrate heights in the range of 3.7 ± 2.0 nm measured from AFM height images (Figure 4.18 A and B) and display globular shape which is clearly visible in the amplitude image (Figure 4.18 C). We also observed some higher-order oligomers in AFM height range of more than 6nm which could correspond to maximum of 10-mers. Such higher order oligomers might act as seeds for the rapid aggregation of Tau$^{RD\Delta}$.

When measuring the size of oligomers by dynamic light scattering we found a hydrodynamic radius Rh ~6 nm, compared to ~3 nm for monomers (Figure 4.19). Similar to our results, others also found that the 4R repeat domain Tau in solution stays as dimers and displayed a hydrodynamic radius of 3.1 nm (Yao et al., 2003). Several rapidly aggregating mutant TauRD species (for example: P301L 4R Tau) also displayed hydrodynamic radii of ~3.1 nm. Hence the authors concluded that all 4R Tau proteins with or without mutation exists as dimers in solution (Yao et al., 2003). Earlier our group also showed that the Stokes radii of 3.0 nm for the dimers formed from K12 construct (3R repeat domain Tau) based on gel filtration chromatography analysis (Wille et al., 1992). Earlier findings (Wille et al., 1992, Yao et al., 2003) along with the present data argue that Tau$^{RD\Delta}$ oligomers exhibit 6nm radius which corresponds to a tetramer of Tau$^{RD\Delta}$ protein, roughly consistent with SDS gel analysis where we observed dimers, trimers and tetramers. Thus the structurally characterized oligomers could be used to understand the functional properties of Tau$^{RD\Delta}$ oligomers.

Characterization of Tau$^{RD\Delta}$ oligomers

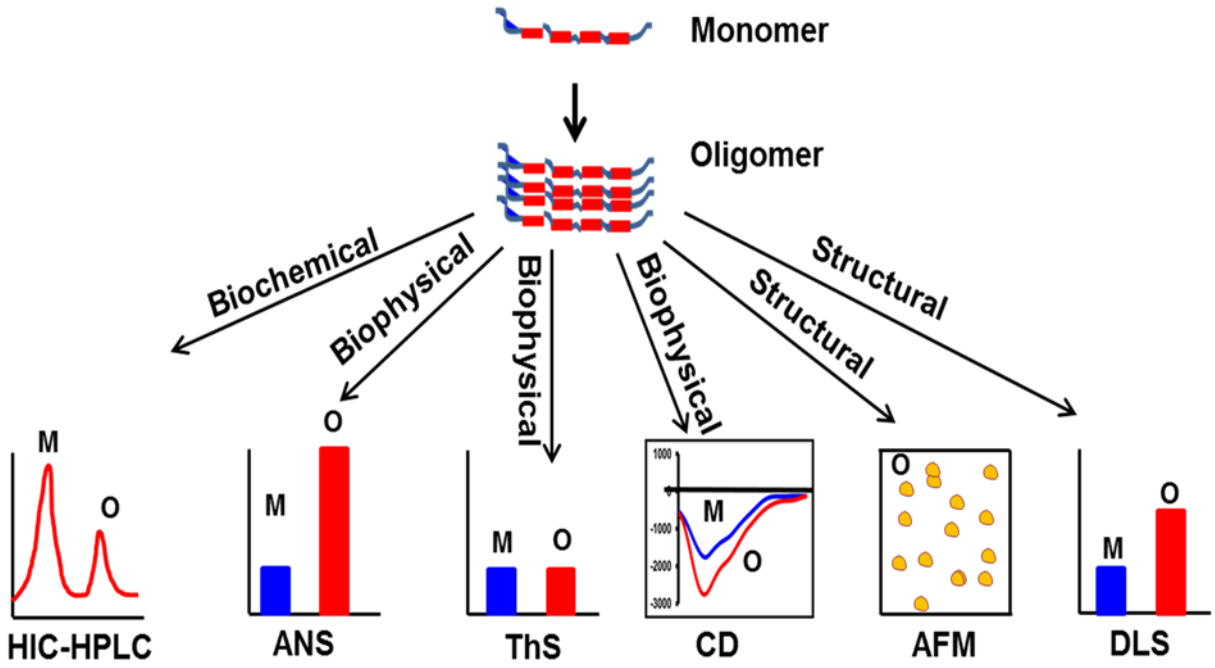

Figure 5.1 Characterization of Tau$^{RD\Delta}$ oligomers
Graphical representation of the characteristics of Tau$^{RD\Delta}$ oligomers. Tau$^{RD\Delta}$ oligomers expose hydrophobic and positively charged residues on their surface (ANS) which aids in the separation of oligomers from the monomers by hydrophobic interaction chromatography methods (HIC). The purified oligomers have altered conformation (ANS) with less or no ß-sheet structure (ThS and CD). The oligomers are roughly globular in shape and in the height ranges from 3.7 ± 2.0 nm (AFM). The hydrodynamic radii for oligomers are ~6 nm (DLS) which corresponds to tetramer consistent with SDS gel analysis.

5.3 Functional properties of pro-aggregation TauRD oligomers

5.3.1 Extracellular effects of Tau$^{RD\Delta}$ oligomers

The major question in the field of Alzheimer disease (and Tauopathies in general) is the toxic species of Tau and the mechanisms of toxicity. Several groups have studied the toxic properties of Tau aggregates, especially PHFs, but more recent evidence suggests that soluble or prefibrillar forms of aggregates are responsible for toxicity and cell death rather than the higher aggregates or PHFs(Haass and Selkoe, 2007). In fact there is a debate whether PHFs are toxic or protective to neurons (Trojanowski and Lee, 2005). In the last decade, Tau oligomers received much attention because the toxic effects of Tau protein preceded NFT formation in mouse models (Andorfer et al., 2005, Spires et al., 2006, Yoshiyama et al., 2007, Polydoro et al., 2009, Van der Jeugd et al., 2012, Eckermann et al., 2007). Tau is primarily an intracellular protein, and it is believed that Tau alone is enough to cause toxicity, at least in familial Tauopathies based on Tau mutations. Consistent with this, Tau inside cells can cause microtubule destruction, disruption of transport, deregulation of

signaling or degradation pathways (Blair et al., 2013, Gotz et al., 2010, Wang et al., 2007, Zempel et al., 2010, Zempel et al., 2013).

On the other hand, Tau can occur outside neurons and has been proposed to cause the spreading of Tau pathology in the brain (Braak and Braak, 1991b). Tau protein (total Tau and phospho Tau) is enhanced in the CSF (cerebro-spinal fluid) of human AD brains (Hampel et al., 2010). The concentration of Tau in the interstitial fluid is 45ng/ml (equivalent to ~1nM) (Yamada et al., 2011) which is 1000 times less than the intracellular concentration of Tau (estimated at ~1µM, (Drubin et al., 1985)). Extracellular tau is also being released from cell lines and neurons via multiple pathways (Chai et al., 2012, Hall and Saman, 2012, Saman et al., 2012, Simon et al., 2012), strongly supporting the notion that secretion of tau protein may be an important biological function or dysfunction of tau, especially in disease. These findings suggest that extracellular tau could be a physiological process and may also have toxic properties.

In support of this, earlier it was shown that, extracellular monomeric Tau is enough to cause the toxicity in neuronal cells by elevating the intracellular calcium level through M1/M3 muscarinic receptor stimulation which leads to endocytosis of extracellular tau thereby causing cell death (Gomez-Ramos et al., 2006, Gomez-Ramos et al., 2008). Moreover extracellular human Tau can spread between CNS neurons through non-synaptic or synaptic mechanisms (Le et al., 2012). Extracellular monomeric Tau protein can be endocytosed and is able to propagate the aggregation of endogenous Tau (Michel et al., 2014). This is possible not only for monomeric Tau protein, but also for the fibrillar form of Tau which can be endocytosed, induces aggregation and propagates trans-cellularly. (Kfoury et al., 2012). The soluble aggregates of Tau could enter via dynamin driven endocytosis (Wu et al., 2013) and proteoglycan mediated macropynocytosis (Holmes et al., 2013).

Tau protein can interact with cell membranes and could modify their properties (Jones et al., 2012). In support of this, Tau oligomers were shown to damage the cell membrane in SH-SY5Y cells (Lasagna-Reeves et al., 2010, Flach et al., 2012) whereas the monomers did not cause the membrane damage. These evidences suggest that even the extracellular Tau might cause toxicity by different mechanisms.

We therefore analyzed the toxic properties of purified $Tau^{RD\Delta}$ oligomers in neuronal cell culture and organotypic slice culture models. Earlier it was demonstrated that the toxicity induced by Aβ-oligomers was dependent on the assay used (Wogulis et al., 2005) We therefore checked the toxicity of $Tau^{RD\Delta}$ oligomers by different assays, including MTT, XTT, alamar blue and LDH release assay. We did not observe any reduction in the cell viability in SH-SY5Y cells and in primary cortical neuronal cells as judged by the above assays (Figure 4.20). There was no membrane disruption by the LDH assay (Figure 4.20) consistent with the data of Kumar et al (Kumar et al., 2014).

We also checked the ability of $Tau^{RD\Delta}$ oligomers to cause toxicity in hippocampal slice culture models, as these mimic the hippocampus of the human brain and retain the connections between neurons and glia cells. The results were unexpected as there was no loss of neurons (analyzed by the density of NeuN positive cells) and no membrane damage (by the LDH release assay) (Figure 4.22). Since the oligomers are cross-linked and might block some active site, we also checked the toxic effects of oligomers before purification, but with the same results (no loss of cell viability and membrane integrity) (Figure 4.21). We conclude that the $Tau^{RD\Delta}$ oligomers are not toxic to neuronal cells and hippocampal slices by standard "classical" assays.

These results are in contrast to other publications (Lasagna-Reeves et al., 2010, Flach et al., 2012, Tian et al., 2013). Since the Tau^{RD} repeat domain protein does not contain the N-terminal or C-terminal domains of Tau, we investigated the relationship between Tau domains and toxicity, using Tau variants with different domain compositions. This, too, did not explain the discrepancies in experimental results (Figure 4.23). We therefore assume that they are due to different methods of oligomer preparation.

The $Tau^{RD\Delta}$ mouse model showed pronounced tau pathology at 10 months of age, including loss of spines, which was reversed when the Tau expression was switched off for periods of 1 to 4 months (Sydow et al., 2011). Therefore we next investigated the more subtle effects such as spine loss caused by these oligomers. As expected we observed pronounced loss of spines up to 50% when $Tau^{RD\Delta}$ oligomers (1µM) were applied extracellularly to rat primary hippocampal neurons.

Oxidative stress plays an important role in AD pathogenesis. (Butterfield et al., 2001) and oxidative stressors play a critical role in neurofibrillary pathology leading to Tau hyperphosphorylation (Borza, 2014). In Tauopathy mouse models, oxidative stress eventually leads to cell death (Cente et al., 2006).Therefore, we investigated whether $Tau^{RD\Delta}$ oligomers cause an increase in intracellular reactive oxygen species in rat primary hippocampal neurons. This was observed within minutes of incubation with oligomers and that was increased with oligomer concentration (Figure 4.25). The mechanism responsible for ROS production by $Tau^{RD\Delta}$ oligomers is not yet understood. A possible pathway may be through the membrane enzyme NADPH oxidase (Gao et al., 2012), as the increase in ROS occurred within a minute. The NADPH oxidase complex generates extracellular superoxide which is converted into hydrogen peroxide outside the cells. This is then able to cross biological membranes and oxidize membrane lipids (Hernandes and Britto, 2012). This would explain the rapid increase in ROS upon addition of $Tau^{RD\Delta}$ oligomers. On the other hand, the mitochondrial membrane potential is not disturbed in oligomer treated cells (as judged by JC1 staining) (data not shown) so that it is unlikely that mitochondrial ROS production is involved within the short time.

There is a strong correlation between the increase in ROS production and calcium elevation. Mitochondria are both generators and targets of ROS. Thus the dysfunction of mitochondrial energy metabolism leads to impairment in calcium homeostasis (Fu et al., 2014). Superoxide ions formed in the extracellular space can enter into cells through the chloride channel-3 and cause the elevation of the intracellular calcium level (Hawkins et al., 2007). Hence we investigated the intracellular calcium level by fura-2 imaging and observed a gradual increase up to 20 minutes, clearly later than the increase in ROS (Figure 4.26). The source of the calcium is not yet known. However, we assume that the calcium should have entered from the extracellular space through the leaky cell membrane as the ROS might oxidize the membrane lipids.

Oxidative stress and calcium elevation have been implicated in Aβ-oligomer mediated neurotoxicity (Fu et al., 2014). Aß-oligomers are also shown to cause synapse loss via calcium dysregulation, Tau phosphorylation and missorting (Zempel et al., 2010). Since we observe calcium dysregulation and synapse loss in neurons treated with $Tau^{RD\Delta}$ oligomers, we asked whether Tau missorting also follows the

calcium elevation to cause the spine loss. Tau$^{RD\Delta}$ oligomers did not cause missorting of Tau in rat primary hippocampal neurons (Figure 4.27). The pathological changes caused by Tau$^{RD\Delta}$ oligomers are summarized in Figure 5.2

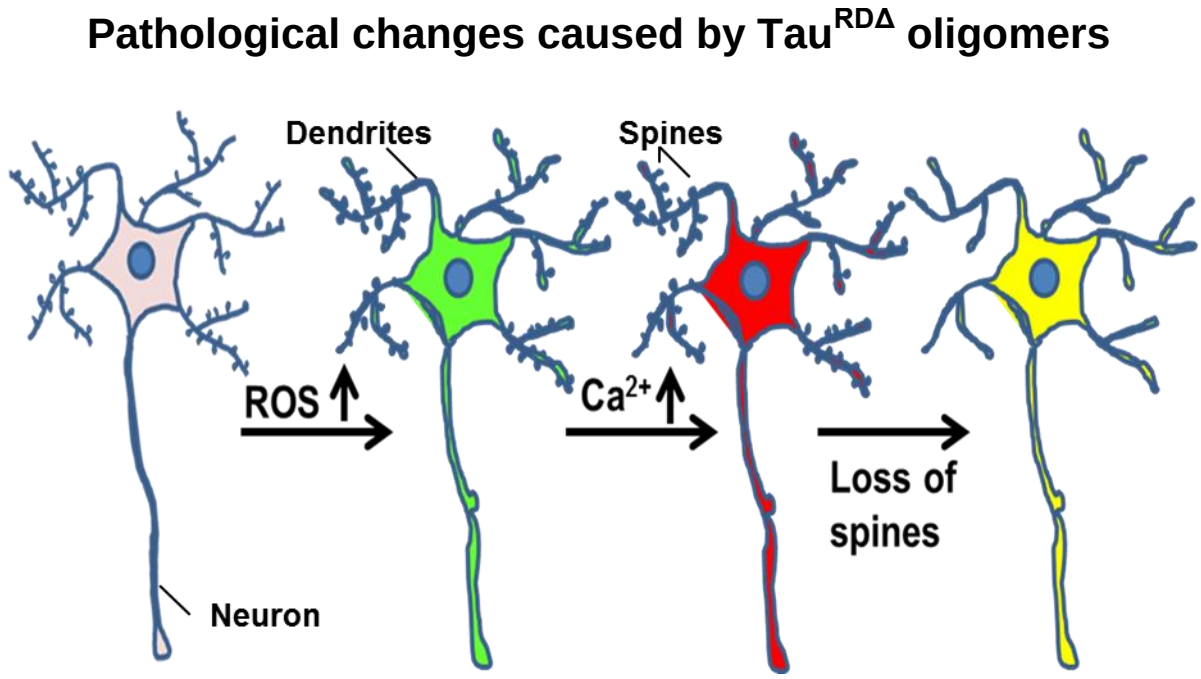

Figure 5.2 Pathological changes caused by Tau$^{RD\Delta}$ oligomers
Tau $^{RD\Delta}$ oligomers induce the ROS production (green color) in rat primary hippocampal neurons within 2 minutes of incubation followed by an increase in the intracellular calcium level (red color) (saturation at 20 min) and later loss of spines at 3 hours (yellow color).

5.3.2 Tau$^{RD\Delta}$ oligomers as intracellular seeds

Since Tau is an intracellular protein and forms neurofibrillary tangles within neurons, it is important to understand the role of purified Tau$^{RD\Delta}$ oligomers in neurons. Studies from model organisms proved that the filaments are formed from monomers (Gotz et al., 2007), and that endogenous and transfected Tau can co-polymerize (Mocanu et al., 2008, Van der Jeugd et al., 2012). *In vitro* and *in vivo* studies showed that seeds are necessary for the filament formation. (Friedhoff et al., 1998b, Schweers et al., 1995, von Bergen et al., 2000, Lasagna-Reeves et al., 2012a). Seeding could take place either by nucleation within cells (as is the case, say, for actin or microtubule assembly), or by transfer of seeds from outside the cells, as discussed below.

Experiments in cultured cells have shown that extracellular Tau aggregates can be endocytosed by cells and can act as seeds to induce the misfolding and aggregation of intracellular Tau (Frost et al., 2009a, Nonaka et al., 2010, Frost et al., 2009b, Guo

and Lee, 2011, Michel et al., 2014). These seeds can spread between CNS neurons via a variety of non-synaptic mechanisms (naked Tau release, exosomes and membrane vesicles) or synaptic mechanisms (Le et al., 2012). Mouse models also showed that injection of brain homogenates from mice expressing mutant Tau into brains of normal mice leads to the conversion of naive Tau protein into NFT like aggregates in the recipient mice (Clavaguera et al., 2009).

The spreading of Tau pathology was initially observed in human brains where the first NFTs occur in the entorhinal cortex, and the pathology progresses in a topographically predictable manner across limbic and association cortices along anatomical connections (Braak stages) (Braak and Braak, 1991a, Braak and Braak, 1991b). This spreading of pathological features could be caused by several mechanisms, e.g. electric or chemical signalling (e.g. cytokines), or by transfer of Tau itself in a pathological state (Brundin et al., 2008). The latter view gained momentum with the discovery that any form of Tau protein (monomer (Michel et al., 2014), oligomer (Lasagna-Reeves et al., 2012b) and fibril (Iba et al., 2013)) can be transferred from neurons to neurons and cause the local accumulation of endogenous Tau (Medina and Avila, 2014, Clavaguera et al., 2015).

It was shown previously that even in vitro prepared PHF can act as seeds (Guo and Lee, 2011). However, recent data of Lasagna-Reeves and coworkers argued against this observation, as PHFs from AD brain injected into wild type mice did not cause propagation of Tau pathology, supporting the notion that AD PHFs do not act as seeds (Lasagna-Reeves et al., 2012a). This could be explained by the procedure - in vitro prepared PHFs were ultrasonicated to break down long fibrils into short ones and oligomers and then delivered into cells (Guo and Lee, 2011). As electron microscopy is not suitable for characterizing small oligomers, the effects of oligomers might have been overlooked.

In most of the above-mentioned studies, the seeds were applied extracellularly and the effects checked intracellularly. We therefore investigated the role of Tau protein as in seeding in SH-SY5Y neuroblastoma cells. We applied the $Tau^{RD\Delta}$ monomers and oligomers extracellularly and then counted ThS positive cells by flow cytometry to analyze the ability of oligomers to be endocytosed and act as seeds. When $Tau^{RD\Delta}$ oligomers were present in the medium for 15 hours we observed a 2 fold increase in

the ThS positive cells compared to monomer treated cells (Figure 4.28). Although the increase in ThS positive cells after oligomer treatment was significant, the overall number of ThS positive cells was very low.

We therefore employed a protein transfection method which is a powerful tool for elucidating a protein function in a cell, and plays an important role in the fields of cell biology and drug discovery (Oba and Tanaka, 2012). Protein transfection approach have been used earlier as well to study the seeding efficiency of Tau aggregates (Guo and Lee, 2011). Using this approach (Xfect protein transfection reagent) we observed that $Tau^{RD\Delta}$ oligomers caused the accumulation of endogenous Tau in SH-SY5Y cells to the ThS positive aggregates, and that oligomers were by far the most efficient Tau species (Figure 4.29 and Figure 4.30). This is consistent with reports that oligomers (but not PHFs) isolated from AD brain caused the spreading of Tau pathology in mice (Lasagna-Reeves et al., 2012a). We observed an increase in the ThS positive cells in $Tau^{RD\Delta}$ monomer delivered cells compared to PBS treated cells. This might be interpreted to mean that the monomeric $Tau^{RD\Delta}$ could self-aggregate (ThS positive), as the analysis shows that the aggregates in SH-SY5Y cells do not contain the endogenous Tau (Figure 4.30). However, since $Tau^{RD\Delta}$ monomer preparations contain a low amount of low-n oligomers (Figure 4.12 A and C) (Kumar et al., 2014) one cannot rule out that they initiate nucleation and hence a ThS response.

The effect of intracellular $Tau^{RD\Delta}$ oligomers (ThS positive cells) was 50 fold higher compared to the effect of oligomers when applied extracellularly to SH-SY5Y cells. (Figure 4.28 and Figure 4.29).

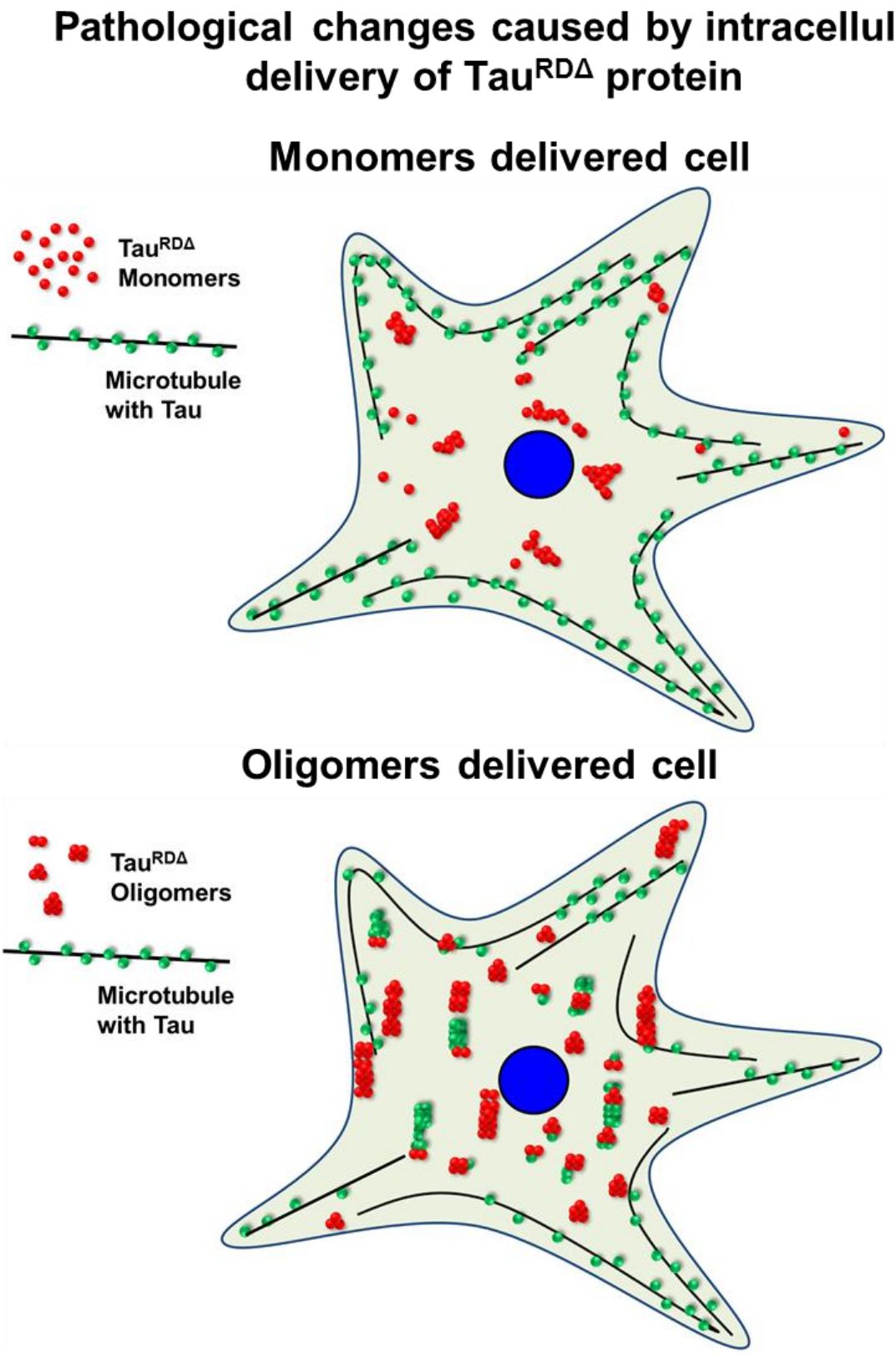

Figure 5.3 Effects of intracellular delivery of Tau$^{RD\Delta}$ protein
Protein transfection (Xfect reagent) of Tau$^{RD\Delta}$ monomer to SH-SY5Y cells induce the self-aggregation of Tau and does not recruit the endogenous Tau from SH-SY5Y cells whereas Tau$^{RD\Delta}$ oligomers recruit the endogenous tau into the growing aggregates and induce the apoptosis (annexin V positive cells).

The mechanism of $Tau^{RD\Delta}$ oligomer entry into the cells is not well understood. We assume that the $Tau^{RD\Delta}$ oligomers can be endocytosed, but the amount of endocytosed Tau is too small to cause the aggregation, or the incubation time is too short. The protein derived from the monomer or oligomer-delivered cells shows almost equal amounts of aggregates in the gel pockets (Figure 4.30) but ThS positive cells were 12 times lower in the case of monomer-treated cells. This suggests the presence of amorphous aggregates, rather than fibers in the monomer delivered cells (Figure 4.29).

Similar to results from the SH-SY5Y cells, we noticed in rat primary hippocampal neurons $Tau^{RD\Delta}$ oligomers cause aggregation of Tau, and that the aggregates are phosphorylated at KXGS motifs (Figure 4.30). This is consistent with earlier results of others that the seeds induce the aggregation of endogenous Tau at elevated phosphorylation (Guo and Lee, 2011, Clavaguera et al., 2009). When oligomers of $Tau^{RD\Delta}$ are present inside cells, they causes early apoptosis (seen by annexin V staining) (Figure 4.31). This effect does not occur when $Tau^{RD\Delta}$ oligomers are added outside cells.

To conclude, $Tau^{RD\Delta}$ oligomers show some toxicity to synapses when present extracellularly. However, toxicity is much more pronounced when oligomers are introduced into cells, leading to strong aggregation and pathology.

6 References

ALZHEIMER, A. 1907. Über eine eigenartige Erkrankung der Hirnrinde. *Allgemeine Zeitschrift für Psychiatrie und Psychisch-gerichtliche Medizin,* 64**,** 146-8.

ANDORFER, C., ACKER, C. M., KRESS, Y., HOF, P. R., DUFF, K. & DAVIES, P. 2005. Cell-cycle reentry and cell death in transgenic mice expressing nonmutant human tau isoforms. *J Neurosci,* 25**,** 5446-54.

ANDORFER, C., KRESS, Y., ESPINOZA, M., DE SILVA, R., TUCKER, K. L., BARDE, Y. A., DUFF, K. & DAVIES, P. 2003. Hyperphosphorylation and aggregation of tau in mice expressing normal human tau isoforms. *J Neurochem,* 86**,** 582-90.

ANDREADIS, A. 2006. Misregulation of tau alternative splicing in neurodegeneration and dementia. *Prog Mol Subcell Biol,* 44**,** 89-107.

ARAI, T., IKEDA, K., AKIYAMA, H., SHIKAMOTO, Y., TSUCHIYA, K., YAGISHITA, S., BEACH, T., ROGERS, J., SCHWAB, C. & MCGEER, P. L. 2001. Distinct isoforms of tau aggregated in neurons and glial cells in brains of patients with Pick's disease, corticobasal degeneration and progressive supranuclear palsy. *Acta Neuropathol,* 101**,** 167-73.

ARRIAGADA, P. V., GROWDON, J. H., HEDLEY-WHYTE, E. T. & HYMAN, B. T. 1992. Neurofibrillary tangles but not senile plaques parallel duration and severity of Alzheimer's disease. *Neurology,* 42**,** 631-9.

BADER, B., NUBLING, G., MEHLE, A., NOBILE, S., KRETZSCHMAR, H. & GIESE, A. 2011. Single particle analysis of tau oligomer formation induced by metal ions and organic solvents. *Biochem Biophys Res Commun,* 411**,** 190-6.

BANCHER, C., BRUNNER, C., LASSMANN, H., BUDKA, H., JELLINGER, K., WICHE, G., SEITELBERGER, F., GRUNDKE-IQBAL, I., IQBAL, K. & WISNIEWSKI, H. M. 1989. Accumulation of abnormally phosphorylated tau precedes the formation of neurofibrillary tangles in Alzheimer's disease. *Brain Res,* 477**,** 90-9.

BARGHORN, S., DAVIES, P. & MANDELKOW, E. 2004. Tau paired helical filaments from Alzheimer's disease brain and assembled in vitro are based on beta-structure in the core domain. *Biochemistry,* 43**,** 1694-703.

BARGHORN, S., ZHENG-FISCHHOFER, Q., ACKMANN, M., BIERNAT, J., VON BERGEN, M., MANDELKOW, E. M. & MANDELKOW, E. 2000. Structure, microtubule interactions, and paired helical filament aggregation by tau mutants of frontotemporal dementias. *Biochemistry,* 39**,** 11714-21.

BEGUM, A. N., JONES, M. R., LIM, G. P., MORIHARA, T., KIM, P., HEATH, D. D., ROCK, C. L., PRUITT, M. A., YANG, F., HUDSPETH, B., HU, S., FAULL, K. F., TETER, B., COLE, G. M. & FRAUTSCHY, S. A. 2008. Curcumin structure-function, bioavailability, and efficacy in models of neuroinflammation and Alzheimer's disease. *J Pharmacol Exp Ther,* 326**,** 196-208.

BERGER, Z., RODER, H., HANNA, A., CARLSON, A., RANGACHARI, V., YUE, M., WSZOLEK, Z., ASHE, K., KNIGHT, J., DICKSON, D., ANDORFER, C., ROSENBERRY, T. L., LEWIS, J., HUTTON, M. & JANUS, C. 2007. Accumulation of pathological tau species and memory loss in a conditional model of tauopathy. *J Neurosci,* 27**,** 3650-62.

BIERNAT, J., GUSTKE, N., DREWES, G., MANDELKOW, E. M. & MANDELKOW, E. 1993. Phosphorylation of Ser262 strongly reduces binding of tau to microtubules: distinction between PHF-like immunoreactivity and microtubule binding. *Neuron,* 11**,** 153-63.

BIESCHKE, J., RUSS, J., FRIEDRICH, R. P., EHRNHOEFER, D. E., WOBST, H., NEUGEBAUER, K. & WANKER, E. E. 2010. EGCG remodels mature alpha-synuclein and amyloid-beta fibrils and reduces cellular toxicity. *Proc Natl Acad Sci U S A,* 107**,** 7710-5.

BLAIR, L. J., ZHANG, B. & DICKEY, C. A. 2013. Potential synergy between tau aggregation inhibitors and tau chaperone modulators. *Alzheimers Res Ther,* 5**,** 41.

BORZA, L. R. 2014. A review on the cause-effect relationship between oxidative stress and toxic proteins in the pathogenesis of neurodegenerative diseases. *Rev Med Chir Soc Med Nat Iasi,* 118**,** 19-27.

BRAAK, H. & BRAAK, E. 1991a. Alzheimer's disease affects limbic nuclei of the thalamus. *Acta Neuropathol,* 81**,** 261-8.

BRAAK, H. & BRAAK, E. 1991b. Neuropathological stageing of Alzheimer-related changes. *Acta Neuropathol,* 82**,** 239-59.

BRANDT, R., HUNDELT, M. & SHAHANI, N. 2005. Tau alteration and neuronal degeneration in tauopathies: mechanisms and models. *Biochim Biophys Acta,* 1739**,** 331-54.

BRUNDEN, K. R., TROJANOWSKI, J. Q. & LEE, V. M. 2009. Advances in tau-focused drug discovery for Alzheimer's disease and related tauopathies. *Nat Rev Drug Discov,* 8**,** 783-93.

BRUNDIN, P., LI, J. Y., HOLTON, J. L., LINDVALL, O. & REVESZ, T. 2008. Research in motion: the enigma of Parkinson's disease pathology spread. *Nat Rev Neurosci,* 9**,** 741-5.

BULIC, B., PICKHARDT, M., SCHMIDT, B., MANDELKOW, E. M., WALDMANN, H. & MANDELKOW, E. 2009. Development of tau aggregation inhibitors for Alzheimer's disease. *Angew Chem Int Ed Engl,* 48**,** 1740-52.

BUTTERFIELD, D. A., DRAKE, J., POCERNICH, C. & CASTEGNA, A. 2001. Evidence of oxidative damage in Alzheimer's disease brain: central role for amyloid beta-peptide. *Trends Mol Med,* 7**,** 548-54.

CASSIMERIS, L. & SPITTLE, C. 2001. Regulation of microtubule-associated proteins. *Int Rev Cytol,* 210**,** 163-226.

CENTE, M., FILIPCIK, P., PEVALOVA, M. & NOVAK, M. 2006. Expression of a truncated tau protein induces oxidative stress in a rodent model of tauopathy. *Eur J Neurosci,* 24**,** 1085-90.

CHAI, X., DAGE, J. L. & CITRON, M. 2012. Constitutive secretion of tau protein by an unconventional mechanism. *Neurobiol Dis,* 48**,** 356-66.

CHEN, Y., DUBE, C. M., RICE, C. J. & BARAM, T. Z. 2008. Rapid loss of dendritic spines after stress involves derangement of spine dynamics by corticotropin-releasing hormone. *J Neurosci,* 28**,** 2903-11.

CHIRITA, C. N., CONGDON, E. E., YIN, H. & KURET, J. 2005. Triggers of full-length tau aggregation: a role for partially folded intermediates. *Biochemistry,* 44**,** 5862-72.

CHIRITA, C. N., NECULA, M. & KURET, J. 2003. Anionic micelles and vesicles induce tau fibrillization in vitro. *J Biol Chem,* 278**,** 25644-50.

CLAVAGUERA, F., BOLMONT, T., CROWTHER, R. A., ABRAMOWSKI, D., FRANK, S., PROBST, A., FRASER, G., STALDER, A. K., BEIBEL, M., STAUFENBIEL, M., JUCKER, M., GOEDERT, M. & TOLNAY, M. 2009. Transmission and spreading of tauopathy in transgenic mouse brain. *Nat Cell Biol,* 11**,** 909-13.

CLAVAGUERA, F., HENCH, J., GOEDERT, M. & TOLNAY, M. 2015. Invited review: Prion-like transmission and spreading of tau pathology. *Neuropathol Appl Neurobiol,* 41**,** 47-58.

CLEVELAND, D. W., HWO, S. Y. & KIRSCHNER, M. W. 1977a. Physical and chemical properties of purified tau factor and the role of tau in microtubule assembly. *J Mol Biol,* 116**,** 227-47.

CLEVELAND, D. W., HWO, S. Y. & KIRSCHNER, M. W. 1977b. Purification of tau, a microtubule-associated protein that induces assembly of microtubules from purified tubulin. *J Mol Biol,* 116**,** 207-25.

COMBS, B. & GAMBLIN, T. C. 2012. FTDP-17 tau mutations induce distinct effects on aggregation and microtubule interactions. *Biochemistry,* 51**,** 8597-607.

COPPOLA, G., CHINNATHAMBI, S., LEE, J. J., DOMBROSKI, B. A., BAKER, M. C., SOTO-ORTOLAZA, A. I., LEE, S. E., KLEIN, E., HUANG, A. Y., SEARS, R., LANE, J. R., KARYDAS, A. M., KENET, R. O., BIERNAT, J., WANG, L. S., COTMAN, C. W., DECARLI, C. S., LEVEY, A. I., RINGMAN, J. M., MENDEZ, M. F., CHUI, H. C., LE BER, I., BRICE, A., LUPTON, M. K., PREZA, E., LOVESTONE, S., POWELL, J., GRAFF-RADFORD, N., PETERSEN, R. C., BOEVE, B. F., LIPPA, C. F., BIGIO, E. H., MACKENZIE, I., FINGER, E., KERTESZ, A., CASELLI, R. J., GEARING, M., JUNCOS, J. L., GHETTI, B., SPINA, S., BORDELON, Y. M., TOURTELLOTTE, W. W., FROSCH, M. P., VONSATTEL, J. P., ZAROW, C., BEACH, T. G., ALBIN, R. L., LIEBERMAN, A. P., LEE, V. M., TROJANOWSKI, J. Q., VAN DEERLIN, V. M., BIRD, T. D., GALASKO, D. R., MASLIAH, E., WHITE, C. L., TRONCOSO, J. C., HANNEQUIN, D., BOXER, A. L., GESCHWIND, M. D., KUMAR, S., MANDELKOW, E. M., WSZOLEK, Z. K., UITTI, R. J., DICKSON, D. W., HAINES, J. L., MAYEUX, R., PERICAK-VANCE, M. A., FARRER, L. A., ALZHEIMER'S DISEASE GENETICS, C., ROSS, O. A., RADEMAKERS, R., SCHELLENBERG, G. D., MILLER, B. L., MANDELKOW, E. & GESCHWIND, D. H. 2012. Evidence for a role of the rare p.A152T variant in MAPT in increasing the risk for FTD-spectrum and Alzheimer's diseases. *Hum Mol Genet,* 21**,** 3500-12.

COUCHIE, D., MAVILIA, C., GEORGIEFF, I. S., LIEM, R. K., SHELANSKI, M. L. & NUNEZ, J. 1992. Primary structure of high molecular weight tau present in the peripheral nervous system. *Proc Natl Acad Sci U S A,* 89**,** 4378-81.

COWAN, C. M. & MUDHER, A. 2013. Are tau aggregates toxic or protective in tauopathies? *Front Neurol,* 4**,** 114.

CRIPPS, D., THOMAS, S. N., JENG, Y., YANG, F., DAVIES, P. & YANG, A. J. 2006. Alzheimer disease-specific conformation of hyperphosphorylated paired helical filament-Tau is polyubiquitinated through Lys-48, Lys-11, and Lys-6 ubiquitin conjugation. *J Biol Chem,* 281**,** 10825-38.

CROWTHER, R. A. & WISCHIK, C. M. 1985. Image reconstruction of the Alzheimer paired helical filament. *EMBO J,* 4**,** 3661-5.

DECKER, T. & LOHMANN-MATTHES, M. L. 1988. A quick and simple method for the quantitation of lactate dehydrogenase release in measurements of cellular cytotoxicity and tumor necrosis factor (TNF) activity. *J Immunol Methods,* 115**,** 61-9.

DICKSON, D. W., AHMED, Z., ALGOM, A. A., TSUBOI, Y. & JOSEPHS, K. A. 2010. Neuropathology of variants of progressive supranuclear palsy. *Curr Opin Neurol,* 23**,** 394-400.

DICKSON, D. W., CRYSTAL, H. A., BEVONA, C., HONER, W., VINCENT, I. & DAVIES, P. 1995. Correlations of synaptic and pathological markers with cognition of the elderly. *Neurobiol Aging,* 16**,** 285-98; discussion 298-304.

DRUBIN, D. G., FEINSTEIN, S. C., SHOOTER, E. M. & KIRSCHNER, M. W. 1985. Nerve growth factor-induced neurite outgrowth in PC12 cells involves the coordinate induction of microtubule assembly and assembly-promoting factors. *J Cell Biol,* 101**,** 1799-807.

ECKERMANN, K., MOCANU, M. M., KHLISTUNOVA, I., BIERNAT, J., NISSEN, A., HOFMANN, A., SCHONIG, K., BUJARD, H., HAEMISCH, A., MANDELKOW, E., ZHOU, L., RUNE, G. & MANDELKOW, E. M. 2007. The beta-propensity of Tau determines aggregation and synaptic loss in inducible mouse models of tauopathy. *J Biol Chem,* 282**,** 31755-65.

EHRNHOEFER, D. E., BIESCHKE, J., BOEDDRICH, A., HERBST, M., MASINO, L., LURZ, R., ENGEMANN, S., PASTORE, A. & WANKER, E. E. 2008. EGCG redirects amyloidogenic polypeptides into unstructured, off-pathway oligomers. *Nat Struct Mol Biol,* 15**,** 558-66.

FARIAS, G. A., MUNOZ, J. P., GARRIDO, J. & MACCIONI, R. B. 2002. Tubulin, actin, and tau protein interactions and the study of their macromolecular assemblies. *J Cell Biochem,* 85**,** 315-24.

FATOUROS, C., PIR, G. J., BIERNAT, J., KOUSHIKA, S. P., MANDELKOW, E., MANDELKOW, E. M., SCHMIDT, E. & BAUMEISTER, R. 2012. Inhibition of tau aggregation in a novel Caenorhabditis elegans model of tauopathy mitigates proteotoxicity. *Hum Mol Genet,* 21**,** 3587-603.

FLACH, K., HILBRICH, I., SCHIFFMANN, A., GARTNER, U., KRUGER, M., LEONHARDT, M., WASCHIPKY, H., WICK, L., ARENDT, T. & HOLZER, M. 2012. Tau oligomers impair artificial membrane integrity and cellular viability. *J Biol Chem,* 287**,** 43223-33.

FRIEDHOFF, P., SCHNEIDER, A., MANDELKOW, E. M. & MANDELKOW, E. 1998a. Rapid assembly of Alzheimer-like paired helical filaments from microtubule-associated protein tau monitored by fluorescence in solution. *Biochemistry,* 37**,** 10223-30.

FRIEDHOFF, P., VON BERGEN, M., MANDELKOW, E. M., DAVIES, P. & MANDELKOW, E. 1998b. A nucleated assembly mechanism of Alzheimer paired helical filaments. *Proc Natl Acad Sci U S A,* 95**,** 15712-7.

FROST, B., JACKS, R. L. & DIAMOND, M. I. 2009a. Propagation of tau misfolding from the outside to the inside of a cell. *J Biol Chem,* 284**,** 12845-52.

FROST, B., OLLESCH, J., WILLE, H. & DIAMOND, M. I. 2009b. Conformational diversity of wild-type Tau fibrils specified by templated conformation change. *J Biol Chem,* 284**,** 3546-51.

FU, Q., GAO, N., YU, J., MA, G., DU, Y., WANG, F., SU, Q. & CHE, F. 2014. Diazoxide pretreatment prevents Abeta1-42 induced oxidative stress in cholinergic neurons via alleviating NOX2 expression. *Neurochem Res,* 39**,** 1313-21.

GAMBLIN, T. C. 2005. Potential structure/function relationships of predicted secondary structural elements of tau. *Biochim Biophys Acta,* 1739**,** 140-9.

GAO, H. M., ZHOU, H. & HONG, J. S. 2012. NADPH oxidases: novel therapeutic targets for neurodegenerative diseases. *Trends Pharmacol Sci,* 33**,** 295-303.

GARCIA-SIERRA, F., GHOSHAL, N., QUINN, B., BERRY, R. W. & BINDER, L. I. 2003. Conformational changes and truncation of tau protein during tangle evolution in Alzheimer's disease. *J Alzheimers Dis,* 5**,** 65-77.

GASYMOV, O. K. & GLASGOW, B. J. 2007. ANS fluorescence: potential to augment the identification of the external binding sites of proteins. *Biochim Biophys Acta,* 1774**,** 403-11.

GERLIER, D. & THOMASSET, N. 1986. Use of MTT colorimetric assay to measure cell activation. *J Immunol Methods,* 94**,** 57-63.

GERSON, J. E., SENGUPTA, U., LASAGNA-REEVES, C. A., GUERRERO-MUNOZ, M. J., TRONCOSO, J. & KAYED, R. 2014. Characterization of tau oligomeric seeds in progressive supranuclear palsy. *Acta Neuropathol Commun,* 2**,** 73.

GHOSHAL, N., GARCIA-SIERRA, F., WUU, J., LEURGANS, S., BENNETT, D. A., BERRY, R. W. & BINDER, L. I. 2002. Tau conformational changes correspond to impairments of episodic memory in mild cognitive impairment and Alzheimer's disease. *Exp Neurol,* 177**,** 475-93.

GLENNER, G. G. & WONG, C. W. 1984. Alzheimer's disease: initial report of the purification and characterization of a novel cerebrovascular amyloid protein. *Biochem Biophys Res Commun,* 120**,** 885-90.

GLENNER, G. G., WONG, C. W., QUARANTA, V. & EANES, E. D. 1984. The amyloid deposits in Alzheimer's disease: their nature and pathogenesis. *Appl Pathol,* 2**,** 357-69.

GOEDERT, M. & JAKES, R. 1990. Expression of separate isoforms of human tau protein: correlation with the tau pattern in brain and effects on tubulin polymerization. *EMBO J,* 9**,** 4225-30.

GOEDERT, M., JAKES, R., SPILLANTINI, M. G., HASEGAWA, M., SMITH, M. J. & CROWTHER, R. A. 1996. Assembly of microtubule-associated protein tau into Alzheimer-like filaments induced by sulphated glycosaminoglycans. *Nature,* 383**,** 550-3.

GOEDERT, M. & SPILLANTINI, M. G. 2001. Tau gene mutations and neurodegeneration. *Biochem Soc Symp***,** 59-71.

GOEDERT, M., SPILLANTINI, M. G. & CROWTHER, R. A. 1992. Cloning of a big tau microtubule-associated protein characteristic of the peripheral nervous system. *Proc Natl Acad Sci U S A,* 89**,** 1983-7.

GOMEZ-ISLA, T., HOLLISTER, R., WEST, H., MUI, S., GROWDON, J. H., PETERSEN, R. C., PARISI, J. E. & HYMAN, B. T. 1997. Neuronal loss correlates with but exceeds neurofibrillary tangles in Alzheimer's disease. *Ann Neurol,* 41**,** 17-24.

GOMEZ-RAMOS, A., DIAZ-HERNANDEZ, M., CUADROS, R., HERNANDEZ, F. & AVILA, J. 2006. Extracellular tau is toxic to neuronal cells. *FEBS Lett,* 580**,** 4842-50.

GOMEZ-RAMOS, A., DIAZ-HERNANDEZ, M., RUBIO, A., MIRAS-PORTUGAL, M. T. & AVILA, J. 2008. Extracellular tau promotes intracellular calcium increase through M1 and M3 muscarinic receptors in neuronal cells. *Mol Cell Neurosci,* 37**,** 673-81.

GOTZ, J., CHEN, F., BARMETTLER, R. & NITSCH, R. M. 2001. Tau filament formation in transgenic mice expressing P301L tau. *J Biol Chem,* 276**,** 529-34.

GOTZ, J., DETERS, N., DOLDISSEN, A., BOKHARI, L., KE, Y., WIESNER, A., SCHONROCK, N. & ITTNER, L. M. 2007. A decade of tau transgenic animal models and beyond. *Brain Pathol,* 17**,** 91-103.

GOTZ, J., LIM, Y. A., KE, Y. D., ECKERT, A. & ITTNER, L. M. 2010. Dissecting toxicity of tau and beta-amyloid. *Neurodegener Dis,* 7**,** 10-2.

GOUX, W. J. 2002. The conformations of filamentous and soluble tau associated with Alzheimer paired helical filaments. *Biochemistry,* 41**,** 13798-806.

GRUNDKE-IQBAL, I., IQBAL, K., TUNG, Y. C., QUINLAN, M., WISNIEWSKI, H. M. & BINDER, L. I. 1986. Abnormal phosphorylation of the microtubule-associated protein tau (tau) in Alzheimer cytoskeletal pathology. *Proc Natl Acad Sci U S A,* 83**,** 4913-7.

GUO, J. L. & LEE, V. M. 2011. Seeding of normal Tau by pathological Tau conformers drives pathogenesis of Alzheimer-like tangles. *J Biol Chem,* 286**,** 15317-31.

GUSTKE, N., TRINCZEK, B., BIERNAT, J., MANDELKOW, E. M. & MANDELKOW, E. 1994. Domains of tau protein and interactions with microtubules. *Biochemistry,* 33**,** 9511-22.

GUTTMANN, R. P., ERICKSON, A. C. & JOHNSON, G. V. 1995. Tau self-association: stabilization with a chemical cross-linker and modulation by phosphorylation and oxidation state. *J Neurochem,* 64**,** 1209-15.

HAASS, C. & SELKOE, D. J. 2007. Soluble protein oligomers in neurodegeneration: lessons from the Alzheimer's amyloid beta-peptide. *Nat Rev Mol Cell Biol,* 8**,** 101-12.

HALL, G. F. & SAMAN, S. 2012. Death or secretion? The demise of a plausible assumption about CSF-tau in Alzheimer Disease? *Commun Integr Biol,* 5**,** 623-6.

HAMPEL, H., BLENNOW, K., SHAW, L. M., HOESSLER, Y. C., ZETTERBERG, H. & TROJANOWSKI, J. Q. 2010. Total and phosphorylated tau protein as biological markers of Alzheimer's disease. *Exp Gerontol,* 45**,** 30-40.

HANGER, D. P., ANDERTON, B. H. & NOBLE, W. 2009. Tau phosphorylation: the therapeutic challenge for neurodegenerative disease. *Trends Mol Med,* 15**,** 112-9.

HAWKINS, B. E., KRISHNAMURTHY, S., CASTILLO-CARRANZA, D. L., SENGUPTA, U., PROUGH, D. S., JACKSON, G. R., DEWITT, D. S. & KAYED, R. 2013. Rapid accumulation of endogenous tau oligomers in a rat model of traumatic brain injury: possible link between traumatic brain injury and sporadic tauopathies. *J Biol Chem,* 288**,** 17042-50.

HAWKINS, B. J., MADESH, M., KIRKPATRICK, C. J. & FISHER, A. B. 2007. Superoxide flux in endothelial cells via the chloride channel-3 mediates intracellular signaling. *Mol Biol Cell,* 18**,** 2002-12.

HE, H. J., WANG, X. S., PAN, R., WANG, D. L., LIU, M. N. & HE, R. Q. 2009. The proline-rich domain of tau plays a role in interactions with actin. *BMC Cell Biol,* 10**,** 81.

HERNANDES, M. S. & BRITTO, L. R. 2012. NADPH oxidase and neurodegeneration. *Curr Neuropharmacol,* 10**,** 321-7.

HOCHGRAFE, K., SYDOW, A., MATENIA, D., CADINU, D., KONEN, S., PETROVA, O., PICKHARDT, M., GOLL, P., MORELLINI, F., MANDELKOW, E. & MANDELKOW, E. M. 2015. Preventive methylene blue treatment preserves cognition in mice expressing full-length pro-aggregant human Tau. *Acta Neuropathol Commun,* 3**,** 25.

HOLMES, B. B., DEVOS, S. L., KFOURY, N., LI, M., JACKS, R., YANAMANDRA, K., OUIDJA, M. O., BRODSKY, F. M., MARASA, J., BAGCHI, D. P., KOTZBAUER, P. T., MILLER, T. M., PAPY-GARCIA, D. & DIAMOND, M. I. 2013. Heparan sulfate proteoglycans mediate internalization and propagation of specific proteopathic seeds. *Proc Natl Acad Sci U S A,* 110**,** E3138-47.

HORIGUCHI, T., URYU, K., GIASSON, B. I., ISCHIROPOULOS, H., LIGHTFOOT, R., BELLMANN, C., RICHTER-LANDSBERG, C., LEE, V. M. & TROJANOWSKI, J. Q. 2003. Nitration of tau protein is linked to neurodegeneration in tauopathies. *Am J Pathol,* 163**,** 1021-31.

HYMAN, B. T., AUGUSTINACK, J. C. & INGELSSON, M. 2005. Transcriptional and conformational changes of the tau molecule in Alzheimer's disease. *Biochim Biophys Acta,* 1739**,** 150-7.

IBA, M., GUO, J. L., MCBRIDE, J. D., ZHANG, B., TROJANOWSKI, J. Q. & LEE, V. M. 2013. Synthetic tau fibrils mediate transmission of neurofibrillary tangles in a transgenic mouse model of Alzheimer's-like tauopathy. *J Neurosci,* 33**,** 1024-37.

JEGANATHAN, S., VON BERGEN, M., BRUTLACH, H., STEINHOFF, H. J. & MANDELKOW, E. 2006. Global hairpin folding of tau in solution. *Biochemistry,* 45**,** 2283-93.

JEGANATHAN, S., VON BERGEN, M., MANDELKOW, E. M. & MANDELKOW, E. 2008. The natively unfolded character of tau and its aggregation to Alzheimer-like paired helical filaments. *Biochemistry,* 47**,** 10526-39.

JONES, E. M., DUBEY, M., CAMP, P. J., VERNON, B. C., BIERNAT, J., MANDELKOW, E., MAJEWSKI, J. & CHI, E. Y. 2012. Interaction of tau protein with model lipid membranes induces tau structural compaction and membrane disruption. *Biochemistry,* 51**,** 2539-50.

KAMPERS, T., FRIEDHOFF, P., BIERNAT, J., MANDELKOW, E. M. & MANDELKOW, E. 1996. RNA stimulates aggregation of microtubule-associated protein tau into Alzheimer-like paired helical filaments. *FEBS Lett,* 399**,** 344-9.

KFOURY, N., HOLMES, B. B., JIANG, H., HOLTZMAN, D. M. & DIAMOND, M. I. 2012. Trans-cellular propagation of Tau aggregation by fibrillar species. *J Biol Chem,* 287**,** 19440-51.

KHLISTUNOVA, I., BIERNAT, J., WANG, Y., PICKHARDT, M., VON BERGEN, M., GAZOVA, Z., MANDELKOW, E. & MANDELKOW, E. M. 2006. Inducible expression of Tau repeat domain in cell models of tauopathy: aggregation is toxic to cells but can be reversed by inhibitor drugs. *J Biol Chem,* 281**,** 1205-14.

KUHLA, B., HAASE, C., FLACH, K., LUTH, H. J., ARENDT, T. & MUNCH, G. 2007. Effect of pseudophosphorylation and cross-linking by lipid peroxidation and advanced glycation end product precursors on tau aggregation and filament formation. *J Biol Chem,* 282**,** 6984-91.

KUMAR, S., TEPPER, K., KANIYAPPAN, S., BIERNAT, J., WEGMANN, S., MANDELKOW, E. M., MULLER, D. & MANDELKOW, E. 2014. Stages and Conformations of Tau Repeat Domain during Aggregation and Effects on Neuronal Toxicity. *J Biol Chem*.

LASAGNA-REEVES, C. A., CASTILLO-CARRANZA, D. L., GUERRERO-MUOZ, M. J., JACKSON, G. R. & KAYED, R. 2010. Preparation and characterization of neurotoxic tau oligomers. *Biochemistry,* 49**,** 10039-41.

LASAGNA-REEVES, C. A., CASTILLO-CARRANZA, D. L., SENGUPTA, U., CLOS, A. L., JACKSON, G. R. & KAYED, R. 2011. Tau oligomers impair memory and induce synaptic and mitochondrial dysfunction in wild-type mice. *Mol Neurodegener,* 6**,** 39.

LASAGNA-REEVES, C. A., CASTILLO-CARRANZA, D. L., SENGUPTA, U., GUERRERO-MUNOZ, M. J., KIRITOSHI, T., NEUGEBAUER, V., JACKSON, G. R. & KAYED, R. 2012a. Alzheimer brain-derived tau oligomers propagate pathology from endogenous tau. *Sci Rep,* 2**,** 700.

LASAGNA-REEVES, C. A., CASTILLO-CARRANZA, D. L., SENGUPTA, U., SARMIENTO, J., TRONCOSO, J., JACKSON, G. R. & KAYED, R. 2012b. Identification of oligomers at early stages of tau aggregation in Alzheimer's disease. *FASEB J,* 26**,** 1946-59.

LE, M. N., KIM, W., LEE, S., MCKEE, A. C. & HALL, G. F. 2012. Multiple mechanisms of extracellular tau spreading in a non-transgenic tauopathy model. *Am J Neurodegener Dis,* 1**,** 316-33.

LEE, G., COWAN, N. & KIRSCHNER, M. 1988. The primary structure and heterogeneity of tau protein from mouse brain. *Science,* 239**,** 285-8.

LIRA-DE LEON, K. I., GARCIA-GUTIERREZ, P., SERRATOS, I. N., PALOMERA-CARDENAS, M., FIGUEROA-CORONA MDEL, P., CAMPOS-PENA, V. & MERAZ-RIOS, M. A. 2013. Molecular mechanism of tau aggregation induced by anionic and cationic dyes. *J Alzheimers Dis,* 35**,** 319-34.

MA, Q. L., ZUO, X., YANG, F., UBEDA, O. J., GANT, D. J., ALAVERDYAN, M., TENG, E., HU, S., CHEN, P. P., MAITI, P., TETER, B., COLE, G. M. & FRAUTSCHY, S. A. 2013. Curcumin suppresses soluble tau dimers and corrects molecular chaperone, synaptic, and behavioral deficits in aged human tau transgenic mice. *J Biol Chem,* 288**,** 4056-65.

MAEDA, S., SAHARA, N., SAITO, Y., MURAYAMA, S., IKAI, A. & TAKASHIMA, A. 2006. Increased levels of granular tau oligomers: an early sign of brain aging and Alzheimer's disease. *Neurosci Res,* 54**,** 197-201.

MANDELKOW, E. M. & MANDELKOW, E. 2012. Biochemistry and cell biology of tau protein in neurofibrillary degeneration. *Cold Spring Harb Perspect Med,* 2**,** a006247.

MASTERS, C. L., SIMMS, G., WEINMAN, N. A., MULTHAUP, G., MCDONALD, B. L. & BEYREUTHER, K. 1985. Amyloid plaque core protein in Alzheimer disease and Down syndrome. *Proc Natl Acad Sci U S A,* 82**,** 4245-9.

MATTSON, G., CONKLIN, E., DESAI, S., NIELANDER, G., SAVAGE, M. D. & MORGENSEN, S. 1993. A practical approach to crosslinking. *Mol Biol Rep,* 17**,** 167-83.

MAURER, K., VOLK, S. & GERBALDO, H. 1997. Auguste D and Alzheimer's disease. *Lancet,* 349**,** 1546-9.

MEDINA, M. & AVILA, J. 2014. The role of extracellular Tau in the spreading of neurofibrillary pathology. *Front Cell Neurosci,* 8**,** 113.

MESSING, L., DECKER, J. M., JOSEPH, M., MANDELKOW, E. & MANDELKOW, E. M. 2013. Cascade of tau toxicity in inducible hippocampal brain slices and prevention by aggregation inhibitors. *Neurobiol Aging,* 34**,** 1343-54.

MICHEL, C. H., KUMAR, S., PINOTSI, D., TUNNACLIFFE, A., ST GEORGE-HYSLOP, P., MANDELKOW, E., MANDELKOW, E. M., KAMINSKI, C. F. & KAMINSKI SCHIERLE, G. S. 2014. Extracellular monomeric tau protein is sufficient to initiate the spread of tau protein pathology. *J Biol Chem,* 289**,** 956-67.

MIETELSKA-POROWSKA, A., WASIK, U., GORAS, M., FILIPEK, A. & NIEWIADOMSKA, G. 2014. Tau protein modifications and interactions: their role in function and dysfunction. *Int J Mol Sci,* 15**,** 4671-713.

MIGNEAULT, I., DARTIGUENAVE, C., BERTRAND, M. J. & WALDRON, K. C. 2004. Glutaraldehyde: behavior in aqueous solution, reaction with proteins, and application to enzyme crosslinking. *Biotechniques,* 37**,** 790-6, 798-802.

MOCANU, M. M., NISSEN, A., ECKERMANN, K., KHLISTUNOVA, I., BIERNAT, J., DREXLER, D., PETROVA, O., SCHONIG, K., BUJARD, H., MANDELKOW, E., ZHOU, L., RUNE, G. & MANDELKOW, E. M. 2008. The potential for beta-structure in the repeat domain of tau protein determines aggregation, synaptic decay, neuronal loss, and coassembly with endogenous Tau in inducible mouse models of tauopathy. *J Neurosci,* 28**,** 737-48.

MORRISON, J. H. & HOF, P. R. 1997. Life and death of neurons in the aging brain. *Science,* 278**,** 412-9.

MUDHER, A., SHEPHERD, D., NEWMAN, T. A., MILDREN, P., JUKES, J. P., SQUIRE, A., MEARS, A., DRUMMOND, J. A., BERG, S., MACKAY, D., ASUNI, A. A., BHAT, R. & LOVESTONE, S. 2004. GSK-3beta inhibition reverses axonal transport defects and behavioural phenotypes in Drosophila. *Mol Psychiatry,* 9**,** 522-30.

MUKRASCH, M. D., BIBOW, S., KORUKOTTU, J., JEGANATHAN, S., BIERNAT, J., GRIESINGER, C., MANDELKOW, E. & ZWECKSTETTER, M. 2009. Structural polymorphism of 441-residue tau at single residue resolution. *PLoS Biol,* 7**,** e34.

MUKRASCH, M. D., BIERNAT, J., VON BERGEN, M., GRIESINGER, C., MANDELKOW, E. & ZWECKSTETTER, M. 2005. Sites of tau important for aggregation populate {beta}-structure and bind to microtubules and polyanions. *J Biol Chem,* 280**,** 24978-86.

MYERS, A. J., PITTMAN, A. M., ZHAO, A. S., ROHRER, K., KALEEM, M., MARLOWE, L., LEES, A., LEUNG, D., MCKEITH, I. G., PERRY, R. H., MORRIS, C. M., TROJANOWSKI, J. Q., CLARK, C., KARLAWISH, J., ARNOLD, S., FORMAN, M. S., VAN DEERLIN, V., DE SILVA, R. & HARDY, J. 2007. The MAPT H1c risk haplotype is associated with increased expression of tau and especially of 4 repeat containing transcripts. *Neurobiol Dis,* 25**,** 561-70.

NACHARAJU, P., KO, L. & YEN, S. H. 1997. Characterization of in vitro glycation sites of tau. *J Neurochem,* 69**,** 1709-19.

NAGY, Z., ESIRI, M. M., JOBST, K. A., MORRIS, J. H., KING, E. M., MCDONALD, B., LITCHFIELD, S., SMITH, A., BARNETSON, L. & SMITH, A. D. 1995. Relative roles of plaques and tangles in the dementia of Alzheimer's disease: correlations using three sets of neuropathological criteria. *Dementia,* 6**,** 21-31.

NEVE, R. L., HARRIS, P., KOSIK, K. S., KURNIT, D. M. & DONLON, T. A. 1986. Identification of cDNA clones for the human microtubule-associated protein tau and chromosomal localization of the genes for tau and microtubule-associated protein 2. *Brain Res,* 387**,** 271-80.

NONAKA, T., WATANABE, S. T., IWATSUBO, T. & HASEGAWA, M. 2010. Seeded aggregation and toxicity of {alpha}-synuclein and tau: cellular models of neurodegenerative diseases. *J Biol Chem,* 285**,** 34885-98.

OBA, M. & TANAKA, M. 2012. Intracellular internalization mechanism of protein transfection reagents. *Biol Pharm Bull,* 35**,** 1064-8.

PAGE, B., PAGE, M. & NOEL, C. 1993. A new fluorometric assay for cytotoxicity measurements in-vitro. *Int J Oncol,* 3**,** 473-6.

PATTERSON, K. R., REMMERS, C., FU, Y., BROOKER, S., KANAAN, N. M., VANA, L., WARD, S., REYES, J. F., PHILIBERT, K., GLUCKSMAN, M. J. & BINDER, L. I. 2011. Characterization of prefibrillar Tau oligomers in vitro and in Alzheimer disease. *J Biol Chem,* 286**,** 23063-76.

PICKHARDT, M., GAZOVA, Z., VON BERGEN, M., KHLISTUNOVA, I., WANG, Y., HASCHER, A., MANDELKOW, E. M., BIERNAT, J. & MANDELKOW, E. 2005. Anthraquinones inhibit tau aggregation and dissolve Alzheimer's paired helical filaments in vitro and in cells. *J Biol Chem,* 280**,** 3628-35.

POLYDORO, M., ACKER, C. M., DUFF, K., CASTILLO, P. E. & DAVIES, P. 2009. Age-dependent impairment of cognitive and synaptic function in the htau mouse model of tau pathology. *J Neurosci,* 29**,** 10741-9.

RAMALHO, R. M., VIANA, R. J., CASTRO, R. E., STEER, C. J., LOW, W. C. & RODRIGUES, C. M. 2008. Apoptosis in transgenic mice expressing the P301L mutated form of human tau. *Mol Med,* 14**,** 309-17.

RIZZU, P., VAN SWIETEN, J. C., JOOSSE, M., HASEGAWA, M., STEVENS, M., TIBBEN, A., NIERMEIJER, M. F., HILLEBRAND, M., RAVID, R., OOSTRA, B. A., GOEDERT, M., VAN DUIJN, C. M. & HEUTINK, P. 1999. High prevalence of mutations in the microtubule-associated protein tau in a population study of frontotemporal dementia in the Netherlands. *Am J Hum Genet,* 64**,** 414-21.

SAHARA, N., MAEDA, S., MURAYAMA, M., SUZUKI, T., DOHMAE, N., YEN, S. H. & TAKASHIMA, A. 2007. Assembly of two distinct dimers and higher-order oligomers from full-length tau. *Eur J Neurosci,* 25**,** 3020-9.

SAMAN, S., KIM, W., RAYA, M., VISNICK, Y., MIRO, S., SAMAN, S., JACKSON, B., MCKEE, A. C., ALVAREZ, V. E., LEE, N. C. & HALL, G. F. 2012. Exosome-associated tau is secreted in tauopathy models and is selectively phosphorylated in cerebrospinal fluid in early Alzheimer disease. *J Biol Chem,* 287**,** 3842-9.

SANTACRUZ, K., LEWIS, J., SPIRES, T., PAULSON, J., KOTILINEK, L., INGELSSON, M., GUIMARAES, A., DETURE, M., RAMSDEN, M., MCGOWAN, E., FORSTER, C., YUE, M., ORNE, J., JANUS, C., MARIASH, A., KUSKOWSKI, M., HYMAN, B., HUTTON, M. & ASHE, K. H. 2005. Tau suppression in a neurodegenerative mouse model improves memory function. *Science,* 309**,** 476-81.

SCHAFER, K. N., CISEK, K., HUSEBY, C. J., CHANG, E. & KURET, J. 2013. Structural determinants of Tau aggregation inhibitor potency. *J Biol Chem,* 288**,** 32599-611.

SCHIRMER, R. H., ADLER, H., PICKHARDT, M. & MANDELKOW, E. 2011. "Lest we forget you--methylene blue...". *Neurobiol Aging,* 32**,** 2325 e7-16.

SCHNEIDER, A. & MANDELKOW, E. 2008. Tau-based treatment strategies in neurodegenerative diseases. *Neurotherapeutics,* 5**,** 443-57.

SCHNEIDER, C. A., RASBAND, W. S. & ELICEIRI, K. W. 2012. NIH Image to ImageJ: 25 years of image analysis. *Nat Methods,* 9**,** 671-5.

SCHWEERS, O., MANDELKOW, E. M., BIERNAT, J. & MANDELKOW, E. 1995. Oxidation of cysteine-322 in the repeat domain of microtubule-associated protein tau controls the in vitro assembly of paired helical filaments. *Proc Natl Acad Sci U S A,* 92**,** 8463-7.

SCHWEERS, O., SCHONBRUNN-HANEBECK, E., MARX, A. & MANDELKOW, E. 1994. Structural studies of tau protein and Alzheimer paired helical filaments show no evidence for beta-structure. *J Biol Chem,* 269**,** 24290-7.

SEMISOTNOV, G. V., RODIONOVA, N. A., RAZGULYAEV, O. I., UVERSKY, V. N., GRIPAS, A. F. & GILMANSHIN, R. I. 1991. Study of the "molten globule" intermediate state in protein folding by a hydrophobic fluorescent probe. *Biopolymers,* 31**,** 119-28.

SERGEANT, N., BRETTEVILLE, A., HAMDANE, M., CAILLET-BOUDIN, M. L., GROGNET, P., BOMBOIS, S., BLUM, D., DELACOURTE, A., PASQUIER, F., VANMECHELEN, E., SCHRAEN-MASCHKE, S. & BUEE, L. 2008. Biochemistry of Tau in Alzheimer's disease and related neurological disorders. *Expert Rev Proteomics,* 5**,** 207-24.

SHARMA, V. M., LITERSKY, J. M., BHASKAR, K. & LEE, G. 2007. Tau impacts on growth-factor-stimulated actin remodeling. *J Cell Sci,* 120**,** 748-57.

SHKUMATOV, A. V., CHINNATHAMBI, S., MANDELKOW, E. & SVERGUN, D. I. 2011. Structural memory of natively unfolded tau protein detected by small-angle X-ray scattering. *Proteins,* 79**,** 2122-31.

SILLEN, A., WIERUSZESKI, J. M., LEROY, A., YOUNES, A. B., LANDRIEU, I. & LIPPENS, G. 2005. High-resolution magic angle spinning NMR of the neuronal tau protein integrated in Alzheimer's-like paired helical fragments. *J Am Chem Soc,* 127**,** 10138-9.

SIMON, D., GARCIA-GARCIA, E., ROYO, F., FALCON-PEREZ, J. M. & AVILA, J. 2012. Proteostasis of tau. Tau overexpression results in its secretion via membrane vesicles. *FEBS Lett,* 586**,** 47-54.

SLAVIK, J. 1982. Anilinonaphthalene sulfonate as a probe of membrane composition and function. *Biochim Biophys Acta,* 694**,** 1-25.

SPIRES, T. L., ORNE, J. D., SANTACRUZ, K., PITSTICK, R., CARLSON, G. A., ASHE, K. H. & HYMAN, B. T. 2006. Region-specific dissociation of neuronal loss and neurofibrillary pathology in a mouse model of tauopathy. *Am J Pathol,* 168**,** 1598-607.

STOPPINI, L., BUCHS, P. A. & MULLER, D. 1991. A simple method for organotypic cultures of nervous tissue. *J Neurosci Methods,* 37**,** 173-82.

SULTAN, A., NESSLANY, F., VIOLET, M., BEGARD, S., LOYENS, A., TALAHARI, S., MANSUROGLU, Z., MARZIN, D., SERGEANT, N., HUMEZ, S., COLIN, M., BONNEFOY, E., BUEE, L. & GALAS, M. C. 2011. Nuclear tau, a key player in neuronal DNA protection. *J Biol Chem,* 286**,** 4566-75.

SYDOW, A., VAN DER JEUGD, A., ZHENG, F., AHMED, T., BALSCHUN, D., PETROVA, O., DREXLER, D., ZHOU, L., RUNE, G., MANDELKOW, E., D'HOOGE, R., ALZHEIMER, C. & MANDELKOW, E. M. 2011. Tau-induced defects in synaptic plasticity, learning, and memory

are reversible in transgenic mice after switching off the toxic Tau mutant. *J Neurosci,* 31**,** 2511-25.

TAI, H. C., SERRANO-POZO, A., HASHIMOTO, T., FROSCH, M. P., SPIRES-JONES, T. L. & HYMAN, B. T. 2012. The synaptic accumulation of hyperphosphorylated tau oligomers in Alzheimer disease is associated with dysfunction of the ubiquitin-proteasome system. *Am J Pathol,* 181**,** 1426-35.

TIAN, H., DAVIDOWITZ, E., LOPEZ, P., EMADI, S., MOE, J. & SIERKS, M. 2013. Trimeric tau is toxic to human neuronal cells at low nanomolar concentrations. *Int J Cell Biol,* 2013**,** 260787.

TOMLINSON, B. E., BLESSED, G. & ROTH, M. 1970. Observations on the brains of demented old people. *J Neurol Sci,* 11**,** 205-42.

TRINCZEK, B., EBNETH, A., MANDELKOW, E. M. & MANDELKOW, E. 1999. Tau regulates the attachment/detachment but not the speed of motors in microtubule-dependent transport of single vesicles and organelles. *J Cell Sci,* 112 (Pt 14)**,** 2355-67.

TROJANOWSKI, J. Q. & LEE, V. M. 2005. Pathological tau: a loss of normal function or a gain in toxicity? *Nat Neurosci,* 8**,** 1136-7.

VAN DER JEUGD, A., HOCHGRAFE, K., AHMED, T., DECKER, J. M., SYDOW, A., HOFMANN, A., WU, D., MESSING, L., BALSCHUN, D., D'HOOGE, R. & MANDELKOW, E. M. 2012. Cognitive defects are reversible in inducible mice expressing pro-aggregant full-length human Tau. *Acta Neuropathol,* 123**,** 787-805.

VISTICA, D. T., SKEHAN, P., SCUDIERO, D., MONKS, A., PITTMAN, A. & BOYD, M. R. 1991. Tetrazolium-based assays for cellular viability: a critical examination of selected parameters affecting formazan production. *Cancer Res,* 51**,** 2515-20.

VON BERGEN, M., BARGHORN, S., BIERNAT, J., MANDELKOW, E. M. & MANDELKOW, E. 2005. Tau aggregation is driven by a transition from random coil to beta sheet structure. *Biochim Biophys Acta,* 1739**,** 158-66.

VON BERGEN, M., BARGHORN, S., LI, L., MARX, A., BIERNAT, J., MANDELKOW, E. M. & MANDELKOW, E. 2001. Mutations of tau protein in frontotemporal dementia promote aggregation of paired helical filaments by enhancing local beta-structure. *J Biol Chem,* 276**,** 48165-74.

VON BERGEN, M., FRIEDHOFF, P., BIERNAT, J., HEBERLE, J., MANDELKOW, E. M. & MANDELKOW, E. 2000. Assembly of tau protein into Alzheimer paired helical filaments depends on a local sequence motif ((306)VQIVYK(311)) forming beta structure. *Proc Natl Acad Sci U S A,* 97**,** 5129-34.

WANG, Y. P., BIERNAT, J., PICKHARDT, M., MANDELKOW, E. & MANDELKOW, E. M. 2007. Stepwise proteolysis liberates tau fragments that nucleate the Alzheimer-like aggregation of full-length tau in a neuronal cell model. *Proc Natl Acad Sci U S A,* 104**,** 10252-7.

WARD, S. M., HIMMELSTEIN, D. S., LANCIA, J. K., FU, Y., PATTERSON, K. R. & BINDER, L. I. 2013. TOC1: characterization of a selective oligomeric tau antibody. *J Alzheimers Dis,* 37**,** 593-602.

WEGMANN, S., JUNG, Y. J., CHINNATHAMBI, S., MANDELKOW, E. M., MANDELKOW, E. & MULLER, D. J. 2010. Human Tau isoforms assemble into ribbon-like fibrils that display polymorphic structure and stability. *J Biol Chem,* 285**,** 27302-13.

WEGMANN, S., MEDALSY, I. D., MANDELKOW, E. & MULLER, D. J. 2013. The fuzzy coat of pathological human Tau fibrils is a two-layered polyelectrolyte brush. *Proc Natl Acad Sci U S A,* 110**,** E313-21.

WEINGARTEN, M. D., SUTER, M. M., LITTMAN, D. R. & KIRSCHNER, M. W. 1974. Properties of the depolymerization products of microtubules from mammalian brain. *Biochemistry,* 13**,** 5529-37.

WILLE, H., DREWES, G., BIERNAT, J., MANDELKOW, E. M. & MANDELKOW, E. 1992. Alzheimer-like paired helical filaments and antiparallel dimers formed from microtubule-associated protein tau in vitro. *J Cell Biol,* 118**,** 573-84.

WILLIAMS, D. W., TYRER, M. & SHEPHERD, D. 2000. Tau and tau reporters disrupt central projections of sensory neurons in Drosophila. *J Comp Neurol,* 428**,** 630-40.

WILSON, D. M. & BINDER, L. I. 1995. Polymerization of microtubule-associated protein tau under near-physiological conditions. *J Biol Chem,* 270**,** 24306-14.

WISCHIK, C. M., HARRINGTON, C. R. & STOREY, J. M. 2014. Tau-aggregation inhibitor therapy for Alzheimer's disease. *Biochem Pharmacol,* 88**,** 529-39.

WITTMANN, C. W., WSZOLEK, M. F., SHULMAN, J. M., SALVATERRA, P. M., LEWIS, J., HUTTON, M. & FEANY, M. B. 2001. Tauopathy in Drosophila: neurodegeneration without neurofibrillary tangles. *Science,* 293**,** 711-4.

WOBST, H. J., SHARMA, A., DIAMOND, M. I., WANKER, E. E. & BIESCHKE, J. 2015. The green tea polyphenol (-)-epigallocatechin gallate prevents the aggregation of tau protein into toxic oligomers at substoichiometric ratios. *FEBS Lett,* 589**,** 77-83.

WOGULIS, M., WRIGHT, S., CUNNINGHAM, D., CHILCOTE, T., POWELL, K. & RYDEL, R. E. 2005. Nucleation-dependent polymerization is an essential component of amyloid-mediated neuronal cell death. *J Neurosci,* 25**,** 1071-80.

WU, J. W., HERMAN, M., LIU, L., SIMOES, S., ACKER, C. M., FIGUEROA, H., STEINBERG, J. I., MARGITTAI, M., KAYED, R., ZURZOLO, C., DI PAOLO, G. & DUFF, K. E. 2013. Small misfolded Tau species are internalized via bulk endocytosis and anterogradely and retrogradely transported in neurons. *J Biol Chem,* 288**,** 1856-70.

YAMADA, K., CIRRITO, J. R., STEWART, F. R., JIANG, H., FINN, M. B., HOLMES, B. B., BINDER, L. I., MANDELKOW, E. M., DIAMOND, M. I., LEE, V. M. & HOLTZMAN, D. M. 2011. In vivo microdialysis reveals age-dependent decrease of brain interstitial fluid tau levels in P301S human tau transgenic mice. *J Neurosci,* 31**,** 13110-7.

YAN, S. D., CHEN, X., SCHMIDT, A. M., BRETT, J., GODMAN, G., ZOU, Y. S., SCOTT, C. W., CAPUTO, C., FRAPPIER, T., SMITH, M. A. & ET AL. 1994. Glycated tau protein in Alzheimer disease: a mechanism for induction of oxidant stress. *Proc Natl Acad Sci U S A,* 91**,** 7787-91.

YAO, T. M., TOMOO, K., ISHIDA, T., HASEGAWA, H., SASAKI, M. & TANIGUCHI, T. 2003. Aggregation analysis of the microtubule binding domain in tau protein by spectroscopic methods. *J Biochem,* 134**,** 91-9.

YOSHIYAMA, Y., HIGUCHI, M., ZHANG, B., HUANG, S. M., IWATA, N., SAIDO, T. C., MAEDA, J., SUHARA, T., TROJANOWSKI, J. Q. & LEE, V. M. 2007. Synapse loss and microglial activation precede tangles in a P301S tauopathy mouse model. *Neuron,* 53**,** 337-51.

YU, J. Z. & RASENICK, M. M. 2006. Tau associates with actin in differentiating PC12 cells. *FASEB J,* 20**,** 1452-61.

ZEMPEL, H., LUEDTKE, J., KUMAR, Y., BIERNAT, J., DAWSON, H., MANDELKOW, E. & MANDELKOW, E. M. 2013. Amyloid-beta oligomers induce synaptic damage via Tau-dependent microtubule severing by TTLL6 and spastin. *EMBO J,* 32**,** 2920-37.

ZEMPEL, H., THIES, E., MANDELKOW, E. & MANDELKOW, E. M. 2010. Abeta oligomers cause localized Ca(2+) elevation, missorting of endogenous Tau into dendrites, Tau phosphorylation, and destruction of microtubules and spines. *J Neurosci,* 30**,** 11938-50.

ZHANG, J., ZHOU, X., YU, Q., YANG, L., SUN, D., ZHOU, Y. & LIU, J. 2014. Epigallocatechin-3-gallate (EGCG)-Stabilized Selenium Nanoparticles Coated with Tet-1 Peptide To Reduce Amyloid-beta Aggregation and Cytotoxicity. *ACS Appl Mater Interfaces,* 6**,** 8475-87.

7 Publications

1. **Kaniyappan S**, Chandupatla RR, Tepper K, Biernat J, Mandelkow EM and Mandelkow E. (2015) Extracellular and intracellular effects of low-n oligomers of pro-aggregant Tau repeat domain. Abstract, ADPD conference, Nice, 2015 (Oral presentation).

2. **Kaniyappan S**, Chandupatla RR, Tepper K, Biernat J, Mandelkow EM and Mandelkow E. (2014) Low molecular weight oligomers of Tau repeat domain (TauRD-ΔK280) cause increase in intracellular ROS and calcium levels accompanied by spine loss. Abstract, SFN conference, Washington D.C, 2014 (Oral presentation)

3. Kumar S, Tepper K, **Kaniyappan S**, Biernat J, Wegmann S, Mandelkow EM, Müller D, and Mandelkow E. (2014). Stages and Conformations of Tau Repeat Domain during Aggregation and Effects on Neuronal Toxicity. Journal of Biological Chemistry, May 13. pii: jbc.M114.554725

Appendix

Chemical composition

Protein purification chemicals:

10 X CB Buffer

Chemical	Weight	Stock	Volume
0.2 M Na-Mes	42.646 g	-	-
10mM Na-EGTA	3.804 g	0.5M	20ml
10mM MgCl2	2 g		1 ml

Make up to 1 liter with double distilled water, pH 6.8. Store at 4°C**.** Prepare the whole solution once or prepare it from stock.

Re Suspension Buffer Composition: For 100 ml

Chemical	Stock	Volume
CB Buffer	10 X	10 ml
DTT	1 M	0.5 ml
PMSF	0.1 M	2 ml
Leupeptin	10 mg/ml	100 µl
Pepstatin A	5 mg/ml	200 µl
benzamidine	1M	200 µl
MQ H2O		87 ml

Mono S A Buffer 10 X

Chemical	10X Stock	Volume for 1X
20 mM Na-MES	0.2 M	100ml
50 mM NaCl	5 M	10ml
2 mM DTT	1 M	2 ml
1 mM Na-EGTA	0.5 M	2 ml
1 mM $MgSO_4$	1 M	1 ml
0.1 mM PMSF	0.1 M	1 ml

Make up to 1Liter; pH 6.8; Sterilize; PMSF and DTT should be added fresh.

Mono S B Buffer (250 ml suffices for a single run)

Chemical	Stock	Volume
20 mM Na-MES	0.2 M	100ml
1M NaCl	5 M	200ml
2 mM DTT	1 M	2 ml
1 mM Na-EGTA	0.5 M	2 ml
1 mM $MgSO_4$	1 M	1 ml
0.1 mM PMSF	0.1 M	1 ml

Make up to 1Liter; pH 6.8; Sterilize; PMSF and DTT should be added fresh.

SDS gel composition

Ingredients	7% resolving gel	10% resolving gel	17% resolving gel	4% stacking gel
40% Acrylamide	10.6 ml	15 ml	25.6 ml	5.4 ml
1M Tris HCl pH 8.8	22 ml	22 ml	22 ml	-
0.25 M Tris HCl pH 6.8	-	-	-	27 ml
H_2O	26.4 ml	22 ml	11.5 ml	-
H_2O + Bromophenol Blue	-	-	-	20.9 ml
10 % SDS	600 µl	600 µl	600 µl	540 µl
TEMED	120 µl	120 µl	120 µl	108 µl
10% APS	65 µl	65 µl	65 µl	150 µl

5X SDS sample buffer

0.32M Tris-HCl, pH 6.8; 10% SDS; 50% Glycerol; 1.43M ß-ME; and

10^{-2}% Bromophenolblue

1X SDS running buffer

0.25M Tris; 0.192M Glycine; 0.1% SDS; make the volume up to 10 liters with doubly distilled water.

10X blotting buffer or Transfer buffer

390 mM Glycine; 480 mM Tris; 0.3% SDS; Make up to 1 liter with doubly distilled water.

1X blotting buffer or Transfer buffer

100 ml of 10X blotting buffer; 50 ml 100% methanol; Make up to 1 liter with doubly distilled water.

10X TBST

100 mM Tris; 1.5 M NaCl; 0.5% Tween 20; Make up to 2.5 liters with doubly distilled water. Adjust the pH to 7.5

Stripping buffer

0.2M glycine; 1mM EDTA-Na; 0.5M NaCl, pH 2.5.

Coomassie Stain:

25% isopropanol; 10% acetic acid; 0.05% coomassie R-250; Make up to 200 ml with doubly distilled water.

Coomassie destaining solution:

Intensive:

2.5 L ethanol; 2.0 L doubly distilled water; and 0.5 L acetic acid

Normal:

250 ml ethanol; 375 ml acetic acid; and 4375 ml doubly distilled water

Silver staining:

Fixative: 30% ethanol and 10% acetic acid

Cross-linking reagent: 30% ethanol; 0.5M sodium acetate; 0.2% sodium thio cyanate and 0.5% glutaraldehyde

Silver nitrate staining solution:

0.1% silver nitrate; and 0.02% formaldehyde

Developing solution:

2.5% sodium carbonate; 0.01% formaldehyde.

Reaction ending solution:

50mM EDTA, pH 8.0

AFM

Adsorption buffer (**PBS)**

137 mM NaCl; 8 mM NH_2PO_4, 2.7 mM KCl; and 1.5 mM KH_2PO_4 adjusted to pH 7.4.

Imaging buffer

10 mM Tris–HCl; 50 mM KCl; adjusted to pH 7.4.

Cell culture chemicals:

SH-SY5Y cells culture medium:

15% FBS; 1% penicillin and streptomycin; diluted in DMEM medium followed by filter sterilization.

SH-SY5Y cells freezing medium:

50% FCS; 30% DMEM; 20% DMSO;

Preparation and sterilization using syringe filters. The filtered solution diluted 1:1 to the culture medium.

Primary rat neuronal cell growing:

Plating medium:

10% Horse serum; 1% penicillin and streptomycin; 1mM pyruvate; diluted in DMEM medium followed by filter sterilization.

Neurobasal medium: (Neuron specific medium)

1% penicillin and streptomycin; 2% B27 serum supplement; 2mM L-glutamine

make up the volume to 500 ml with neurobasal medium. All the additives should be filter sterilized before the addition.

Neurobasal medium with AraC: (To inhibit the growth of the astrocytes)

AraC diluted with Neurobasal medium at a 1:6000 ratio for rat neuronal cells; 1:3000 for mouse neuronal cells.

Tissue culture:

Slice culture media:

MEM media – 50% (200ml) , HBSS – 25% (100 ml), horse serum – 25% (100ml) , penicilin and streptomycin – 1% (4ml) , glucose – 0.9%, (1.8g) . The culture media was prepared, filter sterilized and stored at 4°C until further use.

2X Lysis buffer

100 mM Tris-HCl, pH 7.4; 20% glycerol ; 2% NP 40 detergent; 10mM DTT; 2mM EGTA; 40mM NaF and 2mM Na_3VO_4.

Working lysis buffer

2X lysis buffer; 150mM NaCl; 1X complete protease mini, 5mM CHAPS, 100U benzonase and 5µM okadaic acid. Make up these chemicals with distilled water to the desired volume.

Sarcosyl extraction: Buffer H

10mM Tris-HCl, pH 7.4; 0.8M NaCl; 1mM EGTA; 10% Sucrose; 1mM PMSF and 1X protease inhibitor mix.

Acknowledgement

I would like to express my thanks to Dr. Eckhard Mandelkow and Dr. Eva-Maria Mandelkow for giving me the opportunity to carry out my thesis in their lab and for mentoring me. My thanks go to Dr. Jacek Biernat, Dr. Thomas Timm, Dr. Katharina Tepper for their valuble suggestions and help. I share the credit of my work on AFM with Dr. Johannes Overbuschman. I would like to thank light microscopy facility and the IT department of DZNE for technical assistance. I would also like to thank the secretaries of DZNE and MPI, Hamburg for helping me with administrative matters.

I would like to thank Dr. Madhankumar Anandhakrishnan, who helped me during difficult phases of this project by giving suggestions and ideas. He was a solution giver and kept me always as an optimistic.

I owe thankfulness to Mr. Ram Reddy Chandupatla for helping me in several experiments during the most critical time of the thesis work.

I would like to thank Dr. Yatender Kumar, Dr. Satish Kumar for their useful suggestions and help. I express my thanks to Dr. Maria Joseph for her help in the lab and outside during the early phase of my PhD.

I would also like to thank the all the lab members for helping me in various stages of my PhD.

My sincere thanks to Mr. Dilip Joy, Dr. Avinash Gandhi, Dr. Hemanth Nag for having confidence in me and motivating me to pursue research.

Last but not least, my heartfelt thanks to my family members who supported me during the ups and downs of my life.

Publications: (Peer reviewed journals)

Kumar S, Tepper K, **Kaniyappan S**, Biernat J, Wegmann S, Mandelkow EM, Müller D, and Mandelkow E. (2014). Stages and Conformations of Tau Repeat Domain during Aggregation and Effects on Neuronal Toxicity. Journal of Biological Chemistry, May 13. pii: jbc.M114.554725

Conference abstract publications: (Selected)

Kaniyappan S, Chandupatla RR, Tepper K, Biernat J, Mandelkow EM and Mandelkow E. (2015) Extracellular and intracellular effects of Low-n oligomers of pro-aggregant tau repeat domain (TauRD-ΔK280). ADPD conference, Nice, 2015. (Oral presentation)

Kaniyappan S, Chandupatla RR, Tepper K, Biernat J, Mandelkow EM and Mandelkow E. (2014) Low molecular weight oligomers of Tau repeat domain (TauRD-ΔK280) cause increase in intracellular ROS and calcium levels accompanied by spine loss. SFN conference, Washington D.C, 2014 (Oral presentation)